공학박사학위논문

디젤 엔진에서 가상 질소산화물 센서에 관한 연구

Study on the Virtual NOx Sensor for Diesel Engines

2013년 8월

서울대학교 대학원

기계항공공학부

이 준 용

디젤 엔진에서 가상 질소산화물 센서에 관한 연구

Study on the Virtual NO_x Sensor for Diesel Engines

지도교수 민 경 덕

이 논문을 공학박사 학위논문으로 제출함

2013 년 8 월

서울대학교 대학원

기계항공공학부

이 준 용

이준용의 공학박사 학위논문을 인준함

2013 년 6 월

위 원 장 고 상 근 (인)

부위원장 민 경 덕 (인)

위 원 송 한 호 (인)

위 원 이 동 준 (인)

위 원 이 진 욱 (인)

Acknowledgements

This project on my Ph.D thesis would not be achieved without the helps and advices of following people.

First and foremost, I would like to express my respect and gratitude to my advisor, Professor Kyoungdoug Min. During the graduate course, my knowledge and personality were grown up with his invaluable advices. He gave the inspirations of this study and his guidance and encouragement were the source of power overcoming many difficulties during the project. I would like to give special thanks to the project members who offered assistance, valuable discussions and beautiful memories of friendship. Seungha Lee, Jeongwoo Lee, Seunghyun Lee and Cheolwhan Lee. This work would never have been achieved without their efforts and patients. I also would like to thank my colleagues Wonah Park and Daebong Jung for not only their helps for research but also emotional support during this project. Additionally, I would like to thank Jaeman Park who is my ex-roommate and DIY colleague and Namho Kim who gave me endless support for research and had joyful lab life together. I would like to thank Taeyoung Lee who is greatest friend of mine for his help and wonderful friendship.

It was an honor to have the opportunity to work with Hyundai motor group and I appreciated the financial, material supports.

I would like to present my deepest respect and gratitude to my parents, Jungchan Lee and Hyosoon Shin for their great sacrifice, thoughtful consideration, unimaginable patience and endless love. I extended my thanks to Jiyong Lee my proud brother for his support. I would like to thank my beloved wife, Hayeon Kim who has been together during my whole Ph.D course with infinite faith and endless love. I also would like to thank my wife's parents who gave me confidence.

Abstract

Study on the Development and Application of Virtual NO_x Sensor for Diesel Engines

Junyong Lee
Department of Mechanical and Aerospace Engineering
The Graduate School
Seoul National University

To meet the stringent emission regulations on diesel engines, engine-out emissions have been lowered by adapting new combustion concepts such as low-temperature combustion and after-treatment systems have also been used to reduce tailpipe emissions. To optimize the control of both in-cylinder combustion and the efficiency of an after treatment system to reduce NO_x, the amount of real-time NO_x emissions should be determined.

Thus, many studies on a virtual NO_x sensor using physical and phenomenological models have been reported. Previous studies have shown reliable NO_x estimations; however, there were several limiting factors, such as complexity of the model for a real-time application, the necessity of various calibration constants, fitting processes for empirical equations and the demand for training for numerical models.

In this study, to overcome the limits of previous studies, a real-time nitric oxide estimation model was developed based on the in-cylinder pressure and on data available from the ECU. As computational fluid dynamics can describe the process of NO formation which is not directly obtainable from experiments on a physical basis, the NO formation model was developed based on both the analysis of CFD results as well as on a physical model. Furthermore, the in-cylinder pressure is used

to predict the amount of NO formation under various engine operating conditions as the pressure reflects the change in the combustion characteristics. The estimation model consisted of a simple calculation process; therefore, the model could predict the cycle-by-cycle NO in real-time. The validation results show that the model presented can predict engine-out NO well; thus, this model can be applied to engines and after-treatment systems as a useful tool to control the engine-out NO without the use of a NO_x sensor. In addition to being a virtual NO sensor, the estimation model can be applied to 1-D simulations, such as GT-SUITE and AMESIM, and demonstrate improved NO estimation results as the model is able to predict the NO level as same standard as the 3-D CFD simulation.

Then, a newly developed NO estimation model was implemented on the embedded system bypassed from a conventional engine control unit for real-time estimation of NO during steady-states and transient engine operations. The results of the model were compared to real-time measurement of engine-out NO of a conventional Diesel engine at representative steady state operating points which cover the entire NEDC region. Also, EGR rate and main injection timing were varied to verify the predictability of the model under various conditions. The results showed that the model predicts steady state results well with R^2 value of 0.96 for 76 HP-EGR cases. In addition, to verify transient estimation of NO, the engine-out NO was measured by a fast NO analyzer and compared with the results of the model during simple ramp transition conditions.

Additionally, the engine-out NO emissions measured by a fast NO_x analyzer and the estimated NO emissions were compared during ECE-15 and EUDC cycles. Furthermore, to extend the NO model to a complete NO_x estimation model, an empirical NO_2 estimation model was proposed based on the experiments under steady-state conditions. The in-house EGR estimation model was also applied in the NO_x estimation model for accurate cycle-by-cycle estimation and used as an input during transient engine operations.

This systematic research on the development of a virtual NO_x sensor contributes to real-time NO_x monitoring for transient NO_x control and after-treatment system control.

Keywords: Virtual NO_x (Nitrogen Oxides) sensor, In-cylinder pressure, Diesel engine, CFD (Computational Fluid Dynamics), NEDC (New European Driving Cycle).

Student Number: 2007-22992

Contents

List of Tables

List of Figures

Acronym

A	A constant in equation (2.16)
ABDC	after Bottom Dead Center
AFR	Air to Fuel Ratio (by mass)
ATDC	after Bottom Dead Center
BBDC	before Bottom Dead Center
BMEP	Break Mean Effective Pressure
BSFC	Break Specific Fuel Consumption
BTDC	before Top Dead Center
CAD	Crank Angle Degree
CN	Cyano Radical
CO	Carbon Monoxide
CO2	Carbon Dioxide
CFD	Computational Fluid Dynamics
DAQ	Data Acquisition
DCE	Dynamic Compensation based Estimation
DOC	Diesel Oxidation Catalyst
DPF	Diesel Particulate Filter
ECFM-3Z	Extended Coherent Flame Model in 3 zones
ECU	Engine Control Unit
EGR	Exhaust Gas Recirculation
EPA	Environmental Protection Agency
EUDC	Extended Urban Driving Cycle
EURO	European Emission Standard
EVC	Exhaust Valve Close
EVO	Exhaust Valve Open
EZM	Extended Zeldovich Mechanism
FIE	Fuel Injection Equipment

FTP-75	Federal Test Procedure
GVWR	Gross Vehicle Weight Rating
HCCI	Homogeneous Charge Compression Ignition
HCN	Hydrogen Cyanide
HLDT	Heavy Light-Duty Truck
HRR	Heat Release Rate
IMEP	Indicated Mean Effective Pressure
ISFC	Indicated Specific Fuel Consumption
IVC	Intake Valve Close
IVO	Intake Valve Open
k	Specific Heat Ratio
LDV	Light Duty Vehicle
LHV	Low Heating Value
LLDT	Light Light-Duty Truck
LNT	Lean NO_x Trap
LTC	Low Temperature Combustion
MAF	Mass Airflow Sensor
MDPV	Medium Duty Passenger Vehicle
MFB	Mass Fraction Burned
MI	Main Injection
MK	Modulated Kinetics
NADI	Narrow Angle Direct Injection
NEDC	New European Driving Cycle
NH	Monohydride
NMHC	Non-Methane Hydrocarbon
NO	Nitrogen Oxide
NO_2	Nitrogen Dioxide
NO_x	Nitrogen Oxides
NVH	Noise, Vibration and Harshness
OBD	On Board Diagnosis

OLS	Orthogonal Least Squares
PCI	Premixed Compression Ignition
PCCI	Premixed Charge Compression Ignition
PLTDC	Premixed Low Temperature Diesel Combustion
PM	Particular matter
PMP	Particulate Measurement Programme
RPM	Revolutions per Minute
RGF	Residual Gas Fraction
SFTP	Supplemental Federal Test Procedure
SOC	Start of Combustion
SCR	Selective Catalytic Reduction
TDC	Top Dead Center
TPA	Three Pressure Analysis
UEGO	Universal Exhaust Gas Oxygen Sensor
UHC	Unburned Hydrocarbon
UNIBUS	Uniform Bulky Combustion System
VCR	Variable Compression ratio

Chapter 1. Introduction

1.1 Background and Motivation

1.1.1 Nitrogen oxides formation

NO_x is a group of nitric oxide (NO) and nitrogen dioxide (NO_2). The known sources of NO_x formation are thermal NO_x, fuel NO_x, prompt NO_x, etc.

Thermal NO_x occurs when nitrogen in theair is oxidized in high temperature and the formation rate is highly dependent on temperature. The thermal NO_x formation is endothermic reaction. Thus, the formation of NO increases as the temperature increases due to heat from combustion with enough oxygen and nitrogen. The nitrogen concentration is much higher than oxygen concentration in air. Thus, the oxygen concentration is a dominant factor that determines the NO formation. The flame temperature is peak at stoichiometric condition. Therefore, the maximum NO formation occurs at slightly lean condition close to stoichiometry [1].

When the fuel containing organically bound nitrogen is oxidized during combustion, fuel NO_x can be occurred. Because the bonding strength of organic nitrogen in fuel is much weaker than that of nitrogen molecules in air, the organic nitrogen can be easily oxidized. Coal contains 0.5 ~ 2 % of nitrogen so fuel NO_x is major issue in plant [2, 3]. However, diesel or gasoline fuels that are used in conventional vehicles contain negligibly small organic nitrogen. Thus, the fuel NO_x can be ignored in this study.

Nitrogen and hydrocarbon in fuel rich flame are rapidly change into the forms of N, nitrogen monohydride (NH), cyano radical (CN)- or hydrogen cyanide (HCN) and then they are oxidized to NO_x. Nitrogen oxides from this process are called

prompt NO_x. Prompt NO_x is formed inside the flame and related to combustion process of fuel. It occurs at relatively low temperature and fuel rich conditions than at condition of thermal NO_x formation. Nevertheless, the amount of prompt NO_x is very small compared to thermal NO_x. So it can be negligible except for conditions that total amount of NO_x is very small [4].

1.1.2 The effect of nitrogen oxides on health and environment

Combustion of fossil fuels from stationary sources and in motor vehicles is the major source of anthropogenic emissions [5]. NO is rapidly changed into NO_2 by atmospheric oxidants such as ozone in ambient conditions [6]. NO_x can cause serious problems on environment and human health widely. United States environmental protection agency (EPA) is referencing that ozone can be generated over reaction of NO_x and volatile organic compounds in the presence of heat and sunlight. Thus, children, elderly and people who have lung diseases like asthma are at risk for negative effects from ozone including reduction in lung function, increased respiratory symptoms and possibly premature deaths [7]. Berglund et al. observed in animal experiments that NO_2 caused biochemical and morphological changes in lung tissue resulting in deceased pulmonary function [8]. Crutzen et al. reported that NO_x is one of very relevant components in the formation of ground level ozone [9]. Ricciardolo et al. investigated the effect of nitric oxide in disease of the respiratory system such as lung [10]. Kone et al. reported that NO may contribute to the evolution of commonly encountered renal diseases, including immune-mediated glomerulonephritis, postischemic renal failure, radiocontrast nephropathy, obstructive nephropathy and acute and chronic renal allograft rejection [11]. Pacher et al. reviewed the role of nitric oxide and peroxynitrite on cardiac diseases, vascular diseases, circulatory shock, local inflammation, cancer, stroke and other forms of reperfusion injury, neurodegenerative disorders, diabetes and diabetes complications [12].

And it also contributes to formation of acids as rain, snow or other forms. They can spread by the wind to far distances and they can cause deterioration of not only buildings and cars but also water and soil quality. The only small change of PH of water can decimate fish in lakes and streams. The increase of nitrogen causes eutrophication which results in oxygen depletion that reduces underwater creatures. Additionally, toxic chemicals can be formed from reaction of NO_x with other substances and nitrogen dioxide cause the reduction of visibility in urban areas [7, 13].

1.1.3 Nitrogen oxides emission from diesel engines

Among the source of NO_x formation, thermal NO_x is predominant product in internal combustion engines and the main source of it is oxygen and nitrogen from air. In diesel engines, most NO forms in the high-temperature burned gas region and its formation rate is highest near the stoichiometric regions. Therefore, NO formation process is strongly dependent on the fuel distribution and fuel-air mixing, but the fuel-air distributions are not uniform in the burned gas region [14].

NO_x emission from diesel engines is more important than that from gasoline engines although the level of engine-out NO_x emission is much higher in gasoline engines in conventional operating regions because of their own combustion characteristics. In general, gasoline engines are operating based on premixed combustion at or close to stoichiometric condition. This leads the maximum performance of three-way catalyst as described in Figure 1.1. Therefore, very low level of tailpipe NO_x emission can be accomplished after catalyst in gasoline engines.

On the other hand, the combustion in the diesel engine is based on diffusion flame. Although the combustion occurs locally at close to stoichiometric condition following the flame, the overall air/fuel ratio (AF) in cylinder is much higher compared to that of gasoline engine. The efficiency of NO_x conversion is very high

close to stoichiometric condition and rapidly decreases at lean region. Because NO_x conversion efficiency of three-way catalyst when used in diesel engine is very low because of lean combustion, only diesel oxidation catalyst (DOC) is generally used in diesel engines and high level of NO_x emission can come out without filtering [15-18].

1.1.4 Emission regulations for NO_x from diesel engines

Recently, global environmental issues, such as global warming and depletion of natural resources, have been major issues. As a result, authorities around the world have imposed stringent emission regulations on the automotive industries. In Europe, phased emission regulation program named Euro is on progress and this regulation is widely used in many countries as a global standard for diesel engines. Table 1.1 shows European emission standards for passenger cars and figure 1.3 shows the diagram of the emission standards and necessary technologies to overcome the emission limits. In case of Euro 5 which was enforced in 2009, 30 % of NO_x and 80 % of particular matter (PM) should be reduced compared to Euro 4 which was enforced in 2005. Therefore, manufacturers have been tried to overcome the standards in many ways. To reduce NO_x emission, heavy exhaust gas recirculation (EGR) was applied to lower the combustion temperature and diesel particulate filter (DPF) has been used to reduce PM drastically. However, to clear Euro 6, NO_x emission should be reduced over half of Euro 5 standard. The reduction of engine-out NO_x emission by improvement of conventional combustion has limit because of the stability of combustion. Therefore, in short term, it seems not to be able to avoid adapting lean NO_x trap (LNT) or selective catalytic reduction (SCR) to clear Euro 6. Moreover, phase 2 of Euro 6 will be enforced in 2017. It will be adapting the concept of real driving emission and the emission test cycle will be extended into more wide operating region containing higher load conditions and will be experiencing more acceleration and deceleration. Nevertheless, the level of the emissions should be kept [19-21].

Emissions of vehicles are tested over the new European driving cycle (NEDC) test cycle which is combination of ECE-15 and extended urban driving cycle (EUDC) by a chassis dynamometer procedure. The test procedure for Euro 3 was modified to exclude engine warm-up period of 40 s before the beginning of emission test. The units of all emissions are calculated in g/km. The Euro 5 and Euro 6 regulations suggested a new method of PM mass emission measurement (similar to the US 2007 procedure) developed by the UN/ECE Particulate Measurement Programme (PMP) and modifies the limit of PM mass emission to account for differences in results comparing the old and the new method. The Euro 5 and Euro 6 also introduced the limit of a particle number (PN) emission in addition to the mass-based limits [22].

In United States, EPA regulates the vehicle emissions based on the clean air act amended in 1990. For cars and light trucks, tier 1 standards were published in 1991 and phased in between 1994 and 1997. All new light-duty vehicles (LDV) applied tier 1 standards including passenger cars, light light-duty trucks (LLDT) below 6000 lbs gross vehicle weight rating (GVWR) and heavy light-duty trucks (HLDT) above 6000 lbs GVWR. The emissions of LDVs were measured using the federal test procedure (FTP 75) and the units of emissions were expressed in g/mile. The NO_x emission was limited to 1 g/mile for vehicles of 50,000 miles/ 5 years and 0.97 to 1.53 g/mile for vehicles of 100,000 miles/ 10 years. This level was slightly higher than Euro 1 standards considering the sum of NO_x and HC emissions. Additionally, supplemental federal test procedure was phased in between 2000 and 2004. Aggressive highway driving (US 06) cycle and urban driving emission cycle with the operation of vehicle's air conditioning system (SC 03) were included in supplemental federal test procedure (SFTP). The weighted standards were used for non-methane hydrocarbon (NMHC) and NO_x while carbon monoxide (CO) was measured alone. Tier 2 regulation was phased in between 2004 and 2009. Tier 2 covers heavier vehicle categories including medium-duty passenger vehicles (MDPV) which have 8,500 to 10,000 lbs GVWR. In Tier 2, the emission standards

are the same regardless of type of fuel. Vehicles which are using gasoline, diesel and or even alternative fuels should satisfy the same limits. It means larger vehicles with large engines should apply more advanced technology to meet the standards. Tier 2 standards consist of 8 permanent and 3 temporary certification levels of different stringency. The emission standards for each certification bins over FTP are shown in Table 1.2. The NO_x emission should be reduced by 20 times in Tier 2 bin 5 compared to Tier 1 standards and the level of Tier 2 bin 5 is similar to Euro 6 standard. Tier 2 also regulates emission limits over SFTP which includes US 06 and SC 03 driving cycles except for MDPVs [23]. Car manufacturers should clear the standards to sell their vehicles to each country or area. Therefore, the emission standards have been a big challenge and a driving force for research and development of new eco-friendly technologies.

1.1.5 NO_x reduction technologies and challenges in diesel engines

Although diesel engines have higher thermal efficiency because of their high compression ratio and lean operation characteristics, engine-out emissions performance have been weakness compared to gasoline engine especially for NO_x and PM. As mentioned in 1.1.1, the formation of thermal NO_x is very sensitive to burned gas temperature and the oxygen concentration. Figure 1.2 shows the region of NO_x and soot formation with respect to local temperature and local equivalence ratio. Thermal NO is formed over 2200 K at close to stoichiometric condition. Thus, to reduce the engine-out NO_x emission, the burned gas temperature has to be lowered by decrease of oxygen concentration or initial temperature. The EGR has been main idea to reduce the NO_x emission. The effects of the EGR can be divided into three parts. First one is dilution effect. As EGR gas occupies part of fresh air, the oxygen concentration is lowered and it results in decrease of flame temperature [24, 25]. In other way, the heat capacity of EGR gas is higher than fresh air because carbon dioxide (CO_2) and water is contained in EGR. The high heat capacity results

in decrease of the in-cylinder temperature. This is called thermal effect of EGR [26]. Another effect of EGR is chemical effect. Because the dissociation of water from EGR is highly endothermic reaction which occurs at high temperature, the peak cylinder temperature can be reduced [27]. The dilution effect is known as the most significant one among all effects in diesel engines [28].

Therefore, the EGR has been most useful method to reduce engine-out NO_x emission and many researches have been done. Ladommatos et al. investigated the effects of EGR on the formation and emission of NO_x to obtain understanding which would lead to more effective use of EGR to reduce NO_x. They found that cooling of the EGR increased the effectiveness of EGR in suppressing NO_x [29]. Because of the delay of air control during transient state which is longer than other operation variables, such as injection strategies, unexpected engine-out emissions can be occurred. Muller et al. developed a dynamic EGR state estimator for production engine control.

On the other hand, when the fuel injection is maintaining after the ignition of fuel, the liquid fuel is rapidly vaporized in flame region. Then, there can be a fuel rich region about equivalence ratio of 4~5 and it is not avoidable in conventional diesel combustion. However, generated soot can be oxidized if the burned gas temperature and oxygen concentration is enough.

In summary, if the oxygen concentration or initial temperature is lowered to decrease flame temperature by applying EGR or some other methods to reduce NO_x emission, it will be better environment for PM to be formed and not to be oxidized. NO_x and PM have trade-off relationship in conventional diesel combustion region. Thus, to overcome the trade-off relationship, many researches on simultaneous reduction of NO_x and PM have been conducted.

As technologies about fuel injection equipment (FIE) have been developed, the degree of freedom of injection strategy has increased. Modern fuel injection system,

such as solenoid or piezo injector with common rail, allows the fast response for the change of injection pressure, injection timing, injection quantity and number of injections. Multiple injection strategy contributes to improve noise, vibration and harshness (NVH) and PM emission characteristics of diesel engines. Pierpont et al. investigated the effects of combined use of EGR and multiple injections on simultaneous reduction of PM and NO_x emissions. The results showed that the multiple injection strategies with EGR were effective to reduce emissions but there had been a significant sacrifice in BSFC [30]. Chan et al. confirmed the effect of EGR and multiple injections using 3-D CFD tool. They reported that EGR could reduce NO_x emission by lowering in-cylinder temperature and multiple injections could reduce PM emission by improving fuel-air mixing and leans out the in-cylinder mixture [31]. Park et al. investigated the effect of pilot and post injection strategy on emissions and engine performance. The study was conducted on single cylinder optical diesel engine. They found that pilot injection contributed to control the premixed combustion and post injection helped completion of oxidation process resulting in reduction of PM. They also concluded that the multiple injection strategy with low pressure injection could achieve simultaneous reduction of NO_x and PM emissions [32].

Figure 1.2 also describes the several available combustion modes such as HCCI, PCCI and LTC. In general, the common idea for reducing NO_x emissions that is reducing flame temperature is similar. However, the detailed concepts are slightly different. Kimura et al. introduced new combustion concept called modulated kinetics (MK) which aims low-temperature, premixed combustion system for simultaneous reduction of NO_x and PM emissions. In their MK combustion concept, high EGR was applied and it results in decrease of oxygen concentration and then, NO_x emission can be reduced because of decrease of combustion temperature. In the contrary, smoke increases due to decrease of oxygen concentration. To resolve the trade-off relationship, they increased premixed combustion ratio by retarding injection timing to prolong the ignition delay. Meanwhile, fuel consumption

deterioration and unburned hydrocarbon (UHC) deterioration can be occurred due to increase of premixed combustion ratio. Combustion system optimization, such as gas flow and piston cavity configuration was applied to settle the problems [33]. Then, they tried to expand the operation range of MK combustion with the combination of a low compression ratio, high injection pressure and EGR gas cooling. Low compression ratio and EGR gas cooling prolonged ignition delay and high injection pressure and larger nozzle hole size reduced the injection duration. Thus, the ignition delay could be longer than injection duration as they wanted. Also, they optimized the bowl shape with the large cavity to avoid the increase of HC emission because of low compression ratio especially in cold conditions [34]. Hasegawa et al. introduced uniform bulky combustion system (UNIBUS) which was based on double injection technique with common rail injection system. They found difficulties in combustion and emission control of homogeneous charge compression ignition (HCCI) using single injection at early injection timing. Thus, they implemented the strategy that the first fuel is injected at very early injection timing as much as possible which generates low temperature reaction and then, the second fuel is injected during low temperature reaction as a controller of high temperature reaction. Substantial reduction of NO_x and PM could be found from this strategy [35].

Meanwhile, there have been approaches to consider the reduction of HC and CO emission from wall impingement at early injection by changing injector trajectory and bowl geometry. Walter et al. introduced new dual mode HCCI combustion concept called narrow angle direct injection (NADI). For the part load they optimized injection angle and piston bowl design to prevent wall impingement of fuel at early injection for HCCI combustion. At full load, the combustion mode was switched to conventional diesel combustion to overcome the weakness of HCCI combustion, such as limited operation range and combustion control at high load [36]. On the other hands, to prevent HC and CO emissions from wall impingement of fuel due to early injection for HCCI combustion, Kanda et al. considered a new

approach instead of changing the geometry of injector and combustion chamber. They proposed a premixed charge compression ignition (PCCI) with single injection at close to top dead center (TDC). As a result, wall impingement was reduced but small amount of NO_x increased. They applied high efficiency cooled EGR and modified re-entrant combustion chamber to solve the problems [37]. Jacobs et al. investigated lean and rich premixed compression ignition (PCI) combustion strategies. They found that lean PCI combustion could operate with low NO_x and PM emissions with 5 % increase of fuel consumption and rich PCI combustion could also operate with low NO_x and PM emissions with increase of CO which was needed for aggressive regeneration of lean NO_x trap (LNT) [38]. Lee et al. identified the effects of spray targeting on CO and PM emissions. They examined several nozzles which had different spray angles and the experiments were conducted on PCCI combustion region with high level of EGR and low compression ratio. They found that the optimum targeting spots could be configured and CO and PM emission were reduced without deterioration of NO_x emission when the spray was targeted at the edge of the piston bowl. It was believed that targeting that spot enhanced mixing of fuel and air [39].

Alriksson et al. investigated the possibilities of extending operation range of low temperature combustion (LTC) up to 50 % of engine loads. They applied very high EGR (~65 %) and relatively low compression ratio (14) to a single cylinder research engine. The results showed that the LTC could be accomplished to 50 % of engine loads with zero NO_x and PM while the deterioration of fuel consumption, HC and CO emission were remained as addressable problems [40]. Colban et al. examined the effects of boost pressure on engine performances and engine-out emissions using a single cylinder diesel engine. The systematic study was conducted on two different LTC regimes, early injection strategy with heavy EGR and late injection strategy with moderate EGR rate. Increased boost pressure reduced NO_x and soot emissions and improved combustion efficiency. The more benefits of boost pressure were shown in dilution-controlled LTD regime [41]. Yun et al. introduced

the new combustion concepts called premixed low temperature diesel combustion (PLTDC). They achieved low NO_x and PM emissions without deterioration of fuel efficiency on operating conditions of 1500 rpm and 3/6 IMEP with different injection strategies that were single injection strategy for 3 bar IMEP and triple injection strategy for 6 bar IMEP. They also concluded that engine-out PM emissions could be sacrificed to achieve zero NO_x or better fuel efficiency for a DPF equipped vehicles [42]. Sarangi et al. investigated the effects of intake pressure and EGR rate on emissions and performance at conventional and LTC regimes using single cylinder diesel engine. They also conducted variation of injection timing and injection pressure. Increased intake pressure improved isfc and reduced the HC emissions. Low PM and HC emission could be obtained by higher injection pressure. They also concluded that LTC could be characterized by locally rich fuel-oxygen charge [43]. Furthermore, the characteristics of LTC and PCCI have been investigated using optical diagnostics on specially designed optical research engines or constant volume vessels [44-50].

Additionally, there have been approaches to reduce peak temperature by reducing compression ratio or using variable compression ratio (VCR) equipment. Hountalas et al. examined the potential benefits in exhaust emissions to investigate the necessity of applying variable compression ratio technology on heavy-duty diesel engines. They concluded that the benefit of VCR technology was questionable compared to the complexity of the engine configuration and the control [51].

Moreover, there have been approaches using characteristics of alternative fuels, such as biodiesel and dimethyl ether, to reduce NO_x and PM simultaneously. Yoshimoto et al. investigated the use of a stable emulsified fuel composed of vegetable oils discarded from restaurants on engine performance. They performed tests on a single cylinder diesel engine and they found the “biodiesel” fuel could reduce NO_x and PM emissions without worsening break specific fuel consumption (BSFC) [52]. They also conducted tests using water emulsified biodiesel fuel consist

of 30 % volume fraction of water. The results showed that the combined use of biodiesel fuel and 21 % of EGR could reduce NO_x without increase of PM [53].

Also, there have been studies to take advantages of use of different fuels by using them simultaneously. Nazar et al. investigated the effect of substituting renewable alternative fuels such as karanja oil (KO) and biodiesel of karanja oil (BDK) for conventional diesel as pilot fuels in a LPG inducted dual fuel engine. A diesel engine was operated with karanja oil, bio-diesel obtained from karanja oil (BDK) and diesel as pilot fuels while LPG was used as primary fuel. LPG supply was varied from zero to the maximum value that the engine could tolerate. The engine output was kept at different constant levels of 25%, 50%, 75%, and 100% of full load. The thermal efficiency improved at high loads. Smoke level was reduced drastically at all loads. CO and HC levels were reduced at full load. There was a slight increase in the NO level. Combustion parameters indicated an increase in the ignition delay. Peak pressure and rate of pressure rise were not unfavorably affected. There was an increase in the peak heat release rate with LPG induction. The amount of LPG that could be tolerated without knock at full load was 49%, 53% and 61% on energy basis with karanja oil, BDK and diesel as pilots. On the whole it is concluded that LPG can be inducted along with air in order to reduce smoke levels and improve thermal efficiency of vegetable oil and bio-diesel fuelled diesel engines [54]. Curran et al. investigated in-cylinder fuel blending of gasoline with diesel fuel on a multi-cylinder light-duty diesel engine as a strategy to control in-cylinder fuel reactivity for improved efficiency and lowest possible emissions. Gasoline was introduced with a port-fuel-injection system. Parameter sweeps included gasoline-to-diesel fuel ratio, intake charge mixture temperature, in-cylinder swirl level, and diesel start-of-injection timing. In addition, engine parameters were trimmed for each cylinder to balance the combustion process for maximum efficiency and lowest emissions. An important observation was the strong influence of intake charge temperature on cylinder pressure rise rate. Experiments were able to show increased thermal efficiency along with greater than 90% decreases in NO_x and PM [55].

Kokjohn et al. characterized dual-fuel PCCI operation and investigated dual-fuel PCCI combustion strategy in the light-duty engine using a multi-dimensional CFD code, the KIVA-CHEMKIN code, and a multi-zone modeling. Sweeps of injection timing and premixed gasoline percentage were evaluated and an operating regime map to achieve high efficiency – low NO_x –low noise combustion was generated. It was found that highly-efficient dual-fuel operation with moderate rates of pressure rise (5 to 8 bar/deg) and near zero soot and NO_x could be achieved by using a single, early cycle direct-injection. Additionally, it was found that, by introducing a gradient in fuel reactivity, the combustion duration could be extended to reduce the rate of pressure rise. Using this method, premixed operation was achieved with low rates of pressure rise without using EGR. Furthermore, it was found out that the extended combustion duration was primarily due to the gradient in fuel reactivity [56].

Furthermore, there have been efforts to reduce NO_x emissions by real-time combustion control. Chen et al. investigated the alternative EGR control strategy of using universal exhaust gas lambda (UEGO) sensor in spite of using intake mass airflow (MAF) sensor as a feedback [57]. They reported that engine-out NO_x emission during transient operation was significantly reduced by using the control method. Catania et al. developed predictive zero-dimensional combustion model for model based diesel engine feed-forward control. The model was applied to conventional and premixed charge compression ignition (PCCI) diesel engines and showed promising results in a low computational time [58].

Meanwhile, in spite of advance in reduction technologies of engine-out NO_x, the level of reduction has been insufficient to clear the emission standards. Therefore, there have been lots of researches about reducing NO_x emission using additional after-treatment systems resulting in reduction of tail-pipe NO_x. Representative after-treatment systems for reducing NO_x are lean NO_x trap (LNT) and selective catalytic reaction (SCR).Touns et al. proposed a NO_x trap catalyst model which describes trapping phases. NO_x trap catalysts are known to work within two phases: One is trapping NO_x when an engine runs at “lean” condition and the other is regeneration

(NO_x reduction) when an engine operates at "rich" condition. The model includes gas temperature and composition variations, and it can be easily connected to global engine simulations to design optimized regeneration strategies. Furthermore, the model is able to deal with slow and fast reaction dynamics occurring in the NO_x trap using only one simple first order differential equation [59]. Nieuwstadt et al. proposed a lean NO_x trap model which is not a representation of any lean NO_x trap in particular but rather exhibits all generic features that a control strategy needs to check for and how these features change over the entire operating envelope of the lean NO_x trap. The model was developed considering five features: 1. NO_x storage dyanmics (NO_x storage and release), 2. Oxygen storage dynamics (Oxygen storage and release), 3. Temperature dyanmics (Heat generation by oxidation of reductant), 4. Sulfur poisoning & 5. Sulfur release (Desulfation of the trap) [60]. Parks et al. studied N_2 selectivity of lean NO_x trap regeneration with in-cylinder technique. Engine and bench experiments were performed, and the results showed that excess reductant delivery during regeneration leads to high NH_3 emissions and poor N_2 selectivity. Specific design of in-cylinder regeneration technique that minimizes excess reductant or allow O_2 purge can optimize N_2 selectivity of the lean NO_x trap catalyst [61]. He developed a model for a lean NO_x trap (LNT) used in diesel application. The LNT model was utilized to evaluate the effect of inlet CO concentration, inlet H_2 concentration, inlet gas temperature and trap size on NO_x conversion performance of the LNT. The model could predict the cumulative NO_x emissions at the trap outlet over the FTP cycle and gave a quantitative estimation of each option. The inlet gas temperature was found to have a significant impact on NO_x trap performance (NO_x conversion efficiency of the LNT) [62].

For more reduction of NOx emissions, the use of SCR is necessary. Willand et al. examined the potential of an SNCR (selective non catalytic reduction) process for NOx reduction as an alternative to catalytic exhaust treatment systems. Aqueous urea was used as the reducing species. By injecting aqueous urea directly into the combustion chamber a maximum NOx reduction of 65% could be achieved at full

load and increased exhaust gas temperature. The main results of injection into the exhaust area were: below a reaction temperature of 600°C in the exhaust area, no NOx reduction through the SNCR process occurs. Above 700°C a NOx conversion rate of about 20 % is attained when injecting urea in stoichiometric ratio. Through adding glycerine or hydrogen peroxide as suppliers of OH radicals it was possible to reduce the lower temperature limit down to 600°C and to increase the NOx conversion rate up to 40 % [63]. Koebel et al. discusses the fundamental problems and challenges for urea-SCR when it is extended to mobile applications. They referred that reduction of catalyst volume with maintain high selectivity over a wide temperature range is important and control strategy for urea dosing, the high freezing point of urea and long-term stability of catalyst would be problems to overcome [64]. Song et al. introduced closed-loop control architecture which combines model-based feed forward control to improve transient response of urea-SCR system. Their control strategy also improved steady-state response [65]. Thomas Hammer et al. investigated mechanisms of plasma enhanced selective catalytic reduction of NO_x on a V_2O_5-WO_3/TiO_2-catalyst for temperatures between 100 °C and 200 °C by applying various analytical methods. It was found out that the removal of NO and NO_2 at the indicated temperature is mainly caused by catalytic reduction, not by adsorption or NH_4NO_3(s)-formation. Plasma induced conversion of NO to NO_2 increased NO_x-reduction rates but NH_3 did not; hence, the PE-SCR process has the potential for NO_x-reduction in diesel exhaust at low temperature [66]. They also investigated potential of plasma enhanced selective catalytic reduction (PE-SCR) for diesel-exhaust treatment at temperatures between 60 °C and 180 °C (temperature range relevant for ECE-15 test cycle). Monolithic V_2O_5-WO_3/TiO_2-catalysts with cell densities of 150 cpsi and 200 cpsi were used for selective catalytic reduction. It was found out that 60 % NO_x reduction were obtained at the cold start and energy costs for plasma induced NO_x reduction could be reduced by reactor scaling. In a test cycle, the PE-SCR method showed good response to engine load changes. In conclusion, the PE-SCR method using ammonia-based reducing agents has good potential for NO_x reduction in ECE-15 test cycle [67]. Müller et al.

introduced an initial version of selective catalytic reduction (SCR) to fulfill EURO-4 emission limits. Low sulfur fuel was used for particulate emission control and urea was used a reducing agent for this SCR technique. NO_x reduction efficiency of an engine map controlled open-loop SCR system is about 65 %. The efficiency can be improved significantly by using closed-loop control and a highly efficient oxidation catalyst. The most important disadvantage of all alternatives to SCR other than cost was the increase of CO_2 emission [68]. Steven J. Schmieg et al. investigated the effect of various reactor operating conditions on NO_x reduction performance of three different catalyst formulations which are Cu-zeolite, Fe-zeolite & Vanadium-based to obtain useful guidance in the design and operation of urea-SCR lean NO_x emission control systems. The effects of NO:NO_2 ratio on the steady-state NO_x reduction activity at typical diesel engine exhaust temperatures (150~550℃) are examined. Transient measurements were also performed to determine the impact of NH_3:NO_x ratio and NH_3 storage on catalyst performance. The impacts of hydrocarbon poisoning and sulfur poisoning/regeneration were also examined [69]. Hosoya et al. studied the effects of urea selective catalytic reduction (SCR) systems as a technique to reduce NO_x emissions from heavy-duty diesel engines. Proto type urea SCR system was composed of NO oxidation catalyst, SCR catalyst and ammonia (NH_3) reduction catalyst. The NO_x reduction performance of urea SCR system was improved by a new zeolite type catalyst and mixer for urea distribution at steady state operating conditions. NO_x reduction performance of the urea SCR system was evaluated over JE05 mode of Japan. The NO_x reduction efficiency of the urea SCR catalyst system was 72% at JE05 mode. In addition, with improved oxidation activity of urea SCR catalyst, the NO_x reduction performance is improved in low temperature condition. Several kinds of un-regulated matters were detected including NH_3 and N_2O leak from the exhaust gas. It is necessary to have further study for detailed measurements for un-regulated emissions from urea solution [70]. Cho et al. focused to evaluate the performance of urea-SCR system in a heavy-duty diesel engine and the research was preceded in four steps. First, optimal urea

injection conditions for system were developed. Second, optimal geometric conditions for a urea injection system were investigated by a numerical simulation technique. The simulation results contribute to determine the layout of engine test. Before performing engine test, SCR reactor was used to observe basic performance on SCR. This observation was made on effective NO_x reduction according to gas temperatures, SVs (space velocity) and ARs (aspect ratio). Finally, the engine test was carried out based on experimental results. The urea injector was located at the opposite direction of exhaust gases emitted to an exhaust pipe, and an optimal quantity of a urea was estimated using accurate programming technique under several engine loads and speeds. Furthermore, NO_x emission and applied amounts of urea were investigated with respect to driving modes under the condition of with/without SCR [71]. Kushal Narayanaswamy et al. investigated and modeled different supplier SCR catalysts. A global ammonia SCR mechanism was used and kinetic parameters for selective catalytic reduction of NOx by ammonia were developed for both copper (Cu) – zeolite and iron (Fe) – zeolite SCR catalysts. The kinetic analysis was performed using a commercial 1-D after-treatment code coupled with an optimizer. The optimized kinetics have been validated extensively with laboratory reactor data for various operating conditions on three supplier catalysts – two copper and one iron based formulations. Both steady and transient tests are performed and the developed SCR models are shown to agree with the experimental measurements reasonably well [72]. Schmieg et al. investigated the effects of NO_x (as NO or NO2), hydrocarbon concentration level (HC:NOx ratio), oxygen concentration, NO concentration, catalyst space velocity, catalyst temperature and the co-presence of hydrogen on steady-state NOx reduction activity. Using these results, a control strategy was developed to maximize NOx conversion over the wide-ranging exhaust conditions likely to be encountered in light-duty diesel applications [73].

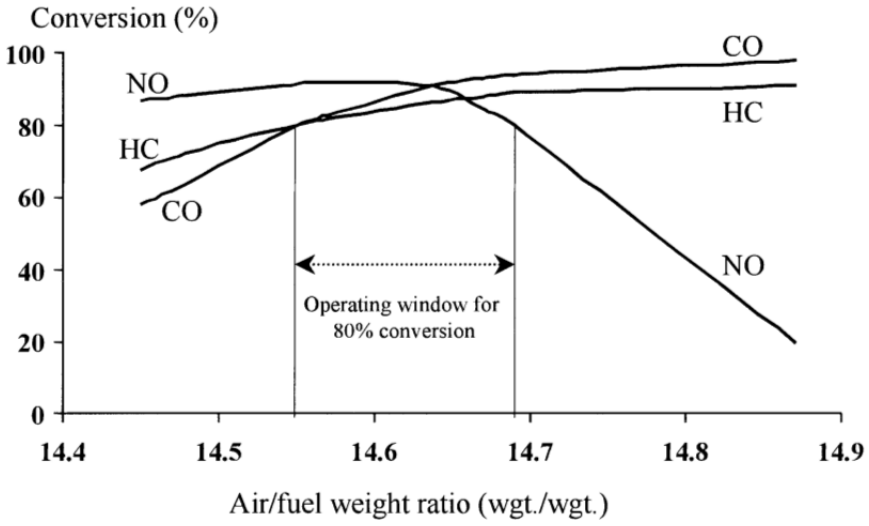

Figure 1.1 Three way catalyst performance determined by engine air to fuel ratio [17].

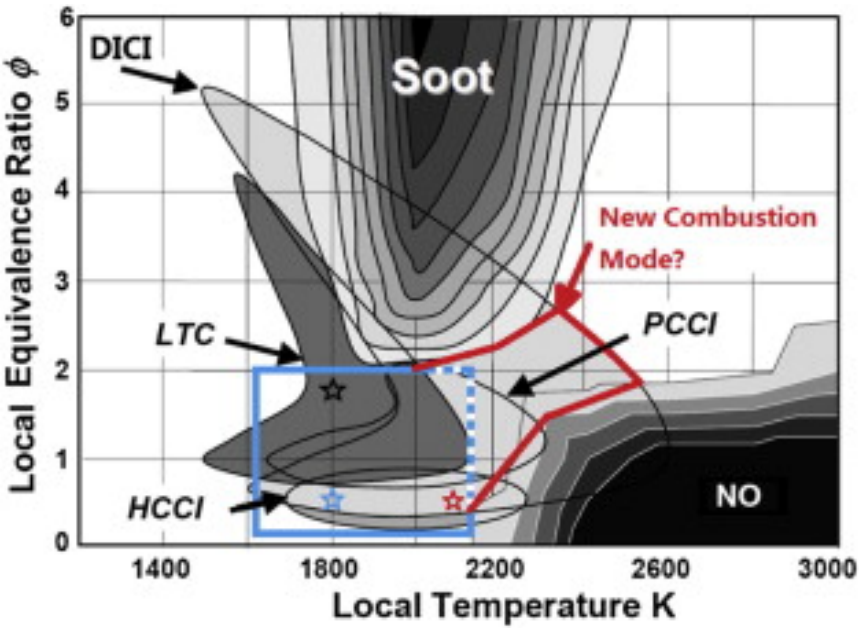

Figure 1.2 Emission formation region and the combustion strategies for emission reduction of diesel engines [74].

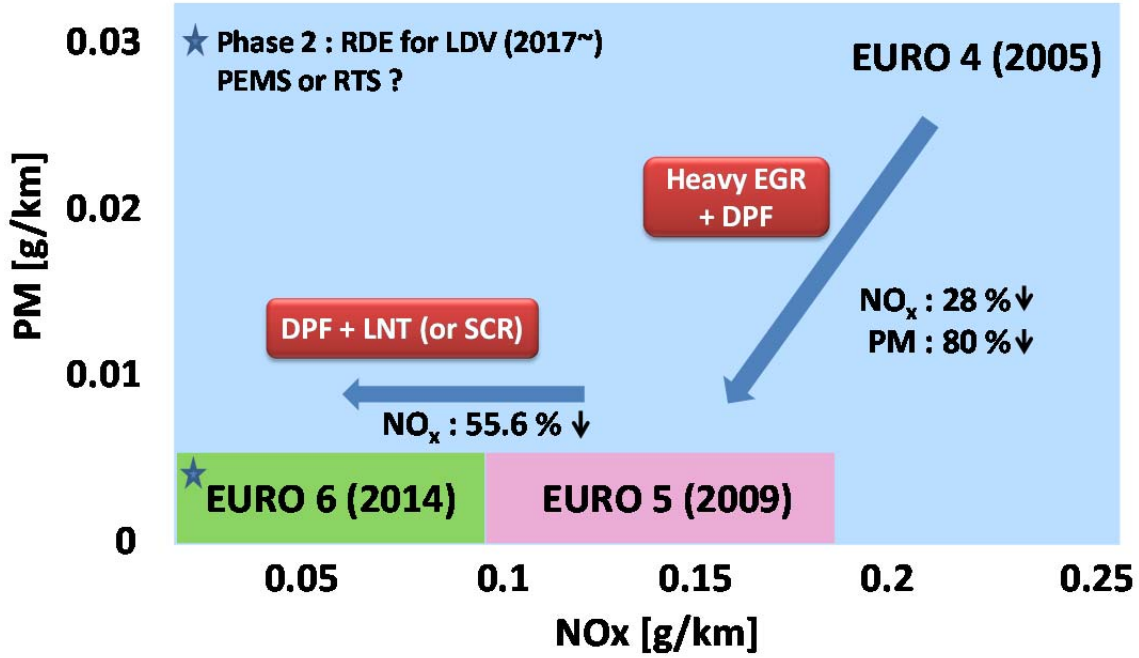

Figure 1.3 Forecast of the future market sales of vehicles.

Table 1.1 European emission standards for passenger cars, [g/km] [22].

Tier	Year	CO	THC	NMHC	NOx	HC+NOx	PM
Euro 1	1992	2.72 (3.16)	-	-	-	0.97 (1.13)	0.14 (0.18)
Euro 2	1996	1	-	-	-	0.7	0.08
Euro 3	2000	0.64	-	-	0.5	0.56	0.05
Euro 4	2005	0.5	-	-	0.25	0.3	0.025
Euro 5	2009	0.5	-	-	0.18	0.23	0.005
Euro 6	2014	0.5	-	-	0.08	0.17	0.005

Table 1.2 Tier 2 emission standards, FTP 75 [g/mi] [23].

Bin#	Intermediate life (5 years / 50,000 miles)				
	NMOG	CO	NOx	PM	HCHO
Temporary bins					
10	0.125 (0.16)	3.4 (4.4)	0.4	-	0.015 (0.018)
9	0.075 (0.14)	3.4	0.2	-	0.015
Permanent bins					
8	0.1 (0.125)	3.4	0.14	-	0.015
7	0.075	3.4	0.11	-	0.015
6	0.075	3.4	0.08	-	0.015
5	0.075	3.4	0.05	-	0.015

1.2 Literature Review on virtual NO_x sensors

Although there have been numerous researches to reduce NO_x and PM emissions simultaneously, the operation range for new combustion concepts was limited. Also, the poor transient emission characteristics have been difficult to be overcome because of the air system and combustion characteristics of diesel engines. Therefore, it has been not avoidable to use after-treatment systems to satisfy the enforced emission standards. These situations have leads to develop not only real-time combustion control, but also efficient after-treatment system control. The real-time emission and combustion control need real-time emission value and target value. After-treatment system, such as LNT and SCR, also need to obtain information how much NOx is generated and trapped to control operating conditions.

In spite of necessity for real-time monitoring of NO_x emission, the cost of portable NO_x sensors is not affordable for mass production vehicles. Therefore, there have been many researches on a virtual NO_x sensor in many ways. Computational fluid dynamics (CFD) can describe the process of the in-cylinder fuel-air mixing and the combustion which is not directly visible from experiment on a physical basis. However, CFD is not suitable for real-time application because of high computational time. Thus, semi-empirical models based on the physical model have been used for the real-time application because of their low computational cost and relatively good accuracy.

Semi-empirical models with in-cylinder pressure measurement

Timoney et al. developed a simplified semi-empirical NO_x formation model based on the in-cylinder pressure data and the model was verified in three engines [75]. Their model calculated the adiabatic temperature using the in-cylinder pressure to consider flame front of diffusion flame but the consideration of reactions in the post flame were excluded. The model implemented activation energy of $E_a = 46{,}851$

J/mol for Zeldovich mechanism and 6 empirical constants to relate the estimation value to real measurement. Andersson et al. introduced a fast NO_x model which required a cylinder pressure trace as input data [76]. Based on heat release analysis (HRR), they calculated equilibrium temperature and concentration of combustion products. The results showed reasonable match over 100 ppm of NO_x region. However, in the low NO_x region, the model accuracy was poor. They supposed that the mismatch according to operation range come from the limit of Zeldovich mechanism and they used simple mathematical relation to deal the problem. Arrègle et al. proposed a NO_x formation model based on HRR analysis and demonstrated the sensitivity study of the model [77, 78]. They used three constants to correlate the equation with experimental data. It was found that the small error in the in-cylinder pressure had no remarkable effects on the NO_x estimation itself. Additionally, they found that the error of the temperature of the air/EGR mixture and the admitted fresh air mass had large sensitivity on estimation of NO_x. Hountalas et al. suggested a simplified multi-zone semi-empirical model that considered the temperature distribution of in-cylinder [79]. The model solved the simple chemical mechanism and NO was calculated using the extended Zeldovich mechanism. Guardiola et al. presented a control oriented raw NO_x emission model [80]. The model used in-cylinder pressure data and other operating conditions from ECU. From the in-cylinder pressure analysis, the flame temperature was calculated to estimate the thermal NO_x. The model was trained and validated at various EGR, boost pressure and intake temperature conditions and showed good agreement with experimental results and showed fast calculation time enough to use for real-time application. Lianglin et al. proposed dynamic compensation based estimation (DCE) method to estimate transient NO_x emissions more precisely for SCR dosing control [81]. They used physical based model called crank angle based emission model for steady state estimation and added DCD method to fill the gap of estimated and measured emissions in the ETC driving cycle.

Semi-empirical models w/o in-cylinder pressure measurement

On the other hand, the in-cylinder pressure sensors are not generally used in conventional diesel engines because of the high price. Thus, to increase the applicability of the virtual NO_x sensor, the necessity of the development of NO_x estimation model without in-cylinder pressure measurement have been focused although the accuracy of the model could be lower than the model with the in-cylinder pressure sensor. Andersson et al. modified their predictive fast NOx model such that it is combined with combustion model which consists of fuel injection, ignition delay, and heat release from premixed and diffusion combustion [82]. The developed model was applicable for not only conventional high temperature diesel combustion but also low temperature combustion with high EGR rate. However, the study was limited to single injection operation. Seykens et al. and Willems et al. presented a real-time NO and PM estimation model and an in-cylinder pressure-based control using the estimation model [83, 84]. The NO formation was computed according to the extended Zeldovich mechanism and the N_2O-intermediate route was added to consider low-temperature combustion. Hegarty et al. presented a semi-empirical model for dynamic NO modeling with simple combustion model including Wiebe function and wall temperature model [85]. The developed model was calibrated in steady state results. The model predicted thermal NO from the simplified Zeldovich mechanism and the coefficient, which is a function mapped against the engine speed and torque. Finesso et al. developed a fast predictive model for NOx estimation based on low-throughput combustion model. The combustion model simulates the heat release and pressure trace then NOx could be calculated through thermodynamic submodel and NOx calculation

Numerical models with in-cylinder pressure data

Meanwhile, there have been different approaches using numerical and statistical methods to estimate the NO_x emissions. These strategies contain less physical analysis but the non-linear relations between factors could be derived by training the model with experimental data. It means more training could make the

model more accurate in the boundary of training region. Also, the calculation time could be shorter than semi-empirical approaches once the model training is finished which let the model could be implemented in a real-time application easily. Although numerical models consider less physical relations between input and output, the selection of input data is important. Because the in-cylinder pressure contains many part of combustion, the use of in-cylinder pressure data has been preferred as input data. Traver et al. investigated the neural network based emission estimation using in-cylinder pressure data [86, 87]. They reported that the in-cylinder pressure data could give more combustion information which is directly related with emission formation to the network. The model was trained at steady state conditions and validated on FTP cycle using digital signal processor (DSP) in real-time. They also suggested advanced training method to defeat the analyzer response problem. Wang et al. improved the neural network model for the virtual NO_x sensor [88]. This model tried to use more several key physical models, such as EGR, AFR, burned gas temperature from calculation, CA50, RPM and coolant temperatures, as inputs to a neural network model than other numerical models to enhance the estimation performance. The trained neural network model was used to predict the amount of NO_x.

Numerical models w/o in-cylinder pressure data

In the same manner with semi-empirical models, the absence of in-cylinder pressure is large benefit in cost reduction. Johri et al. developed real-time NO_x and soot virtual sensors using neuro-fuzzy model tree and orthogonal least squares (OLS) for engine diagnostics and controls [89]. The neuro-fuzzy model approach is based on a drive-and-conquer strategy which the operating space is divided into subspaces to divide the complex problem into simpler problems. Additionally, recurrent architecture allowed for estimating transient emission characteristics. The model was trained using a medium duty diesel engine and showed good agreement in NO_x estimation from comparison with the fast NO_x analyzer. Wang et al. developed

neural network model without in-cylinder pressure sensor [88]. To achieve that, in spite of excluding CA50 and burned gas temperature, fuel flow rate, SOI and intake manifold temperature were included. The accuracy of estimation was slightly lower than that with in-cylinder pressure data but still reasonable. They also applied dynamic correction term to estimate transient NO_x. Although the numerical methods have benefits in low cost and fast calculation time, the estimation performance in the outside region over the training boundary and robustness on the change of hardware and environment could be poor than physics-based estimation models.

1.3 Objectives

To reduce real-time NO_x emission, the amount of NO_x formed should be determined for better control and optimization of both in-cylinder combustion and efficiency of after-treatment systems. Therefore, many researches on a virtual NO_x sensor using physics-based models and numerical models have been reported. The previous researches showed reliable NO_x estimation but there are some limiting factors, such as complexity of the model which leads to lack of calculation time for real-time application, necessity of many calibration constants, fitting process for empirical equations and demand on training for numerical models. Furthermore, most of the studies did not consider NO_2 emissions despite the fact that the NO_2/NO_x ratio is significant at higher EGR rate regions for diesel engines. Thus, the objectives of this study are:

1. The development of physics-based NO_x estimation model based on in-cylinder pressure measurement and data available from ECU.

2. Verification of real-time applicability of the model.

3. Investigation on the performance of developed model at steady state conditions and transient driving cycles.

Chapter 2. Development of NO estimation model with in-cylinder pressure measurement

In this chapter, a real-time nitric oxide estimation model was developed based on the in-cylinder pressure measurement and on data available from the ECU. As computational fluid dynamics can describe the process of NO formation which is not directly obtainable from experiments on a physical basis, the NO formation model was developed based on both the analysis of CFD results as well as on a physical model. Furthermore, the in-cylinder pressure is used to predict the amount of NO formation under various engine operating conditions as the pressure reflects the change in the combustion characteristics. The estimation model consisted of a simple calculation process; therefore, the model could predict the cycle-by-cycle NO in real-time. The validation results show that the model presented can predict engine-out NO well; thus, this model can be applied to engines and after-treatment systems as a useful tool to control the engine-out NO without the use of a NO_x sensor. In addition to being a virtual NO sensor, the estimation model can be applied to 1-D simulations, such as GT-SUITE and AMESIM, and demonstrate improved NO estimation results as the model is able to predict the NO level as the same levelas the 3-D CFD simulation. This chapter includes a part of published paper in 2013 [90].

2.1 Computational model and validation

2.1.1 Computational model for the CFD simulation

CFD can describe the process of NO formation, such as the start of NO formation, the NO formation rate, and the duration of NO formation, that is not directly accessible from the experimental data. Therefore, in the present work, the NO formation model was developed based on the analysis of both the CFD results and the physical model. Moreover, the in-cylinder pressure was used to predict NO under various engine operating conditions as it reflects the change in the combustion characteristics.

Computations were performed using the commercial CFD software Star-CD ver. 4.10 [91]. The combustion model was the Extended Coherent Flame Model in 3 zones (ECFM-3Z) [92-94]. To simulate spray atomization and break-up, the Reitz-Diwakar model was used in this study [95]. The O'Rourke model modified by Aamir and Watkins was used for droplet collision [96], and the Bai model was used for the spray impingement process [97]. The extended Zeldovich mechanism was used for NO formation.

2.1.2 Validation of the computational models

The computational models were verified using the experimental results. A 2.2 L conventional diesel engine was used. This engine has a common rail system with a piezo injector that enables injection pressures up to 1800 bar. The detailed specifications of the engine are listed in Table 2.1. The EGR rate of the intake gas was calculated from the carbon dioxide (CO_2) fractions in the exhaust and intake gas. The concentrations of NO and CO_2 in the exhaust gas were measured using an exhaust gas analyzer (HORIBA, MEXA-7100DEGR). Signals from the pressure

transducers were recorded at every 1° crank angle (CA) using a data acquisition system.

At first, the two reference conditions (1500 rpm / bmep 4 bar and 2000 rpm / bmep 6 bar) with a 25% EGR were applied to the simulation and compared with the experimental data. At 1500 rpm, a total of 16.38 mg/str of fuel was injected by the pilot injection, main injection (MI), and post injection, and the main injection timing was before 5 ° BTDC. At 2000 rpm, total of 22.6 mg/str of fuel was injected by the two pilot injections, main injection, and post injection, and the main injection timing was 7 ° BTDC.

A one over eight sector meshes, which has approximately 22700 cells at top dead center (TDC) and 90000 cells at bottom dead center (BDC), was constructed, and a cyclic boundary was applied to achieve symmetry as shown in Figure 2.1. The calculation was started from the intake valve closing time, approximately BTDC 150 °CA, and the initial conditions were obtained from the experimental results. Figures 2.2 and 2.3 show pressure and HRR curves of the simulation and experimental results. The ignition delay, peak pressure, pressure trace, and HRR trace of the simulation agreed with the experimental results.

During the next step, various EGR rates and main injection timing conditions were changed to verify the emission model. The EGR rate was varied from 15% to 25% in 5% increments and the main injection time was advanced and retarded by 2° CA from the base condition. The specific conditions are listed in Table 2.2. Figure 2.4 shows the comparisons between the predicted and measured NO emission. For an exact comparison with the simulation result, only the NO emission was measured. As shown in the Figure 2.4, the predicted NO emission agreed with the measured one. Based on these results, the CFD could be useful tool in describing the combustion and the emission characteristics of the diesel engine.

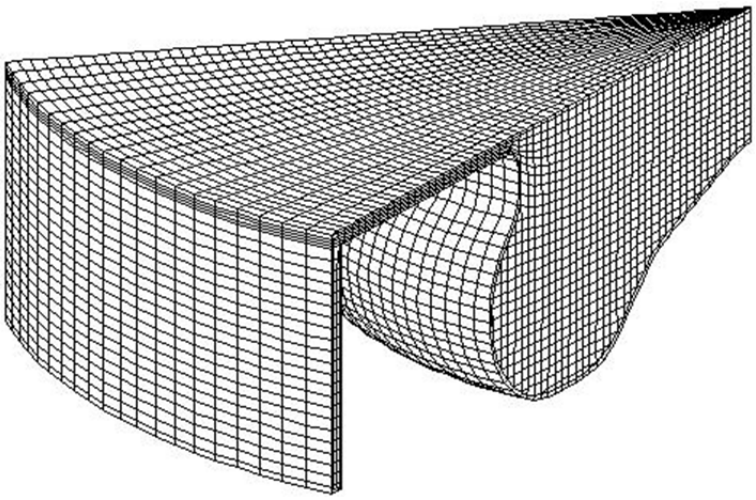

Figure 2.1 1/8 sector mesh at TDC.

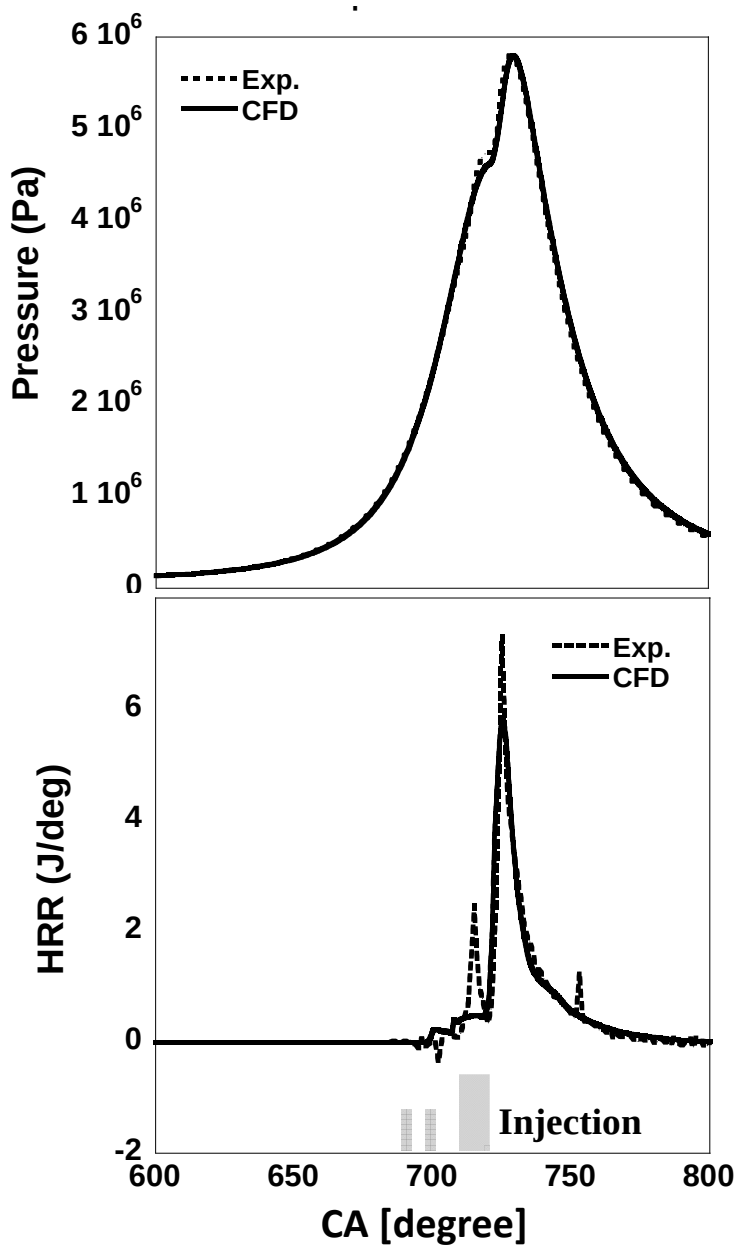

Figure 2.2 Pressure, HRR and injection strategies of CFD and experimental results at 1500 rpm 4 bar.

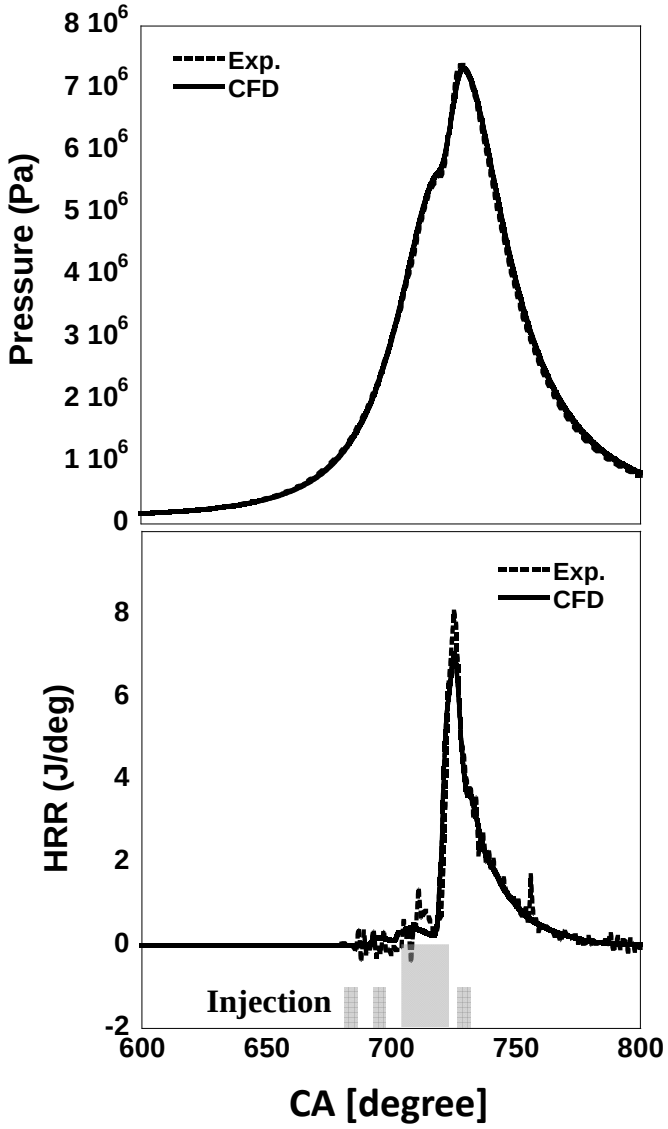

Figure 2.3 Pressure, HRR and injection strategies of CFD and experimental results at 2000 rpm 6 bar.

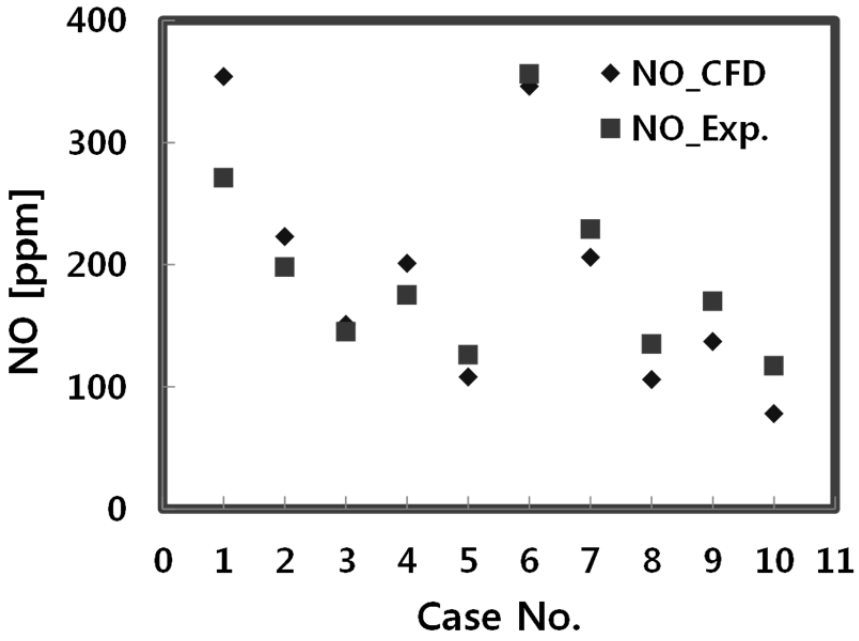

Figure 2.4 Comparisons between predicted and measured NO emissions.

2.2 NO estimation model

2.2.1 Basic assumptions for the NO estimation model

The NO estimation model was developed based on these assumptions.

- NO forms in the high temperature burned gas region, and its formation rate is highest near the stoichiometric regions.
- Most NO forms by the main injection.
- The adiabatic flame temperature and the gas concentrations at start of combustion (SOC) can be substituted for the burned gas temperature and equilibrium gas concentrations.
- The flame forms at the stoichiometric regions; thus, the adiabatic flame temperature is calculated at the Φ=1.

2.2.2 Physical model for NO formation

The extended Zeldovich mechanism is used for NO formation from atmospheric nitrogen [14].

$$N + O_2 = NO + O \tag{2.1}$$

$$O + N_2 = NO + N \tag{2.2}$$

$$N + OH = NO + H \tag{2.3}$$

The rate of NO formation using forward and reverse rate constants is given by equation (2.4).

$$\frac{d[NO]}{dt} = k_1^+[O][N_2] + k_2^+[N][O_2] + k_3^+[N][OH] \qquad (2.4)$$
$$k_1\ [NO][N] \quad k_2\ [NO][O] \quad k_3\ [NO][H]$$

[ ] : species concentrations mol/cm3 , k : reaction constant

Because [N] is much less than the concentration of other species, [N] and d[NO]/dt is set to zero by steady-state approximation. Then equation (2.4) becomes:

$$\frac{d[NO]}{dt} = 2k_1^+[O][N_2]\frac{1-[NO]^2/(K[O_2][N_2])}{1+k_1^-[NO]/(k_2^+[O_2]+k_3^+[OH])} \qquad (2.5)$$

$$K = (k_1^+ / k_1^-)(k_2^+ / k_2^-) \qquad (2.6)$$

NO formation in the post flame area is dominant and the concentrations of O, O_2, OH, H, and N_2 is assumed equilibrium. For convenience, the below notations are used.

$$R_1 = k_1^+[O]_e[N_2]_e = k_1^-[NO]_e[N]_e \qquad (2.7)$$

$$R_2 = k_2^+[N]_e[O_2]_e = k_2^-[NO]_e[O]_e \qquad (2.8)$$

$$R_3 = k_3^+[N]_e[OH]_e = k_3^-[NO]_e[H]_e \qquad (2.9)$$

Where [ ]e denotes equilibrium concentration, for the one-way equilibrium rate for reaction.

Then, equation (2.5) becomes:

$$\frac{d[NO]}{dt} = \frac{2R_1\left\{1-\left([NO]/[NO]_e\right)^2\right\}}{1+\left([NO]/[NO]_e\right)R_1/\left(R_2+R_3\right)} \tag{2.10}$$

When [NO]/[NO]e 《 1, then, from equation (2.10),

$$\frac{d[NO]}{dt} = 2R_1 = 2k_1^+[O]_e[N_2]_e \tag{2.11}$$

The equilibrium oxygen atom concentration is given by

$$[O]_e = \frac{K_{P(O)}[O_2]_e^{1/2}}{\left(\widetilde{R}T\right)^{1/2}} \tag{2.12}$$

$$K_{P(O)} = 3.6\times10^3 \exp\left(\frac{-31090}{T}\right) \tag{2.13}$$

Then the NO formation rate is written as [9]

$$\frac{d[NO]}{dt} = \frac{6\times10^{16}}{T^{1/2}}\exp\left(\frac{-69090}{T}\right)[O_2]_e^{1/2}[N_2]_e \tag{2.14}$$

Figure 2.5-(a) shows that the profile of d[NO]/dt and [NO] through the CFD calculation at 2000 rpm, bmep 6 bar, and EGR 30 % condition. If the NO formation rate can be obtained, the total amount of NO can be calculated by integrating the NO formation rate. However, the integration is time consuming process, thus the integration is substituted by multiplication like Figure 2.5-(b) and equation (2.15) in presented work. To do this, averaged NO formation rate and the duration of NO formation should be calculated. However, the averaged NO formation rate cannot be calculated by using data available from ECU and in-cylinder pressure data because it is only obtained from the CFD result.

2.2.3 Determination of the duration of NO formation

The first step is to determine the duration of NO formation. As the duration cannot be directly accessible from the engine experiment, Mass fraction burned (MFB) was used for determining the duration. At first, the duration from the point of 20 % of [NO] to the point of 90 % of [NO] assumed to represent the duration of NO formation. It is difficult to find the MFB points which match [NO] 0 % and [NO] 100 % because NO formation rate is slow and effected by pilot injection strategy at the early stage of combustion and NO formation is almost steady at the end of the combustion. Therefore [NO] 20 % and [NO] 90 % were chosen the start and end point of NO formation and the difference between [NO] 0% ~ 100% and [NO] 20 % ~ 90% were compensated with a coefficient.

Then, MFB timings which match [NO] 20 % and [NO] 90 % were found from the CFD results. Figure 2.7 shows the results of MFB timings which correspond to [NO] 20 % and [NO] 90 % under the variable conditions given in Table 2.2. MFB 40 is well matched with the [NO] 20 % and MFB 80 is well matched with the [NO] 90 %.

2.2.4 Determination of averaged NO formation rate

Total NO formation can be calculated by multiple of averaged NO formation rate and NO formation duration as expressed in equation (2.15).

$$[NO] = \int \frac{d[NO]}{dt} \cdot dt \approx \left(\frac{d[NO]}{dt} \right)_{average} \times (duration) \qquad (2.15)$$

CFD simulation was carried out confirming that the maximum NO formation rate is suitable to substitute the averaged NO formation rate. The simulations were

conducted at 35 operating points covering the large weighting points of the NEDC cycle. For validating the robustness, EGR rate and main injection timing were varied, and each test points are given in Table 2.2 the corresponding main engine operating data. Figure 2.6 shows the correlation between the averaged NO formation rate and the maximum NO formation rate. The averaged NO formation rate was calculated by CFD simulation using averaged NO formation rate between $[NO]_{20}$ and $[NO]_{90}$. The maximum NO formation rate was calculated by equation (2.16) using maximum burned gas temperature and gas concentration.

$$\left(\frac{d[NO]}{dt}\right)_{\max} = \frac{A}{T_{\max}^{1/2}} \exp\left(\frac{-69090}{T_{\max}}\right)[O_2]^{1/2}[N_2] \tag{2.16}$$

It was shown that the maximum NO formation rate is proportional to the averaged NO formation rate. Therefore, it is concluded that the maximum NO formation rate can be used as a representative value of the averaged NO formation rate.

2.2.5 Calculation of the maximum NO formation rate

The key inputs to calculate the maximum NO formation rate written as equation (2.16) described below. Maximum temperature, O_2 and N_2 concentrations, and constant A are needed to predict the maximum NO formation rate and they are calculated by using available ECU data and in-cylinder pressure.

Gas concentration

Gas concentrations are calculated using data available from ECU such as fuel mass, AF ratio, and EGR rate as follows:

$$O_2 = (1 - X_b) \times O_{2\_air} + X_b \times O_{2\_X_b} \tag{2.17}$$

$$N_2 = (1 - X_b) \times N_{2\_air} + X_b \times N_{2\_X_b} \quad (2.18)$$

Where, O_2 and N_2 correspond to the volume fractions of O_2 and N_2 before combustion starts. And each term is obtained from the below formula [98]:

$$O_{2\_X_b} = \frac{1-\phi}{(1-\varepsilon)\phi + 1 + \psi}, \text{ } O_2 \text{ volume fraction of burned gas} \quad (2.19)$$

$$N_{2\_X_b} = \frac{\psi}{(1-\varepsilon)\phi + 1 + \psi}, \text{ } N_2 \text{ volume fraction of burned gas} \quad (2.20)$$

$$\psi = 3.773(air), \text{ the molar N/O ratio} \quad (2.21)$$

$$\phi = \frac{1/AF}{1/AF_{stoich}}, \text{ fuel/air equivalence ratio} \quad (2.22)$$

$$\varepsilon = \frac{4}{4+y}, \text{ y = 1.8 (diesel), the molar H/C ratio of the fuel} \quad (2.23)$$

$$m_{total} = \frac{AF \times m_{fuel}}{1 - X_b} \quad (2.24)$$

$$X_b = \frac{m_{EGR} + m_r}{m_{total}} = \left(\frac{EGR}{100}\right)(1 - X_r) + X_r \quad (2.25)$$

Where X_b, X_r, m_{EGR}, m_r, and m_{total} correspond to the burned gas fraction, residual gas fraction, EGR mass, residual mass, and total mass of in-cylinder gas respectively. EGR rate is obtained from the ECU (the engine has own EGR model inside the ECU) and the residual gas fraction is calculated from the TPA (Three Pressure Analysis) Engine model of GT-SUITE [99]. The TPA engine model can calculate the burned gas fraction (X_b) from measured intake, exhaust, and in-cylinder pressure. Figure 2.8 shows the TPA model of a single cylinder diesel

engine and Table 2.3 lists the residual fraction results under various EGR conditions. The residual fraction (X_r) almost constant according to the EGR, so averaged value, 0.047, is used.

Maximum burned gas temperature

Predicting the in-cylinder temperature is not simple, instead adiabatic flame temperature was used. To calculate the adiabatic frame temperature, a second order formula was derived from a database. The database was built of the 130 cases of simulation results under various AF, EGR, and initial temperature conditions using the Chemkin-III [100]. The reactant was n-heptane and reduced reaction mechanism which consists of 29 species and 52 reactions was used to simulate diesel fuel chemistry [101]. And it was assumed that combustion occurs at $\Phi = 1$. The finished formula of the adiabatic flame temperature is derived as a function of temperature at SOC and $[O_2]$. T_{SOC}, which means the temperature when the combustion starts, is indirectly determined from the ideal gas state equation

The SOC is determined by HRR analysis which is calculated from the in-cylinder pressure. As shown in Figure 2.9, the minimum value near the main injection timing is set to the SOC because NO mostly forms after the main injection.

Burned gas is compressed during the combustion, therefore the burned gas temperature additionally increased than the burned gas temperature at the SOC. The compression is assumed an isentropic process, so the maximum burned gas temperature can be written like equation (2.26). Where, P_{max} is a measured value and k is the ratio of specific heats which is assumed to be constant, 1.3.

$$T_{\max} = T_{ad}\left(\frac{P_{\max}}{P_{SOC}}\right)^{\frac{k-1}{k}} \tag{2.26}$$

2.2.6 Summary of the NO estimation model

The procedure to determine the formed NO is summarized as shown in Figure 2.10. To establish this procedure, the information available from the pressure sensor and ECU existing engine was taken into account.

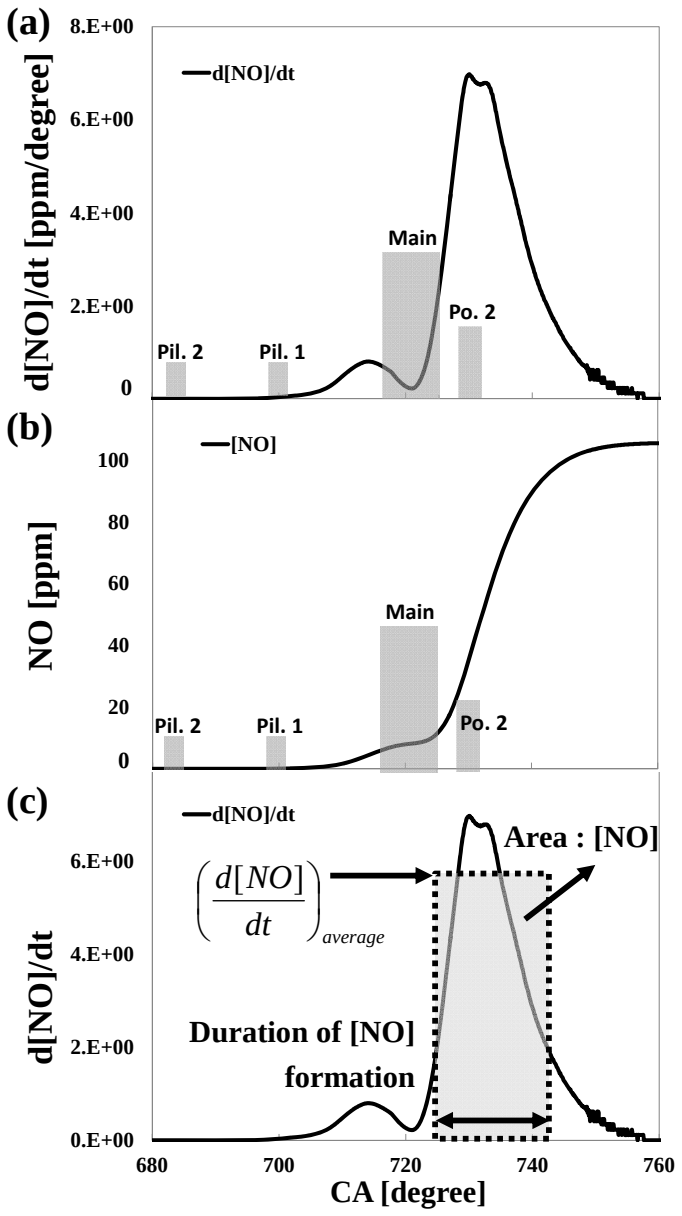

Figure 2.5 Methods of calculating the NO emission (a) dNO/dt (b) integration, and (c) multiplication.

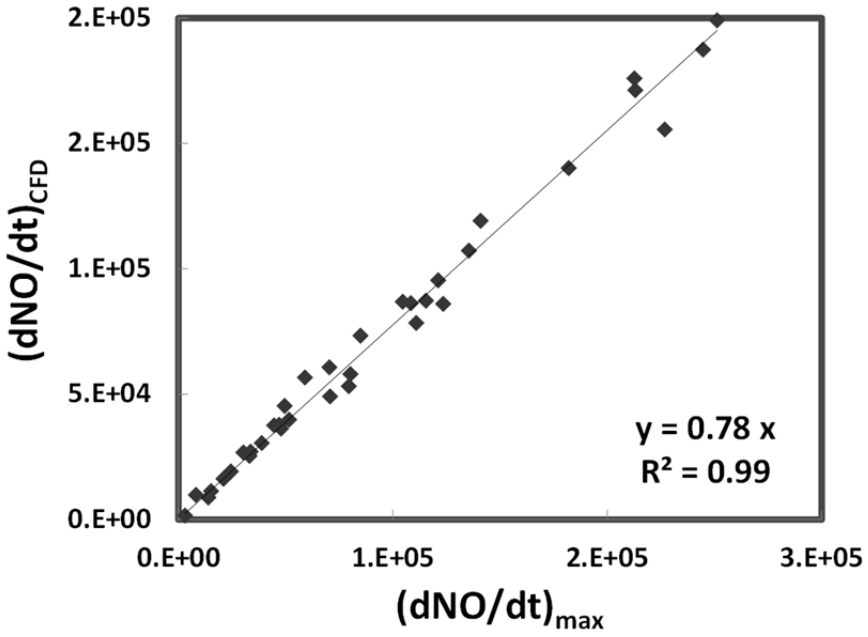

Figure 2.6 Correlation between the averaged NO formation rate (CFD) and the maximum NO formation rate.

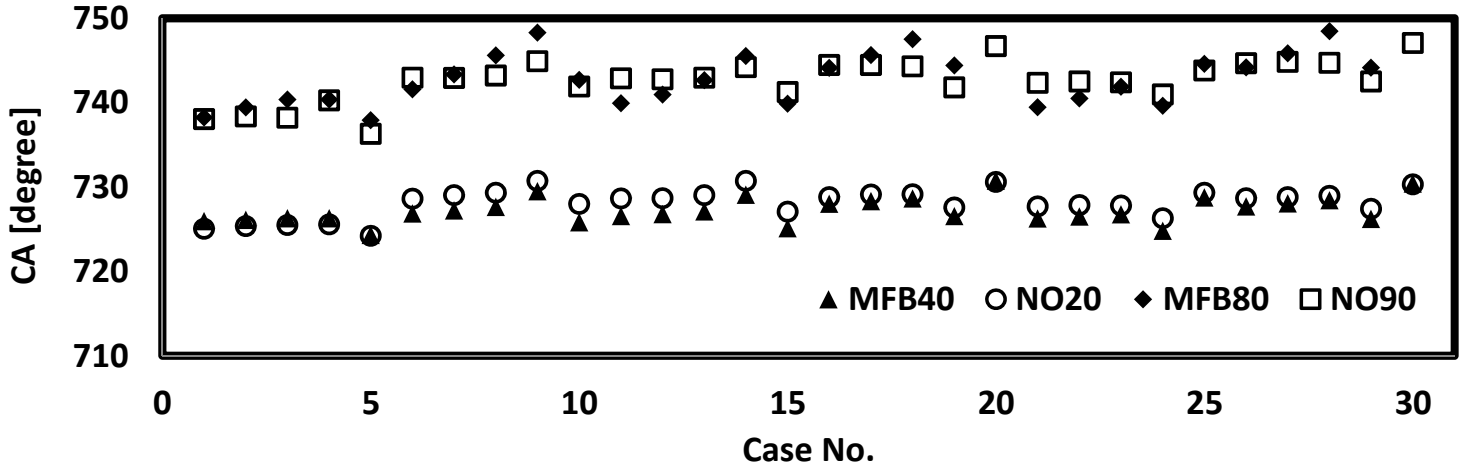

Figure 2.7 Timings of MFB 40, MFB 80, NO 20 % and NO 90 %.

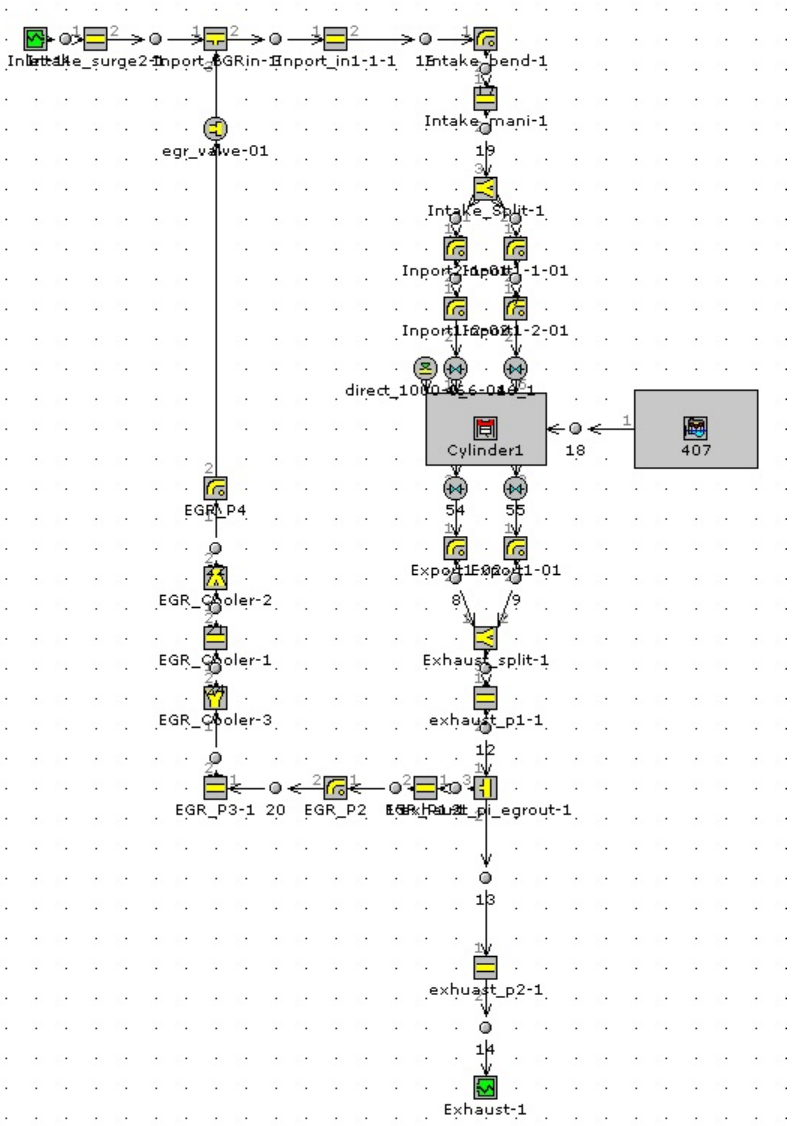

Figure 2.8 the TPA model of a single cylinder diesel engine.

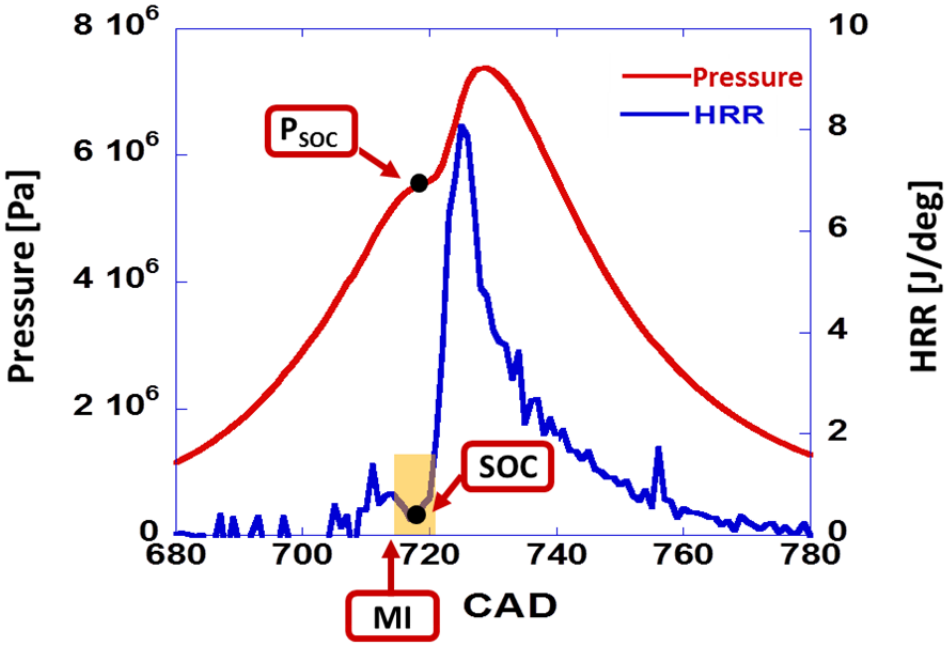

Figure 2.9 Determination of the start of combustion.

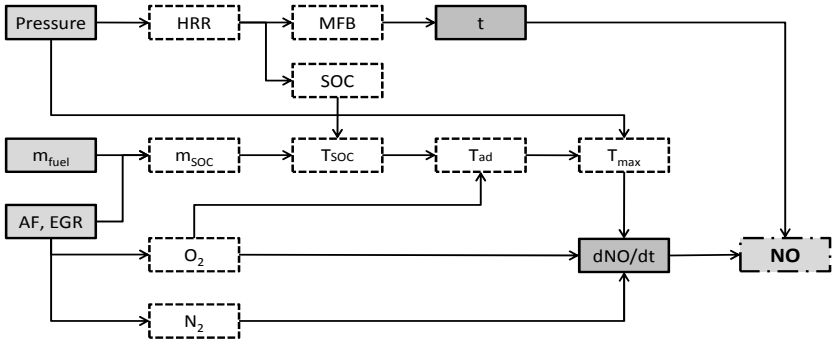

Figure 2.10 Procedure to determine the formed NO.

Table 2.1 Engine specifications.

Criteria	Specification
Layout	In-line 4 cylinder 2.2 L
Max power	200 hp / 3800 RPM
Max torque	44.5 kgm / 1800 RPM~2500 RPM
Bore	85.4 mm
Stroke	96 mm
Displacement volume	550 cc
Connecting rod	145 mm
Compression ratio	16
Valve timing	IVO : 10° BTDC
	IVC : 28° ABDC
	EVO : 54° BBDC
	EVC : 4° ATDC
Fuel injector type	Piezoelectric type
ECU version	EDC 17C

Table 2.2 Conditions for validation of CFD against experiments.

No.	Speed [rpm]	bmep [bar]	EGR [%]	MI [BTDC]
1	1500	4	15	5
2	1500	4	20	5
3	1500	4	25	5
4	1500	4	25	7
5	1500	4	25	3
6	2000	6	15	7.2
7	2000	6	20	7.2
8	2000	6	25	7.2
9	2000	6	25	9.2
10	2000	6	25	5.2

Table 2.3 The residual fraction results under various EGR conditions.

1500 rpm / 4 bar	**Intake EGR [%]**	5.1	7.9	11.6	14.1	18.4	23.3	29.6	34.7
	Residual EGR [%]	4.43	4.45	4.52	4.42	4.53	4.43	4.55	4.59
	In-cylinder EGR [%]	9.3	12	15.6	17.9	22.1	26.7	32.8	37.7
2000 rpm / 4 bar	**Intake EGR [%]**	3.7	6.3	9.9	14.8	18.9	23	31.4	34.5
	Residual EGR [%]	4.88	4.91	4.88	4.69	4.81	4.68	5.1	4.89
	In-cylinder EGR [%]	8.4	10.9	14.3	18.8	22.8	26.6	34.9	37.7

2.3 Model validation with CFD results

The NO estimation model was validated on the basis of combustion simulation result of the diesel engine. The key inputs for predicting NO formation are EGR, AF ratio, and fuel mass which were obtained from the ECU. However, there are difference between real value and ECU value and these differences may cause the error between predicted NO and measured NO. To exclude these errors, CFD simulation was used to validate the model. Because CFD simulation can provide exact inputs such as EGR, AF ratio, and fuel mass to the estimation model, it is helpful tool verifying the model.

The simulation was carried out at 44 operating conditions using the computational models which explained in chapter 2. Table 2.4 lists the simulation conditions which cover the NEDC cycle and swing of EGR and main injection timing. Figure 2.11 shows the validation result. The model showed averaged 7.4 ppm error under 100 ppm of NO and averaged 9.3 % error from 100 ppm to 900 ppm of NO and the standard deviation was 0.98. The results show good quantitative agreement at overall NO range.

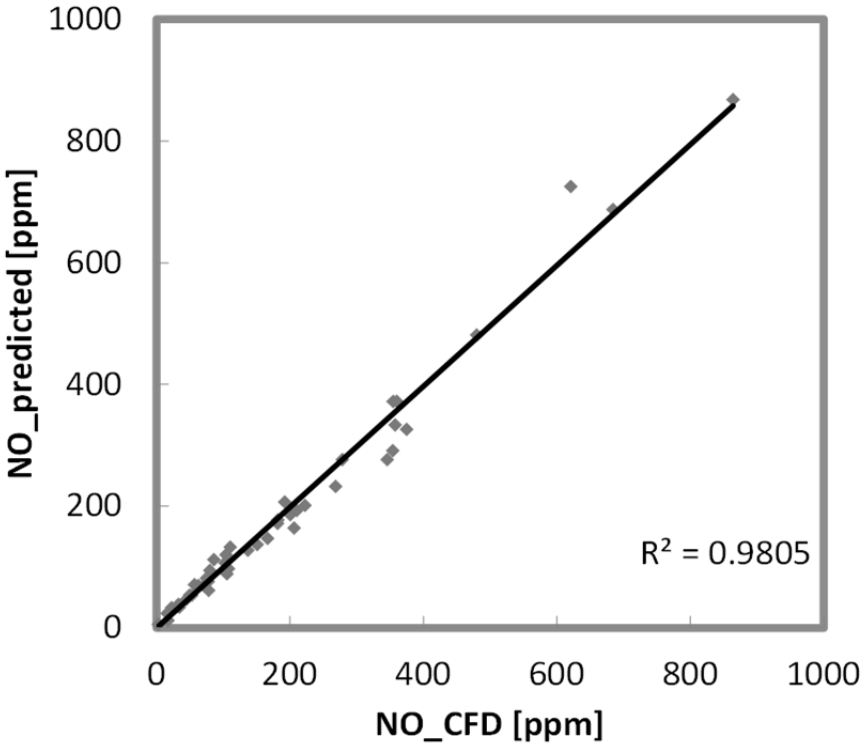

Figure 2.11 Comparison of the predicted results with the CFD results.

Chapter 3. Experimental Apparatus

3.1 Engine setup

To verify the model experimentally, a 2.2 liter 4 cylinder diesel engine shown in Figure 3.1 was used. The engine was equipped with a turbocharger and a common rail direct injection system with piezo injectors. The size of bore and stroke was 85.4 and 96 mm, respectiviely. The compression ratio of the engine was 16. The engine was also equipped with a dual EGR system which includes high pressure EGR (HP-EGR) and low pressure EGR (LP-EGR) system. The specifications of the engine are described in Table 3.1.

For steady and simple ramp conditions, the engine was connected to a 190 kW AC dynamometer (AVL, ELIN) which is capable of measuring not only steady state operations but also transient state operations with the dynamometer controller (FEV, TOM). The specifications of the dynamometer are shown in Table 3.2. Diesel fuel was supplied by low pressure fuel pump from fuel tank. Fuel flow rate was measured by a fuel flow meter (Oval, Ultra mass MK II) which is based on Coriolis force and the specifications of the fuel flow meter are shown in Table 3.3. Temperature of the fuel was controlled to maintain 40 ℃ by fuel temperature controller (SAMBU, SFTC-1400). The coolant temperature was set to 85 ℃ by coolant temperature controller (SAMBU, SWC-1200). The test cell temperature was set to 25 ℃ by building air conditioning system. The engine was controlled by programmable Bosch ECU version of EDC 17C which is connected to PC software. The brief experimental setup is described in Figure 3.2.

For transient driving cycles, the engine was connected to a 340 kW AC dynamometer which is able to operate both steady-state operations and transient state operations with the dynamometer controller (AVL, PUMA). Fuel was supplied through a fuel flow meter (AVL, 733S) while the rest setup is the same.

Figure 3.1 In-line 4 cylinder 2.2 L diesel engine.

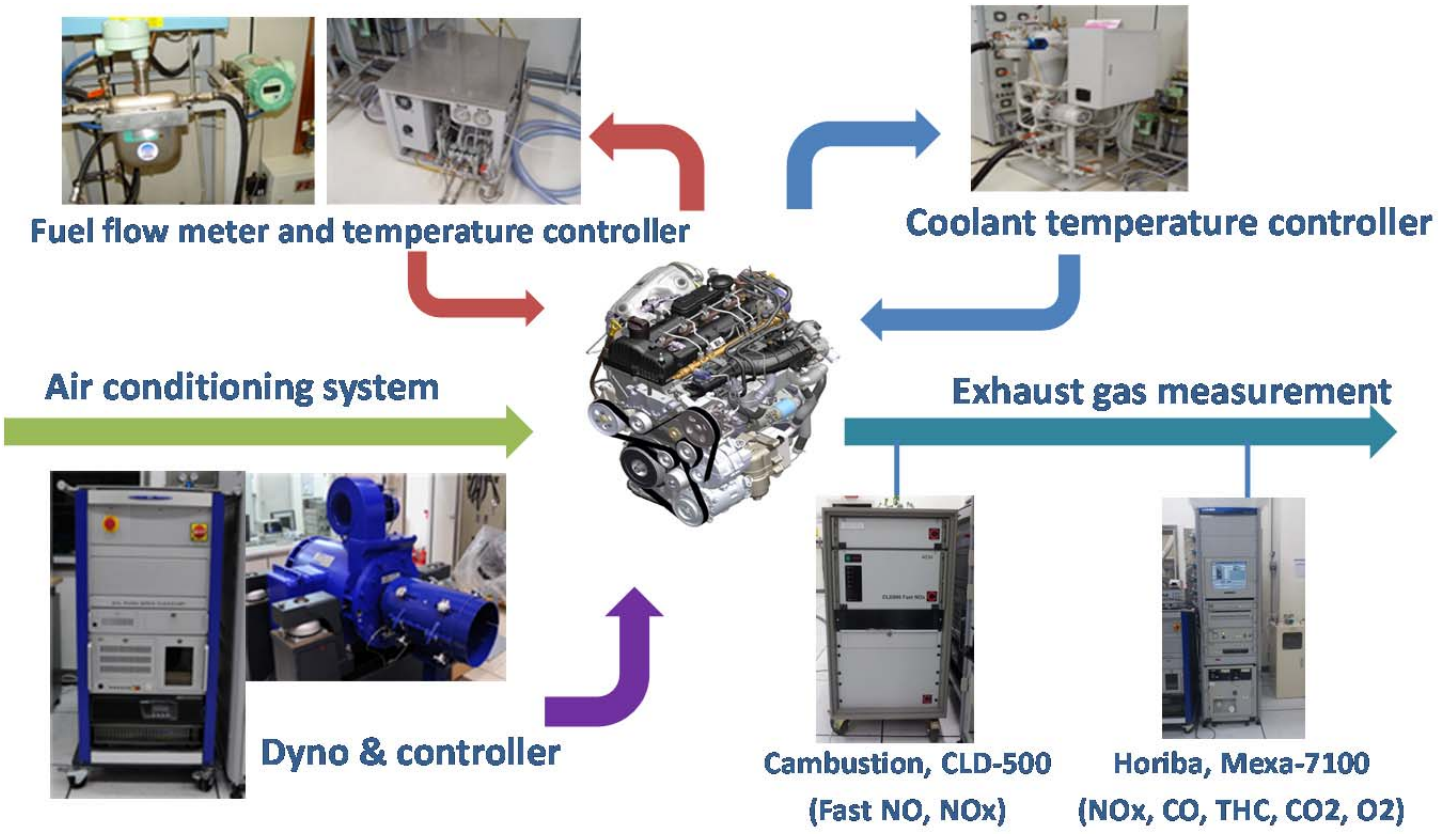

Figure 3.2 In-line 4 cylinder 2.2 L diesel engine.

Table 3.1 Engine specifications.

Specification	Value
Number of cylinder	4
Engine type	Compression ignition
Displacement volume (liter)	2.2
Bore (mm)	85.4
Stroke (mm)	96
Compression ratio	16
Max. Power (HP) / Torque (kg · m)	200 / 44.5
Valve timing	IVO/IVC (10° BTDC / 28° ABDC) EVO/EVC (54° BBDC /4° ATDC)

Table 3.2 Specifications of 190 kW dynamometer.

Item	Specfication
Manufacturer	AVL ELIN
Model	MCA-231
Capacity	190 kW
Type	AC
Maximum rpm	6980
Cooling	Air cooling

Table 3.3 Specifications of fuel flow meter (OVAL).

Item	Specfication
Manufacturer	OVAL
Type	Coriolis type
Model	ULTRA mass MKII CN-003
Transmitter	CT9401
Range of measurement	0 ~ 20 g/sec
Minimum range	1 g/s
Accuracy	± 0.1 %
Allowable measuring density	0.3 ~ 2 g/mL

3.2 In-cylinder pressure measurement

To obtain real-time in-cylinder pressure, glow plug type piezoelectric sensors (Kistler, 6056A) were installed at each cylinder. The sensor signal was amplified by a charge amplifier (Kistler, 5019A). The specifications of the piezoelectric sensor are shown in Table 3.4. Amplified pressure signal delivered to a data acquisition (DAQ) board which is a part of the ES-1000. Also, the signal of a cam position sensor was acquired by the DAQ board.

Table 3.4 Specifications of piezoelectric pressure sensor.

Technical data	
Operating temperature	-40 – 140°C (max. 150°C)
Pressure range	0 – 200 bar (max. 210 bar)
Sensor	
Power supply (Vdd)	5,0 V or 3,3 V
Output signal	ratio metric
Bandwidth	0 to 5 kHz
Accuracy	± 2%
Glow function	
Current 60sec	< 10 A
Temperature after 60sec	> 980°C
Max. temperature	1100°C

3.3 EGR measurement

An EGR rate was calculated by measuring the concentration of carbon dioxide (CO_2) at the intake manifold and the exhaust manifold, respctively. The CO_2 concentrations at each location were measured by exhaust gas analyzer (Horiba, MEXA-7100DEGR). Since the amount of real NO_x formation and estimation of model are very sensitive to the EGR rate as shown in the sensitivity analysis, to obtain the accurate EGR rate of each cylinder, CO_2 concentration at each non-swirl intake port were measured as described as unfilled stars in Figure 3.3.

Measured data set of EGR rates over the whole engine operation regions was directly used as an input of the NO estimation model at steady state cases. This data set was also used to calibrate an EGR estimation model which is included in ECU. The EGR estimation model was used as input of the NO estimation model for transient operations.

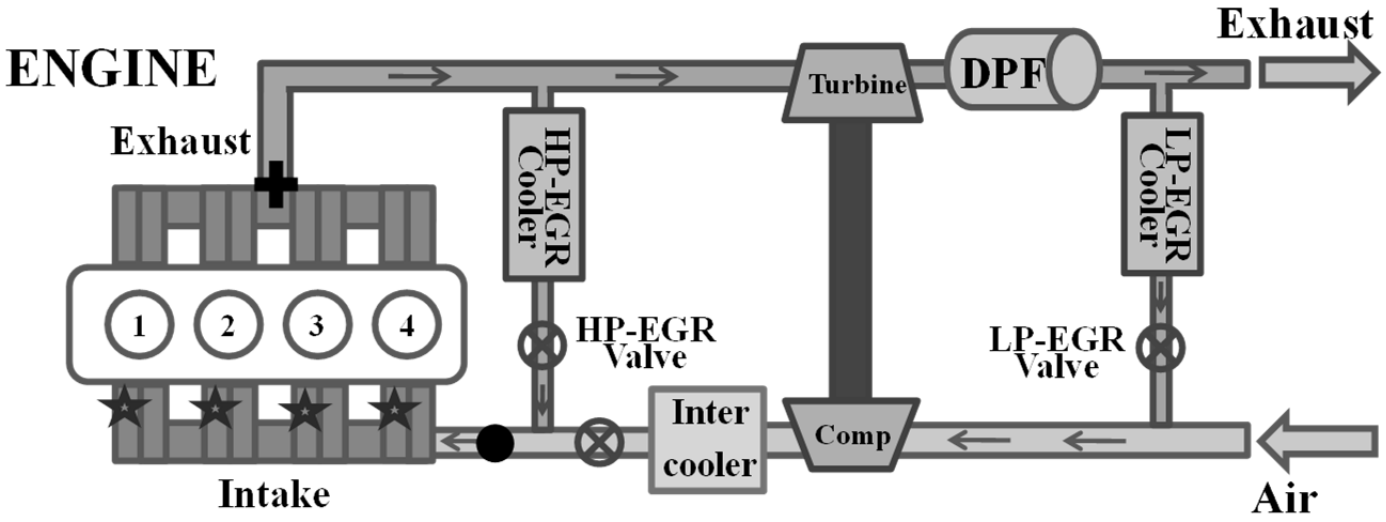

Figure 3.3 The cylinder-by-cylinder measurement of EGR rate.

3.4 NO and NO_x measurement

NO was measured by two pieces of equipment. For the measurement during steady state engine operation cases, the exhaust gas analyzer (Horiba, MEXA-7100DEGR) was used. Also, THC, CO and O2 concentrations are measured by the exhaust gas analyzer. The measuring principles of each emission are shown in Table 3.5. For fast measurement during transient operations, a fast NO analyzer (Cambustion, CLD-500) was used since the equipment had very fast response time (~2 ms). The sampling probe of the fast NO analyzer was installed at the confluence of exhaust gas indicated as a filled black cross in Figure 3.2, where is close to the exhaust valve to minimize sampling delay. The specifications of the fast NO analyzer are shown in Table 3.6.

Table 3.5 Measurement principle of exhaust gas analyzer.

Emissions	Measurement principle
NOx	Chemiluminecence Detector
THC	Flame Ionization Detector
O_2, CO_2, CO	Non Dispersive Infrared Rays

Table 3.6 Specifications of fast NO analyzer.

Item	Specification
Manufacturer	Cambustion
Model	CLD-500
Measurement range	0 ~ 100 ppm to 0 ~ 20,000 ppm
Linearity	±1 % FS to 5,000 ppm ±2 % FS to 10,000 ppm
Response time	2 ms (10 ms with NO_2measurement)
Zero stability	5 ppm for 1 hour

3.5 Real-time calculation of NO

To verify the potential as a real-time application of the developed model, the model was implemented on the embedded system (ETAS, ES-1000) bypassed from ECU for real-time estimation of NO during engine operations.

As demonstrated in Figure 3.4, ECU controls the engine and the engine provides actual feedback to ECU such as boost pressure, rail pressure, AFR, air mass and so on. Simultaneously, real-time in-cylinder pressure and cam position signal from the engine are delivered to ES-1000. Engine control parameters, real-time engine speed, EGR rate, AFR, air mass from ECU were also brought to ES-1000. The developed model was implemented in ES-1000 by using ASCET which is one of graphic based codes and has been used to build conventional ECU logic. All calculations were conducted in ES-1000 and a PC communicates with it through a monitor and logs real-time predicted results.

Figure 3.5 shows the procedure of predicting NO in a cycle. During 360°~270° BTDC, cycle-by-cycle input data such as engine control parameters, injection parameters, real-time engine speed, EGR rate, AFR and air mass from ECU are transferred to the model. After combustion is almost completed, heat release is calculated using pressure data during 90°~270° ATDC. Then, MFB and SOC timing were calculated using heat release data. After that, using input data, gas concentration and T_{SOC} were calculated. T_{ad} was calculated in this step and T_{max} could be calculated using P_{max}. Finally, NO is calculated. Since the calculation was designed to be finished in a cycle, cycle-by-cycle estimation of NO is possible. The specifications of the embedded system are shown in Table 3.7.

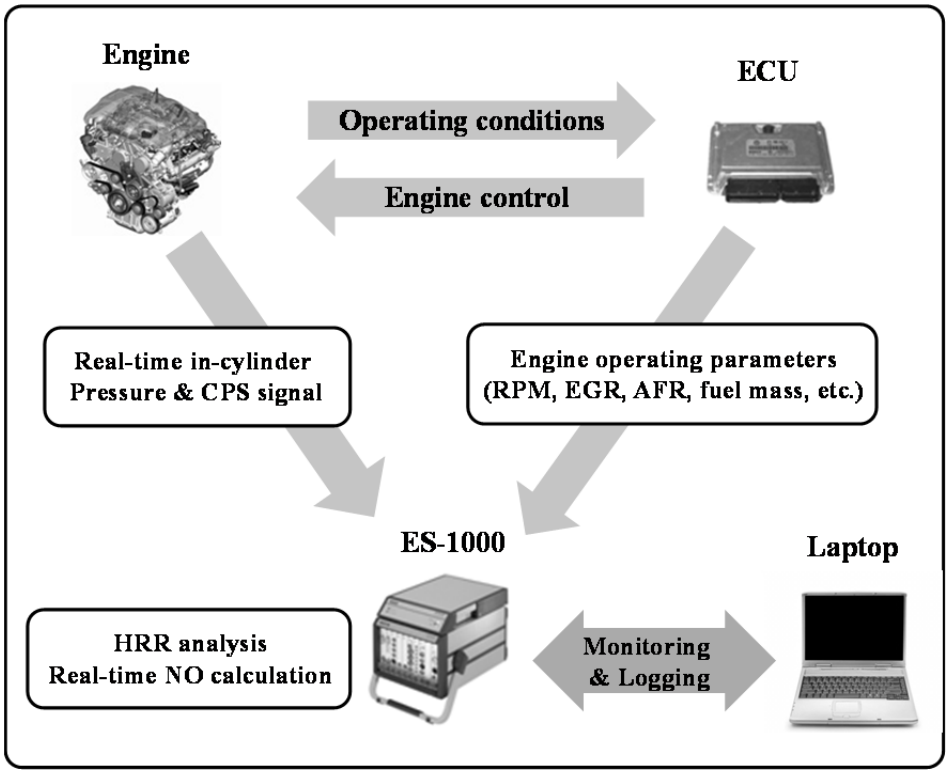

Figure 3.4 The scheme of the real-time NO estimation.

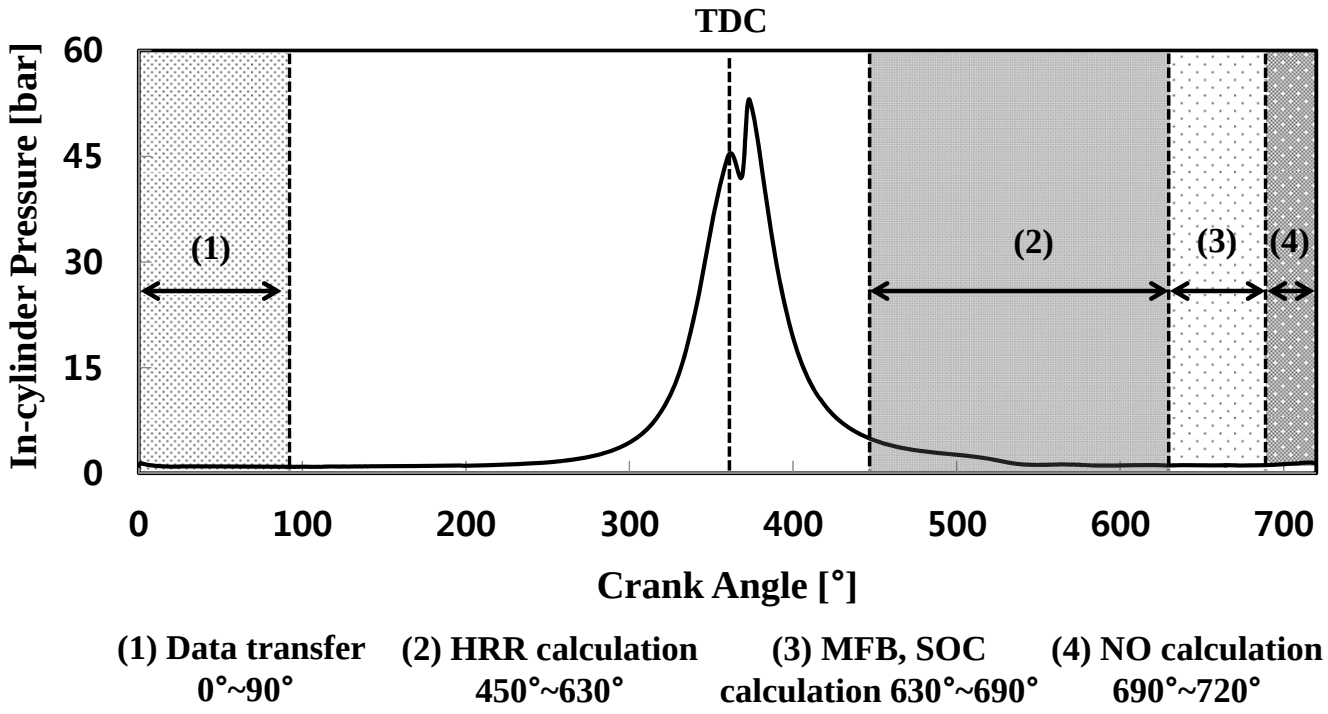

Figure 3.5 NO calculation procedure in a cycle.

Table 3.7 Specifications of the embedded system (ETAS, ES-1000).

Criteria		**Specification**
Simulation Board	CPU	1 GHz
	RAM	256 MB SDRAM
A/D board		16 CH, 100 kHz/CH
D/A board		8 CH
Digital and PWM I/O board	Channel	16 CH input, 16 CH output 2 external trigger
	Frequency	1 Hz to 60 kHz
CAN Communication		4 CAN signal

Chapter 4. The effect of EGR rate on NO estimation model

4.1 Sensitivity analysis

EGR is known as a dominant factor for NO_x emissions from Diesel engines because, by using EGR, combustion temperature can be lowered due to lower oxygen concentration and higher heat capacity than when fresh air is supplied. The effect of EGR rate on the NO estimation in the model can be also inferred in Figure 4.1.

To investigate the effect of EGR rate on NO estimation of the model, a sensitivity analysis was performed. Figure 4.1 demonstrates the effect of the increase of 1 % EGR rate on NO estimation under various conditions which are also used in the experiment that will be explained in the following chapter. It was shown that decrease in both NO in ppm and change of NO in percent due to 1 % EGR over estimation (i.e. 16 % instead of 15 %) is getting larger as the engine operation is in high NO region. It means that as the operating condition head towards a high temperature combustion region (decrease of EGR), the model is more sensitive to the EGR rate. This comes from the exponential term of equation (3). It can be found in Figure 4.1 that in low EGR conditions (under 15 %), NO can be reduced over 12 % by the 1 % increase of EGR.

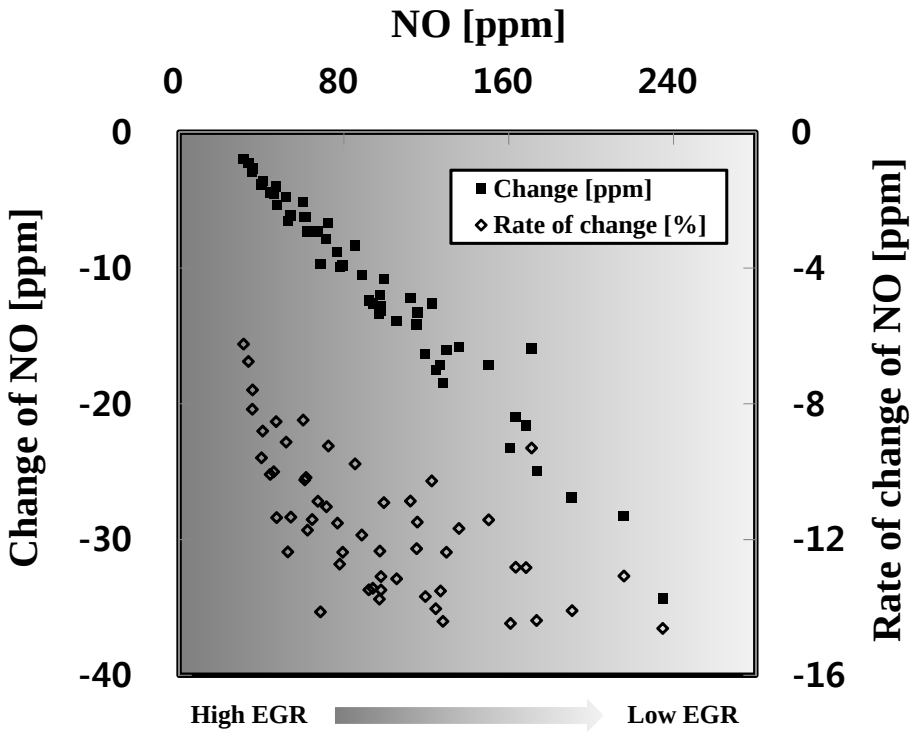

Figure 4.1 The quantitative analysis on the effect of EGR on NO estimation.

4.2 Cylinder-to-cylinder measurement of EGR

EGR rates were measured at each cylinder to see the cylinder-to-cylinder variance. Figure 4.2 shows cylinder-to-cylinder EGR measurement at engine operating condition of 1500 rpm and 4 bar. EGR0 means the EGR rate measured at a filled black circle in Figure 3.3 where the fresh air and the EGR gas are just mixed. Accordingly, EGR1 to EGR4 means EGR rates measured at cylinder 1 to cylinder 4, (at the position where stars are drawn in Figure 3.3) respectively. EGR_avg is the average value of EGR1 to EGR4. It was found that measured EGR values could differ by over 7 % according to the measurement position in this condition. The degree of non-homogeneity was different at each operating condition because the internal gas flow can be changed by engine speed, gas temperature and so on. Differences in EGR rate at each measurement position result from local differences of CO_2 concentration due to short mixing length of fresh air and EGR gas. These results can distort the measurement of actual EGR rates so that NO estimation could also be distorted. To minimize this effect, EGR_avg was used as an input EGR of the model.

On the contrary, non-homogeneity of EGR distribution is not found when only LP-EGR is activated. This is because not only LP-EGR has much longer mixing path, but also the EGR gas can be mixed very well with fresh air as it passes through the compressor as described in Figure 3.3. It was observed that the EGR rate was almost homogeneous wherever it was measured after the compressor when using only LP-EGR.

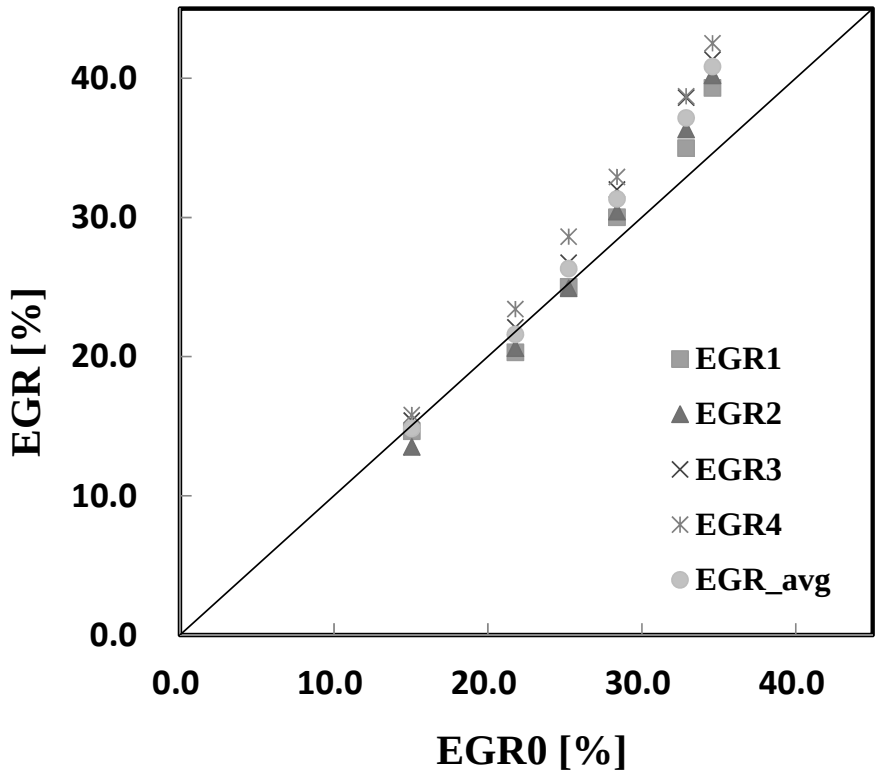

Figure 4.2 Cylinder-to-cylinder variance of the EGR measurement at the engine speed of 1500 rpm and load of BMEP 4 bar according to the EGR measured at EGR0.

4.3 EGR estimation model

Figure 4.3-(a) shows the cylinder-by-cylinder difference of the EGR from the averaged EGR. Using these EGR rates, the amount of NO emissions of each cylinder was predicted, as shown in Figure 4.3-(b). Although the average NO may be similar when an average EGR is used for each cylinder, the cylinder-to-cylinder deviation of NO can be larger than expected.

Therefore, in this study, an in-house EGR estimation model [102] was used and modified to calculate the cylinder-by-cylinder EGR to improve accuracy of NO_x estimation model. Each NO is calculated for each EGR rate, and then, the values are averaged. It can be expected that by accurate predicting the NO of each cylinder, cylinder-by-cylinder combustion control can be performed more appropriately.

Figure 4.5 shows the gas composition of the in-cylinder gas. The mass of the EGR gas can be calculated if the total masses of the in-cylinder gas, fresh air and residual gas are known.

$$m_{IVC} = m_{air} + m_{EGR} + m_{RG} \tag{4.1}$$

The EGR model obtains the mass of fresh air from the ECU, and the total mass of the in-cylinder gas at the intake valve close (IVC) can be derived with the ideal gas equation of state.

$$\frac{P_{IVC} v_{IVC}}{R T_{IVC}} = m_{IVC} \tag{4.2}$$

The in-cylinder pressure is measured using the pressure sensors for the NO model and the in-cylinder volume at the IVC can be calculated from the geometry.

The temperature of the in-cylinder gas at the IVC should be derived to calculate equation (4.1). From the definition of the residual gas fraction,

$$RGF[\%] = \frac{m_{RG}}{m_{air} + m_{EGR} + m_{RG}} \times 100 \tag{4.3}$$

The mass of the residual gas can be derived as

$$m_{RG} = \frac{RGF}{100 - RGF} \times \left(m_{air} + m_{EGR} \right) \tag{4.4}$$

If the heat losses are neglected, the law of conservation of energy is applicable to consider the temperature at the IVC.

$$c_{IVC} T_{IVC,noHT} m_{IVC} = c_{air} T_{air} m_{air} + c_{EGR} T_{EGR} m_{EGR} + c_{RG} T_{RG} m_{RG} \tag{4.5}$$

If the specific heat of the fresh air, EGR gas and residual gas are assumed to be approximately equal, calculation can be simplified by removing the specific heat.

$$T_{IVC,noHT} = \frac{T_{air} m_{air} + T_{EGR} m_{EGR} + T_{RG} m_{RG}}{m_{air} + m_{EGR} + m_{RG}} \tag{4.6}$$

Nevertheless, heat transfer from the cylinder wall to the in-cylinder gas is not negligible. A term that considers the increased gas temperature caused by heat transfer is applied to the equation.

$$T_{IVC} = T_{IVC,noHT} + \Delta T_{IVC,HT} = T_{IVC,noHT} \times \eta_{HT} \tag{4.7}$$

The mass of the EGR gas is calculated as

$$m_{EGR} = \frac{\frac{p_{IVC} v_{IVC}}{R \eta_{HT}} - m_{air}\left(T_{air} + T_{RG} \times \frac{RGF}{100 - RGF} \right)}{T_{EGR} + T_{RG} \times \frac{RGF}{100 - RGF}} \tag{4.8}$$

Then, the EGR rate is calculated as

$$EGR[\%] = \frac{m_{EGR}}{m_{air} + m_{EGR}} \times 100 \tag{4.9}$$

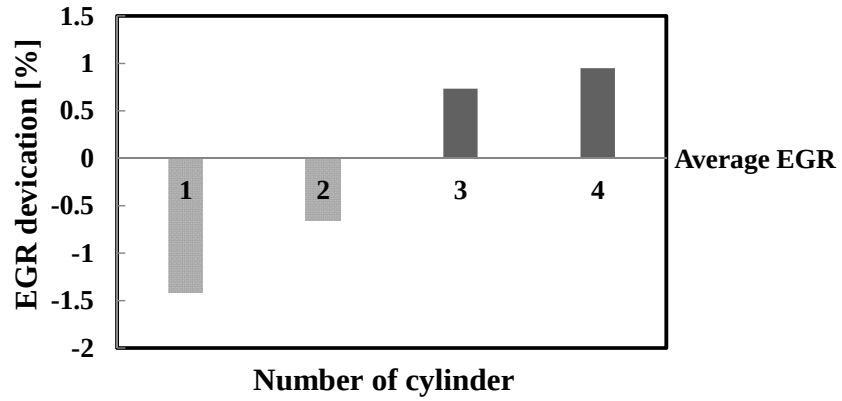

(a) Cylinder by cylinder EGR deviation

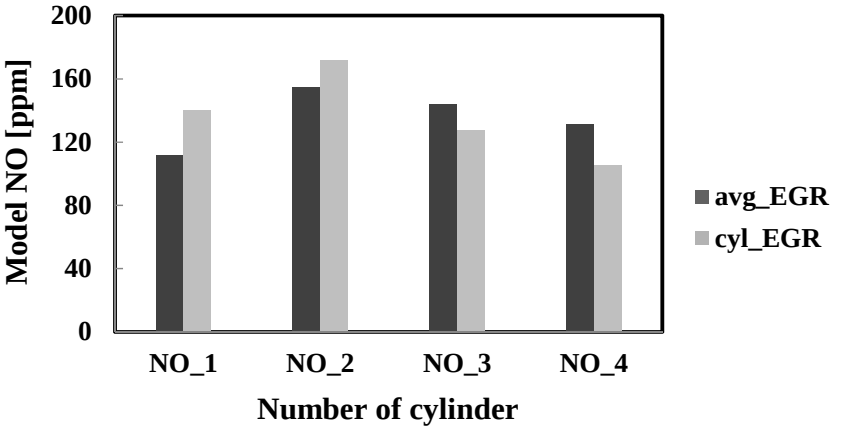

(b) Cylinder by cylinder model NO deviation

Figure 4.3 Cylinder-by-cylinder deviation of (a) EGR and (b) NO at 1500 rpm/ 7 bar condition.

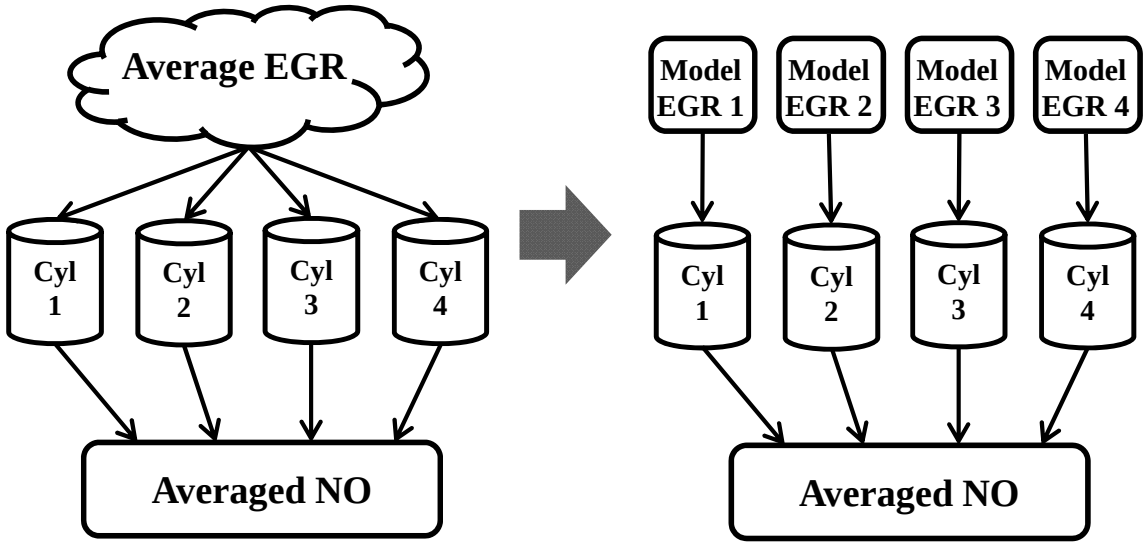

Figure 4.4 Change of NO calculation procedure.

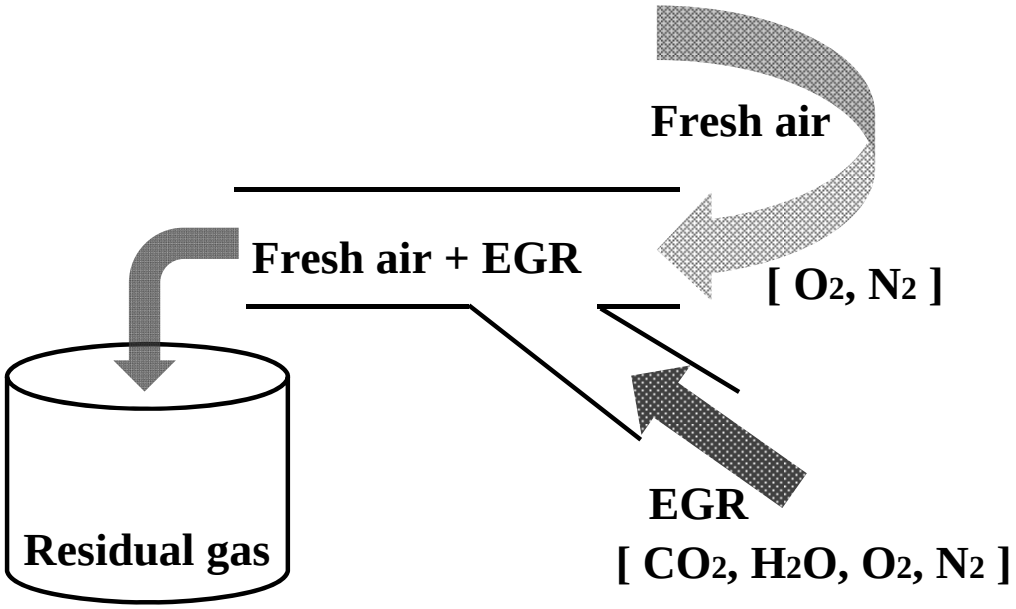

Figure 4.5 The gas composition of the in-cylinder gas.

Chapter 5. NO estimation during steady state and simple ramp transition using a real-time virtual NO sensor

In the present chapter, to investigate the feasibility of the developed model as a real-time application, the model was implemented on the embedded system (ETAS, ES-1000) bypassed from a conventional engine control unit (ECU) for real-time estimation of NO during engine operations. Additionally, the effect of EGR was investigated to emphasize the importance of accurate EGR measurement in the use of the model in real application. Model results were compared to real-time measurement of engine-out NO of a conventional diesel engine at representative steady state operating points which cover the entire NEDC. Also, EGR rate and main injection timing were varied to verify the predictability of the model under various conditions.

In addition, to verify transient estimation of NO, the engine-out NO was measured by a fast NO analyzer and compared with the results of the model during simple ramp transition conditions such as engine speed change, load change and simultaneous change of them.

5.1 Experimental cases

5.1.1 Steady state cases

To compare the steady state results of the model to engine-out NO of a conventional diesel engine, representative steady state operating points which cover the entire NEDC cycle were selected. Also, based on a conventional engine operation map, the EGR rate and the main injection timing sweep were conducted to verify the predictability of the model under various conditions. The other engine operating variables (pilot and post injection strategies, boost pressure, rail pressure, etc.) were fixed at the same engine speed and brake mean effective pressure (BMEP) condition. To investigate the robustness of the model at different methods for EGR supplying, the same experiment was repeated under only HP-EGR and only LP-EGR cases except 1250 rpm/3 bar and 2250 rpm/3 bar conditions. All experiments were performed when the engine was fully warmed-up. The entire experimental cases are shown in Table 5.1.

5.1.2 Simple ramp transition cases

To investigate the transient estimation of NO, the engine-out NO was measured by the fast NO analyzer through simple ramp transient operations and compared to the results of the model. EGR change, RPM change, simultaneous RPM and load change are included. Detailed transient conditions are described in the results part for convenience.

Table 5.1 Experimental cases.

Engine speed [RPM]	BMEP [bar]	Target EGR [%]	Main injection timing [BTDC CAD]
1250	3	42, 35	4.6, 2.6, 0.6
1500	4	40, 35, 30, (25, 20, 15)	5.1, 3.1, 1.1 (1.1)
1500	6	30, 25, 20 (15)	5.1, 3.1, 1.1, (1.1)
1750	6	27, 20, 15	5.9, 3.9, 1.9
1750	8	21, 15, 10	6.4, 4.4, 2.4
2000	6	27, 20, 15	7.2, 5.2, 3.2
2000	8	23, 20, 15	7.6, 5.6, 3.6
2000	10	21, 15	7.9, 5.9, 3.9
2250	3	35, 30	6.5, 4.5, 2.5

5.2 Experimental results

5.2.1 Steady state results

The model was validated on 76 cases using only HP-EGR and 55 cases using only LP-EGR shown in Table 5.1. 30 seconds average value of measured NO was used for the each experimental result and the NO estimation was done with the 100 cycle averaged in-cylinder pressure and other input parameters. The variables which are necessary for NO calculation, such as AFR, air mass, etc., were brought from the ECU for 30 seconds and averaged values were used as input variables. Figure 5.1 shows the validation results of the model on steady state conditions. It was found that the model showed ± 10 ppm error under 100 ppm NO region and about ± 10 % error under 150 ppm NO region compared to the experimental results. The level of accuracy of the model is close to the conventional mass product portable NO_x sensor although there are higher errors at some points.

The R^2 value of the results for HP-EGR and LP-EGR cases were 0.96 and 0.94, respectively. These are a little lower than that is shown in the validation result with CFD (R^2 = 0.98) shown in previous study [90]. However, its correlation is still high enough. The validation results at the LP-EGR cases show the robustness of the model to not only the change of hardware but also the broad range of intake air temperature.

5.2.2 Simple ramp transition results

5.2.2.1 EGR rate change

Figure 5.2 shows the real-time NO estimation of the model and measured NO by the fast NO analyzer simultaneously. At the engine speed of 1200 rpm, the EGR

rate was varied suddenly from 40 % to 10 % and then return to 40 %. The other parameters except the EGR rate, such as fuel mass, injection timing and boost pressure, were all maintained. The EGR rate was controlled by controlling an air control valve using the programmable ECU. It is shown that the model predicts NO very well during the EGR change and the NO fluctuation due to the pulsation of air control during a quasi-unstable state was well reflected in the estimation model.

5.2.2.2 Engine speed change

Figure 5.3 shows the model validation result during engine speed change. The engine speed was varied from 1200 to 1500 RPM and EGR rate was increased, following the map programmed in ECU due to the change of the operation region. It is shown that the model predicted the real-time amount of NO well during RPM and EGR changes.

5.2.2.3 Simultaneous engine speed and load change

To verify the incorporating performance of the model, engine speed and load were changed simultaneously as shown in the upper profile of Figure 5.4. Since almost engine operating variables were mapped on the basis of engine speed and fuel mass, change of them resulted in the simultaneous change of many operating variables such as EGR rate, rail pressure, injection strategy, boost pressure and so on. The validation result showed that the model can predict the real-time NO well in various operating conditions and the transient situations.

5.2.3 Source of error

It is thought that the errors come from the EGR estimation and other inputs such as air flow rate and AFR. From the sensitivity analysis of EGR on NO estimation on chapter 2, it was shown that 1 % error of EGR measurement (estimation) can cause at least 5 % to max 15 % error to NO estimation.

Additionally, accuracy of air flow sensor and input parameters from ECU can affect the calculation of in-cylinder mass and consequently; the estimation of in-cylinder temperature can be affected.

There is also limit of EZM in estimation of NO on various load conditions. The error from model assumptions also exists. The characteristic time for equilibrium of NO formation is short enough to affect the calculation of NO formation rate when the combustion temperature is very high. Determination of NO formation duration also contains error as described in Figure 2.7. The fixed value for residual EGR can be source of error.

As described in Table 2.3, the residual EGR rates are different with varying engine load and speed. However, in this model, the residual EGR rate was fixed to 0.047 for all engine load and speed condition for convenience. This can affect the actual in-cylinder EGR rate and consequently cause same error from EGR measurement.

There were also issues about gas constant and specific heat ratio that participate in calculation of NO. Generally, gas constant and specific heat ratio are dependent on gas concentration and temperature. However, in this model, fixed values were used based on pre-calculation using CFD model.

5.2.4 Improvement of model accuracy using modified R and k

If more accurate gas constant and specific heat ratio are used, the model accuracy could be improved. From Amagat's law, the volume of gas mixture consists of partial volume of each gas as expressed in equation (5.1) [103].

$$\mathrm{V} = V_A + V_B + \cdots \tag{5.1}$$

where V is the volume of gas mixture, V_A and V_B are partial volume of gas A and B relatively.

For n moles of gas mixture, mole fraction (x) can be defined.

$$\frac{V_A}{V} = \frac{n_A}{n} = x_A, \quad \frac{V_B}{V} = \frac{n_B}{n} = x_B \tag{5.2}$$

Molecular weight of gas mixture (M_{mix}) can be calculated using equation (5.3).

$$M_{mix} = M_A x_A + M_B x_B \tag{5.3}$$

where M_A and M_B are molecular weight of gas A and B relatively.

Then, gas constant of gas mixture (R_{mix}) can be derived by equation (4.4)

$$R_{mix} = \frac{\bar{R}}{M_{mix}} \tag{5.4}$$

where $\bar{R}$ is universal gas constant. (8.3244 kJ/kmol·K)

From ideal gas equation, following relation can be derived.

$$\frac{C_v}{R} = \frac{C_p}{R} + 1 \tag{5.5}$$

Using polynomial curvefit method expressed in equation (4.6) and values in Table 5.2, $\frac{C_p}{R}$ can be calculated.

$$\frac{C_p}{R} = c_1 + c_2 T + c_3 T^2 + c_4 T^3 + c_5 T^4 \tag{5.6}$$

where c_1,c_2,c_3,c_4,c_5 are polynomial constants for certain gas and T is temperature.

Then, by substituting it to equation (5.5), $\frac{c_v}{R}$ can be calculated and specific heat ratio ($k = \frac{C_p}{C_v}$) can be calculated.

Figure 5.5 shows the specific heat ratio as a function of EGR rate on various engine load and speed conditions. Increase of EGR rate results in decrease of specific heat ratio. In general, increase of EGR rate also results in decrease of burned gas temperature. Therefore, the use of modified specific heat ratio decreases the maximum burned gas temperature as EGR rate increases. Meanwhile, it is shown that the increase of temperature at the SOC (increased engine load and rpm) decreases the specific heat ratio. Then, the modified specific heat ratio decreases the maximum burned gas temperature than when using a fixed specific heat ratio. The effect of decreased maximum temperature at relatively low temperature region, eg. Increased EGR, is lower than that at relatively high temperature region, eg. Increased engine load and rpm. Consequently, the use of modified specific heat ratio decreases the sensitivity of model on change of maximum burned gas temperature. By using these gas constant and specific heat ratio which consider the gas concentration and temperature, the steady state results were calculated again. Figure 5.6 shows the steady state matching result when modified R and k are used in the model. It is shown that R^2 is improved from 0.96 to 0.972 and it means that the model accuracy can be improved by using modified R and k values for each condition.

5.2.5 Cycle-by-cycle & cylinder-by-cylinder NO estimation

Developed model can basically estimate cycle-by-cycle NO because model receive engine control parameters (AFR, air mass, injection strategy) and pressure data of every cycle. Additionally, cylinder-by-cylinder NO can be estimated if

pressure sensors for each cylinder are used. However, it was not confirmed that cylinder-by-cylinder NO deviation actually exist and model estimates the deviation. Therefore, NO was measured at two sampling points which are at right after exhaust ports of cylinder #1 and cylinder #4 using a fast NO_x analyzer. To confirm the cylinder-by-cylinder NO estimation, pressures at cylinder #1 and cylinder #4 were measured using two pressure sensors. Figure 5.7 shows the comparison results of cylinder-by-cylinder & cycle-by-cycle NO between model and measurement at 1500 rpm and 5.5 bar bmep condition. Similar level of cycle-by-cycle NO variation was found for both of NO estimation and measurement. More NO change can be found in data from fast NO_x analyzer and it comes from difference of real-time measurement and discrete model estimation. Additionally, it was shown that there was actual NO deviation between cylinder #1 and cylinder #4 about 10 ppm and model could predict this deviation well.

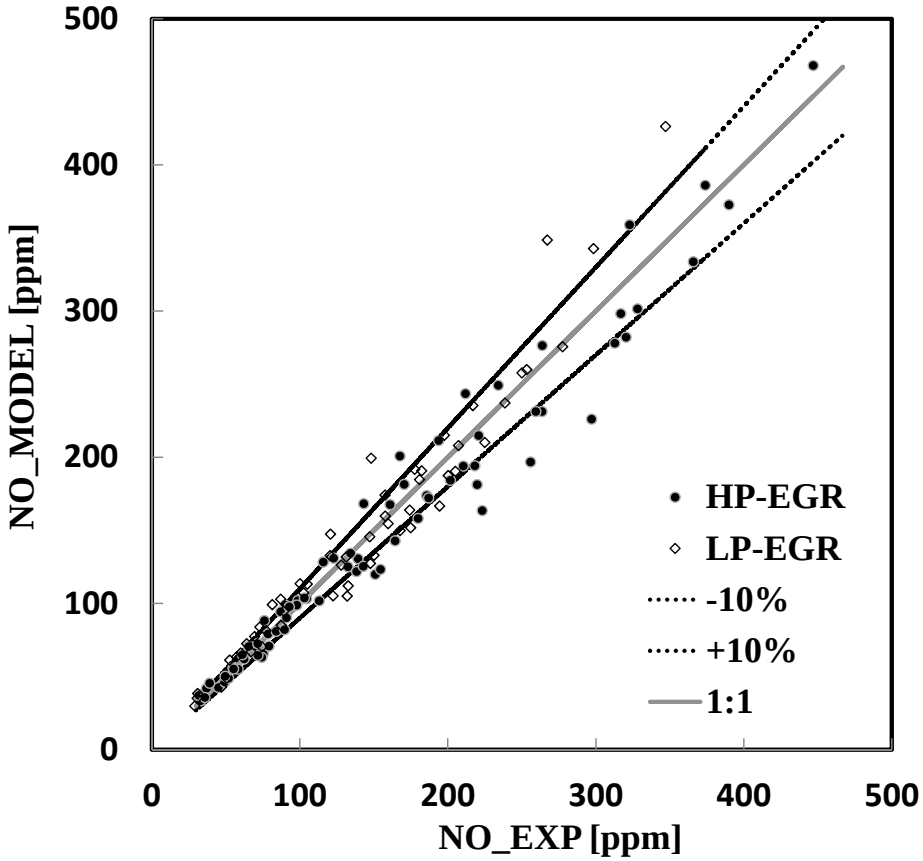

Figure 5.1 The model validation on 131 steady state conditions with experimental results.

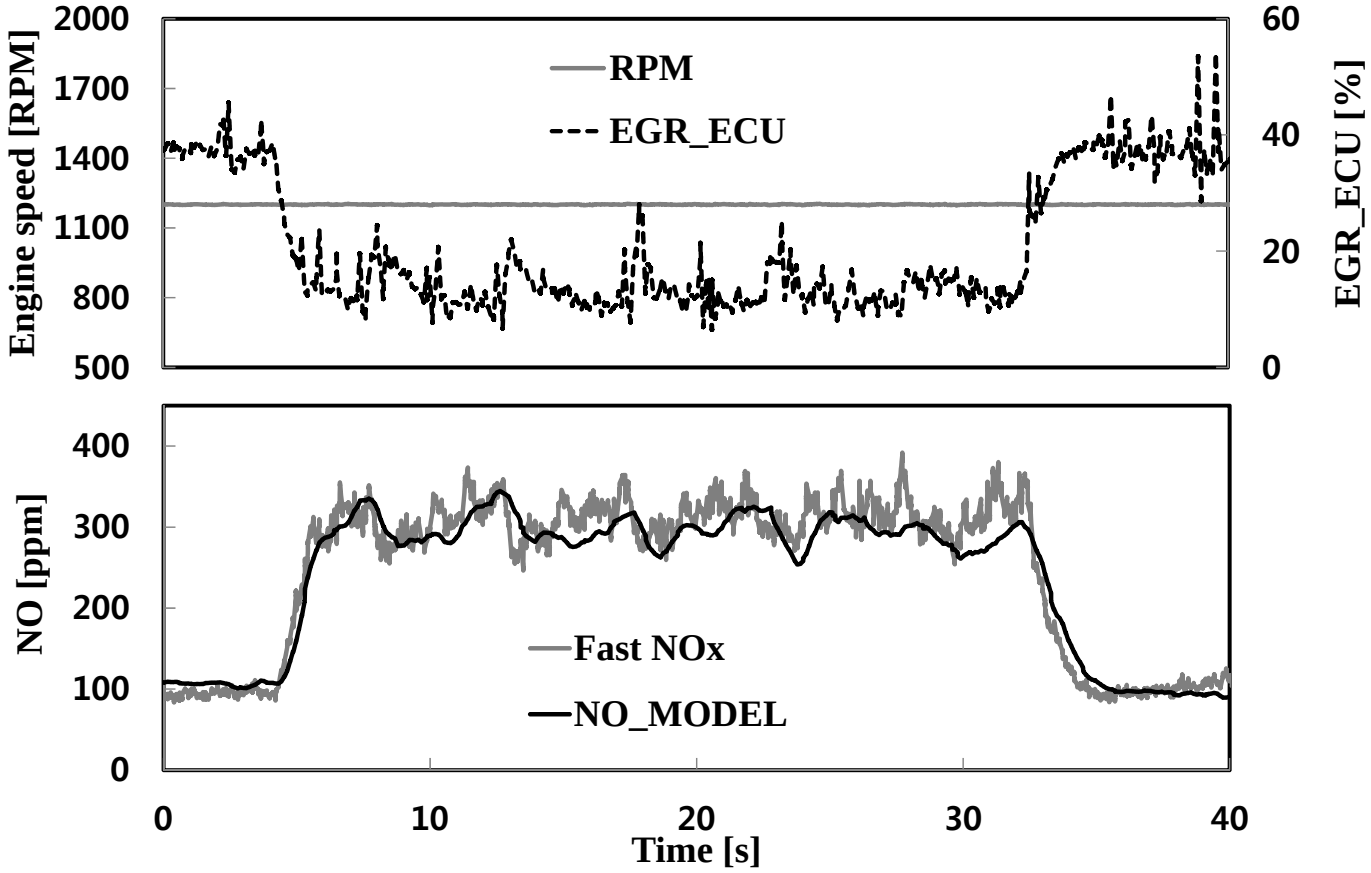

Figure 5.2 Model validation during EGR change.

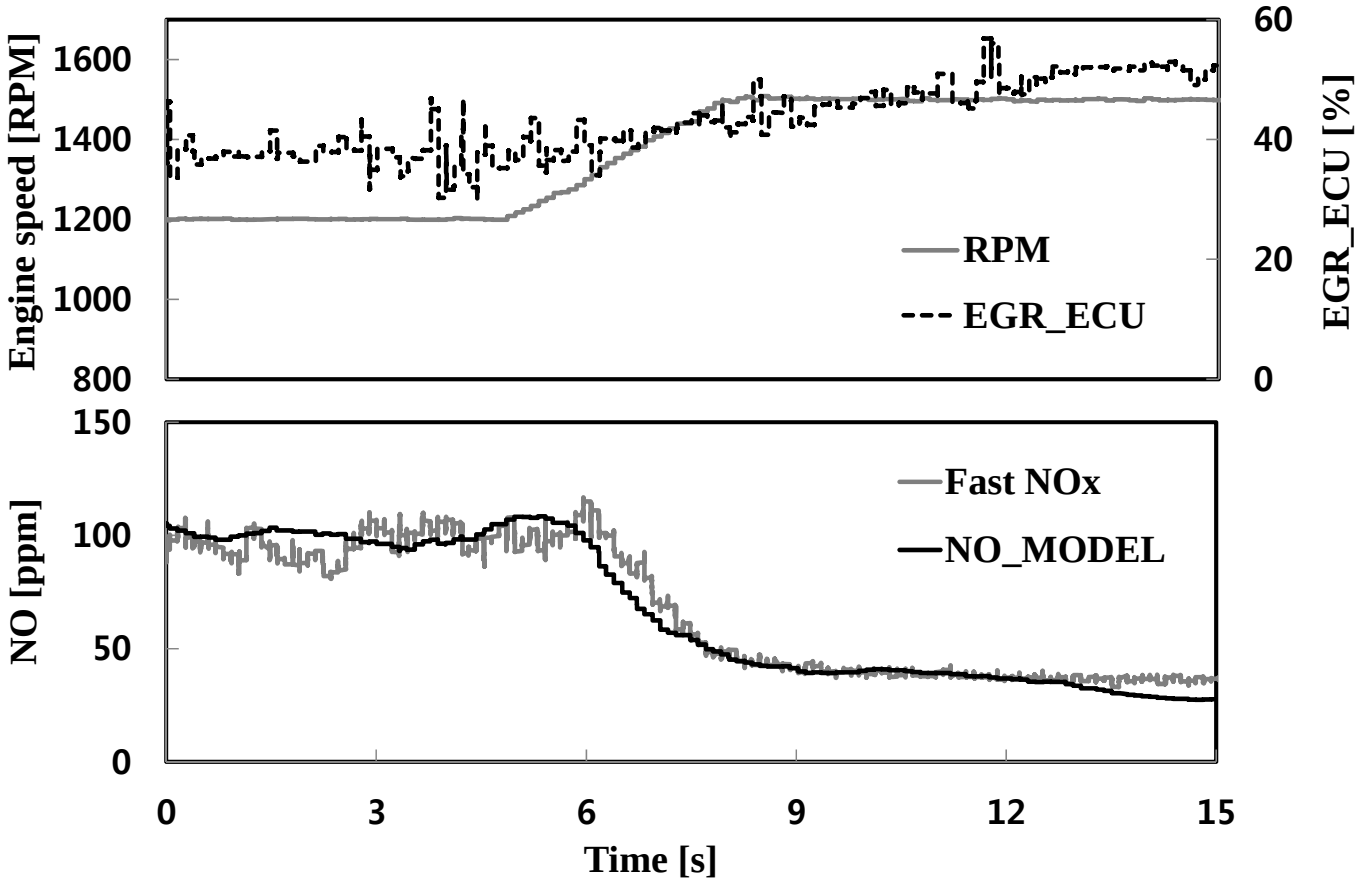

Figure 5.3 Model validation during engine speed change.

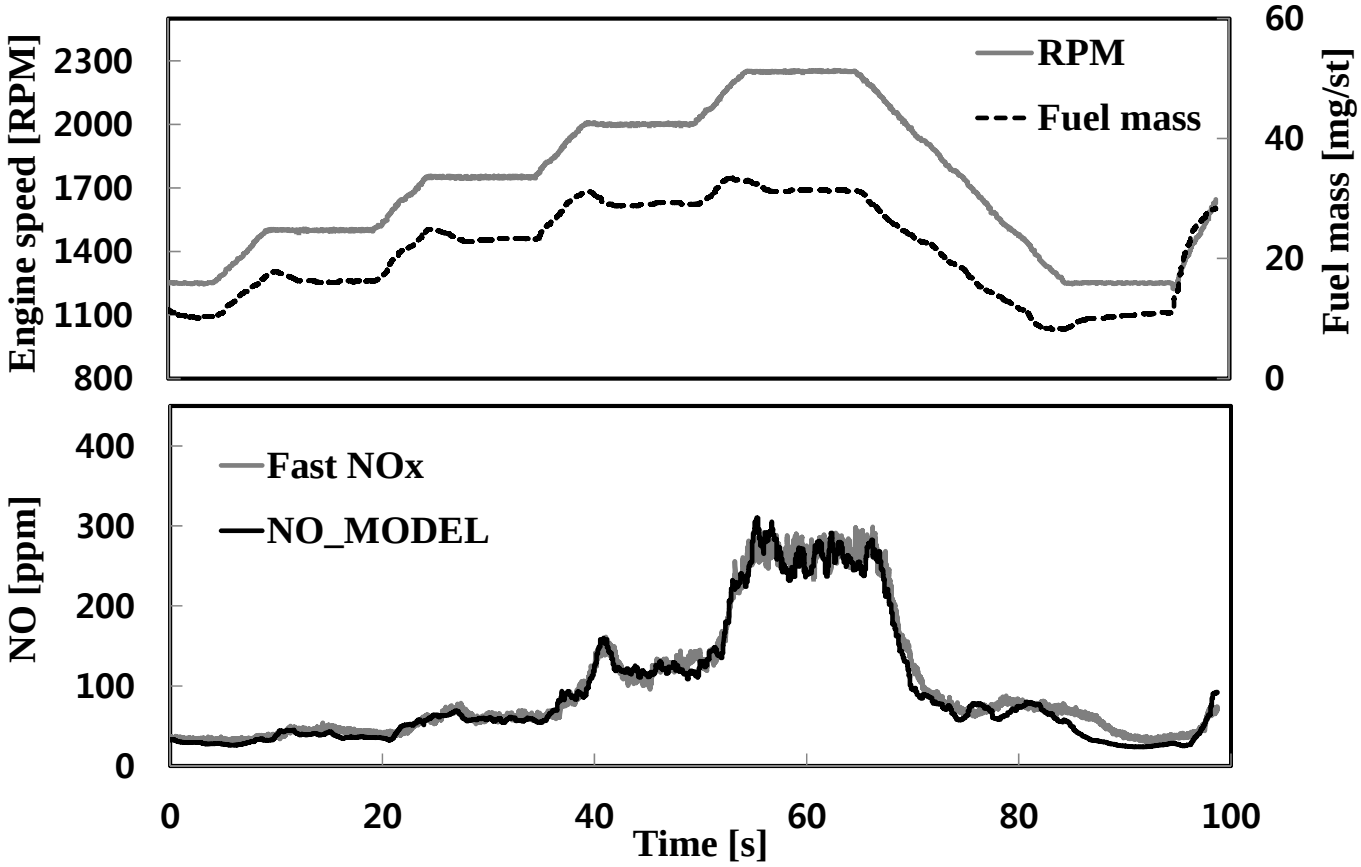

Figure 5.4 Model validation during engine speed change.

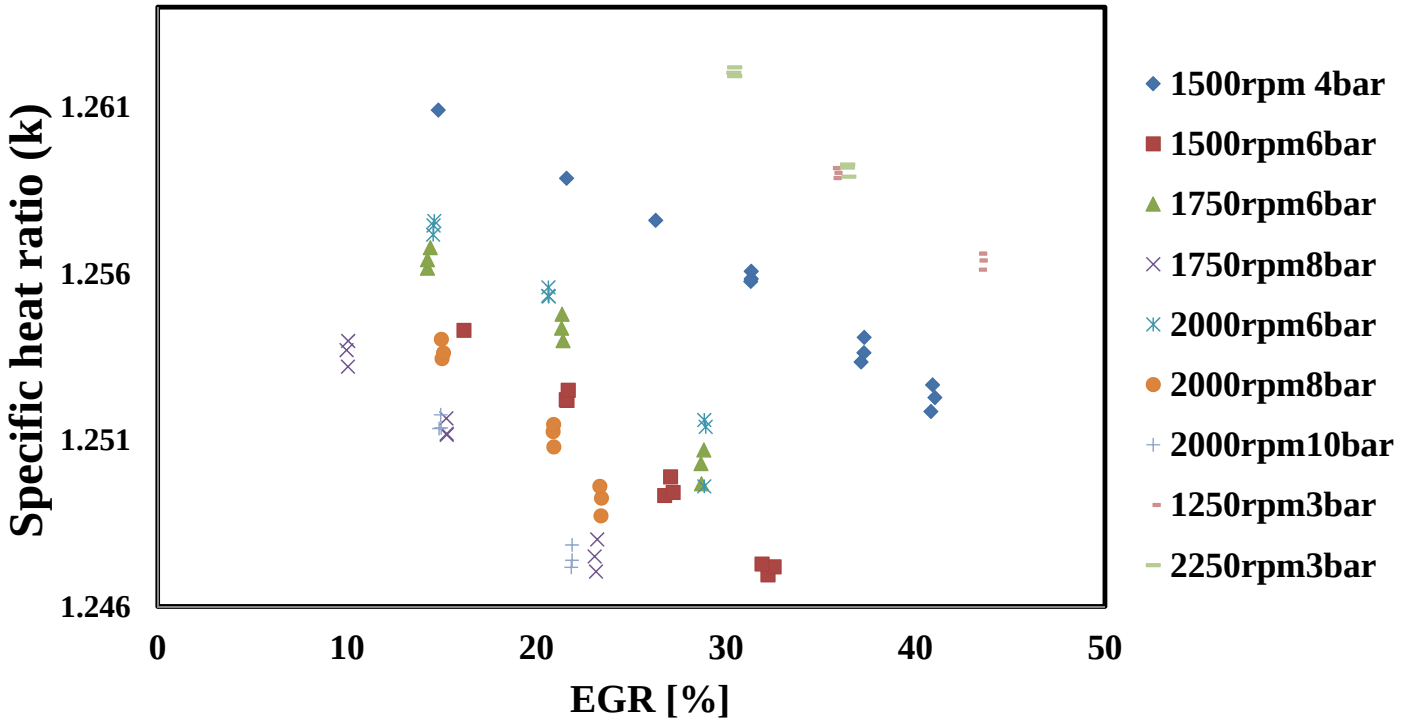

Figure 5.5 Modified specific heat ratio as a function of EGR rate under various engine load and speed conditions.

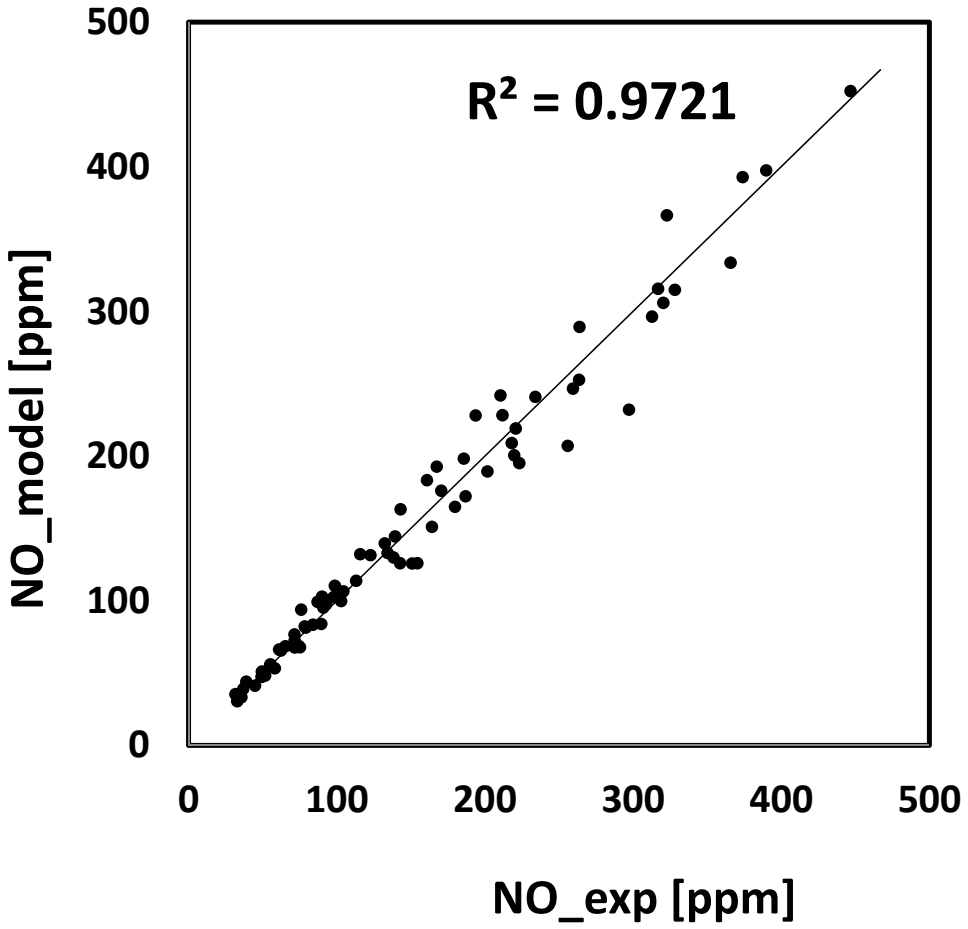

Figure 5.6 The steady state matching result of NO estimation model with experimental results using modified R and k under HP-EGR conditions.

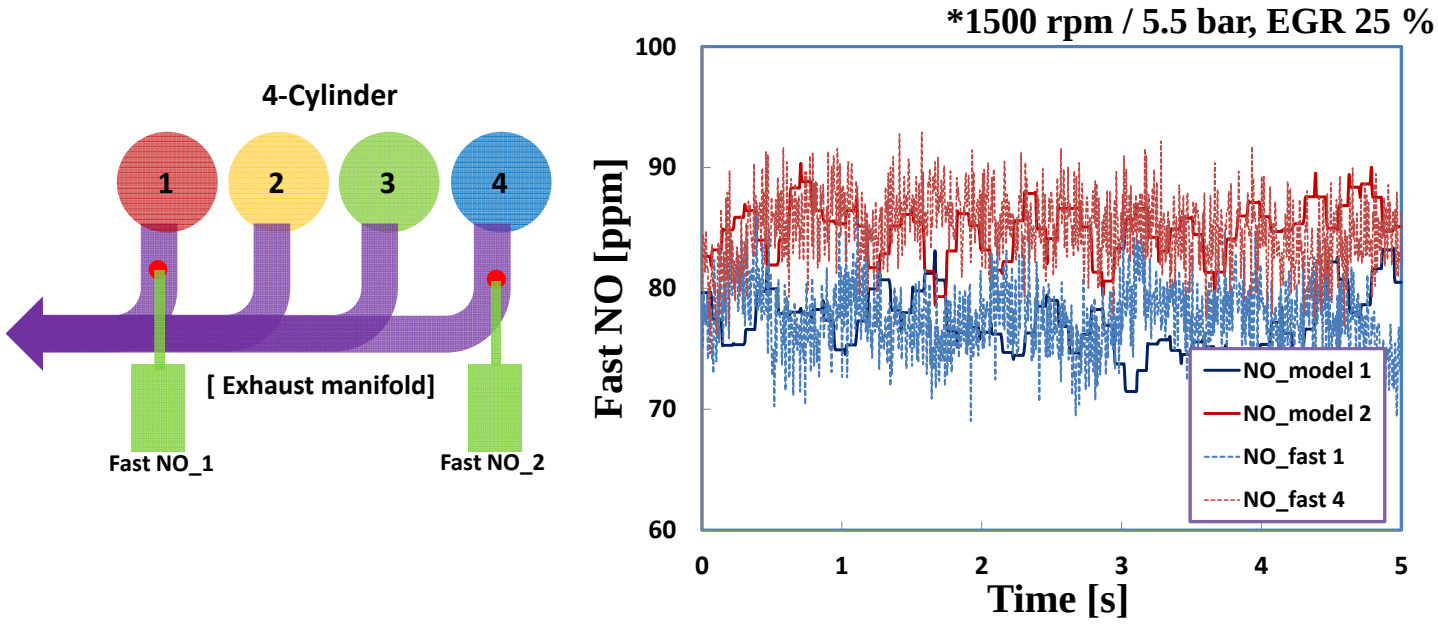

Figure 5.7 The comparison of cycle-by-cycle and cylinder-by-cylinder (cylinder #1 and cylinder #4) NO estimation with measurement using fast NOx analyzer at 1500 rpm and 5.5 bar condition.

Table 5.2 Polynomial curve fit coefficients for modified gas constant and specific heat ratio.

	CO_2(low)	CO_2(high)	H_2O(low)	H_2O(high)	N_2(low)	N_2(high)	O_2(low)	O_2(high)
C1	2.27572	4.45362	3.38684	2.67215	3.29868	2.92664	3.21294	3.69758
C2	0.0099221	0.00314	0.003475	0.0030563	0.0014082	0.001488	0.0011275	0.0006135
C3	1.04E-05	-1.28E-06	-6.35E-06	-8.73E-07	-3.96E-06	-5.68E-07	-5.76E-07	-1.26E-07
C4	6.87E-09	2.39E-10	6.97E-09	1.20E-10	5.64E-09	1.01E-10	1.31E-09	1.78E-11
C5	-2.12E-12	-1.67E-14	-14.50659	-6.39E-15	-2.44E-12	-6.75E-15	-8.77E-13	-1.14E-15
Enthalpy	-4.84E+04	-48967	-30208.1	-2.99E+04	-1.02E+03	-9.23E+02	-1.01E+03	-1.23E+03
Entropy	1.02E+01	-0.955396	2.59023	6.86E+00	3.95E+00	5.98E+00	6.03E+00	3.19E+00

Chapter 6. NO_x estimation during transient state using a real-time virtual NO_x sensor

In this chapter, to verify the performance and to investigate the characteristics of the real-time estimation of the model, the engine-out NO emissions measured by a fast NO_x analyzer and the estimated NO emissions were compared during not only simple ramp transitions, but also ECE-15 and EUDC cycles. Furthermore, to extend the NO model to a complete NO_x estimation model, an empirical NO_2 estimation model is proposed based on the experiments under steady-state conditions. The in-house EGR estimation model was also applied in the NO_x estimation model for accurate cycle-by-cycle estimation and used as an input during transient engine operations. This chapter is part of published conference paper of author in 2013 [104].

6.1 Extend to NO_x (NO_2) estimation model

For most of the proposed NO_x models, the portion of NO_2 in NO_x is not considered because not only do those models assume that the NO is a predominant in-cylinder product but also there is no obvious mechanism, such as the Zeldovich mechanism for NO_2 formation. NO_2/NO ratios are reported that they are negligibly small in spark-ignition engines; however, NO_2 in a diesel engine can be 10 to 30 % of the total exhaust oxides of NO_x [14]. Therefore, NO_2 estimation is needed in the NO_x estimation model for diesel engines.

In the present study, an empirical NO_2 estimation model was developed using experimental data under various engine operating conditions in wide regions. Table 6.1 describes the experimental conditions used in the NO_2 estimation model. Figure 6.1 shows the NO_2/NO_x ratio as functions of the exhaust gas temperature, boost pressure, main injection timing and NO.

The NO_2/NO_x ratio should be expressed as a function of the engine speed and the amount of fuel especially at steady-state operating conditions because almost all engine operating variables, such as boost pressure and main injection timing, are mapped as a function of engine speed and the total fuel injected. Advanced SOI and higher boost pressure are needed to acquire higher torque with increased amount of fuel and it results in increase of combustion temperature and NO formation. Then, NO_2/NO_x decreases as NO increases. However, this is not always valid at a transient state because the actual air system reacts much more slowly than the demanded control and injection system. As shown in Figure 6.1-(d), it was observed that the NO_2/NO_x ratio can simply be expressed as a function of NO and is independent of engine speed and fuel amount. Thus, the NO to NO_x map was made as a form of a 1-D fitting curve, as demonstrated in Figure 6.2. Once the NO is calculated as an output of the NO model, by multiplying the NO to NO_x ratio on table, NO_x comes out as an output of the NO_x model. The values which are not

listed in the table are linearly interpolated. The reason why the fitting map is constructed with a table rather than a formula is that the table is able to counter the sudden gradient changes where it is vague and hard to interpret these rapid sensitivity variations in the formula.

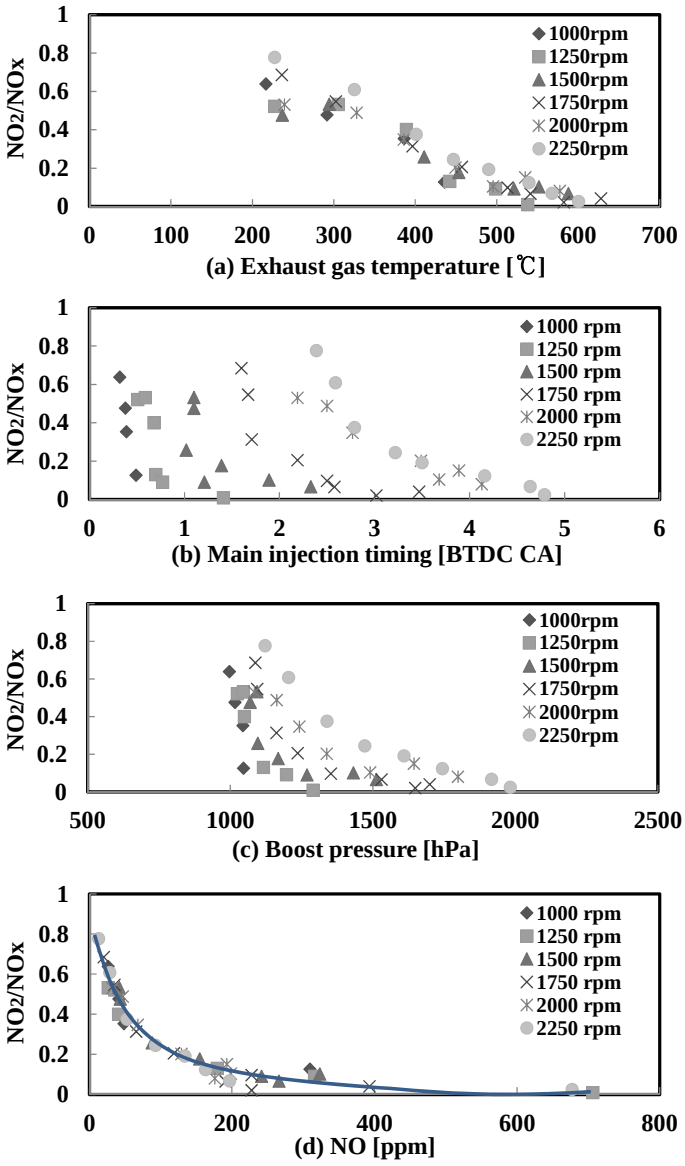

Figure 6.1 The effect of (a) exhaust gas temperature, (b) main injection timing, (c) boost pressure and (d) NO on the NO2/NOx ratio at operating conditions given in Table 6.1.

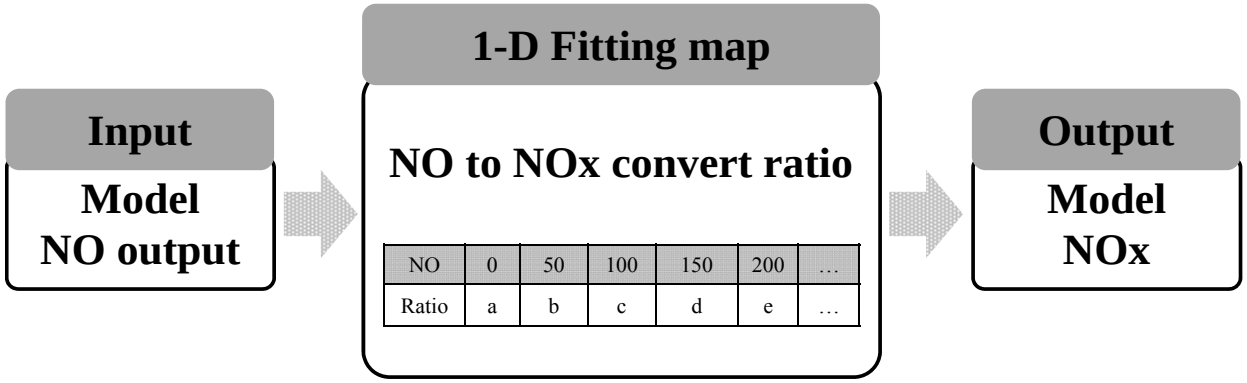

Figure 6.2 The scheme of the NO to NOx table.

Table 6.1 Test conditions for NO to NO_x table.

Engine speed [RPM]	Fuel mass [mg/st]
1000	10, 15, 20, 25
1250	10, 15, 20, 25, 30, 35
1500	10, 15, 20, 25, 30, 35, 40
1750	10, 15, 20, 25, 30, 35, 40, 45
2000	10, 15, 20, 25, 30, 35, 40
2250	10, 15, 20, 25, 30, 35, 40, 45

6.2 Experimental conditions

The validation at the steady-state engine operating conditions and simple transient conditions was performed in previous chapter. In this chapter, to investigate faster, realistic transient estimation of NO emissions, the engine-out NO emissions were measured by a fast NO analyzer under the ECE-15 and EUDC cycle. The engine was fully warmed up to 85 ℃ (both engine oil and coolant temperature at the start of the cycle). The velocity profiles for the ECE-15 and EUDC cycle are shown in Figure 6.3. The velocity profile is converted to engine speed and torque profile in accordance with the gear ratio so that it can be applied to the dynamometer.

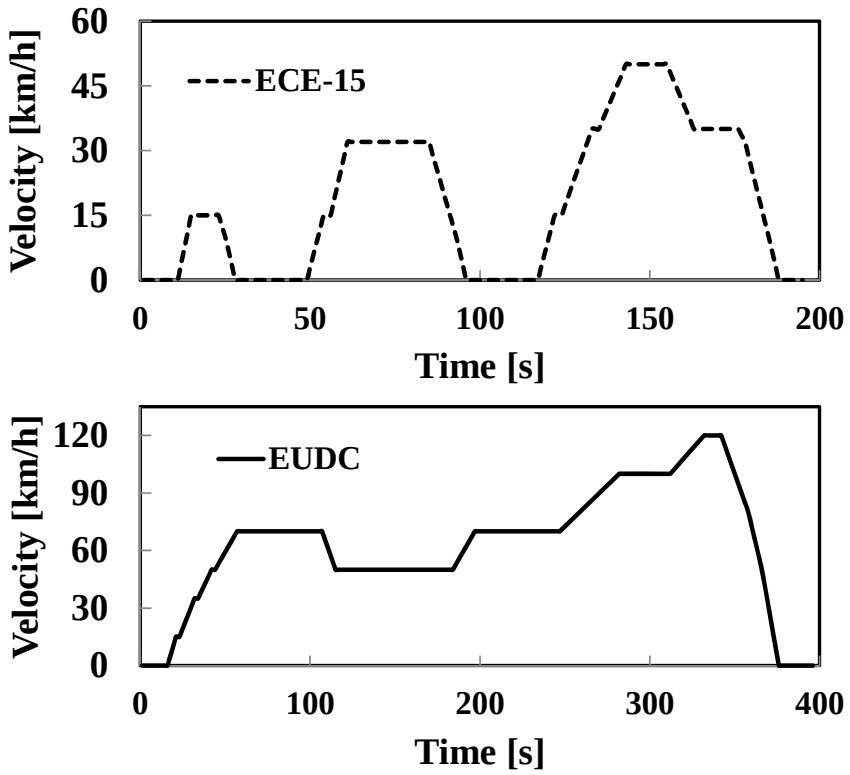

Figure 6.3 Velocity profiles of the ECE-15 and EUDC cycle.

6.3 Results and discussions

Figure 6.4 shows the comparison of the predicted NO (NO_x) and measured NO (NO_x) during the ECE-15 and EUDC cycles in real-time. NO_x was measured by an exhaust gas analyzer (Horiba, MEXA-7100DEGR) because the fast NO analyzer needs an additional NO_x converter to measure NO_x. Additionally, for simultaneous measurement of NO and NO_x, the use of two sets of equipment was needed. It is shown that the model predicts the real-time NO and NO_x emissions well compared with the measurement results.

Much higher peaks of NO than that are expected in similar steady-state conditions are shown in Figure 6.4. This is because when the engine speed and the load is changing, injection parameters, such as injection timing, quantity and multiple injection strategy, can be changed cycle-by-cycle; However, the actual air system, such as boost pressure, fresh air and EGR, cannot respond to demanded control as fast as the other parameters due to its inertia effect and need of emptying and filling process. It causes, for example, the instantaneous mismatch of actual EGR to target EGR and leads to higher or lower production of NO_x than that are expected in steady-state conditions. Therefore, if the cycle-by-cycle NO_x estimation is performed in the ECU, there is a potential that unwanted higher NO_x emission can be lowered by fast combustion control, for example, by retarding the main injection timing.

The image from Figure 6.4-(a) is magnified from 120~150 s in Figure 6.5. In addition, the result of the simultaneous NO measurement using the exhaust gas analyzer is also described. It is shown that the exhaust gas analyzer had a measurement delay of approximately 5 seconds compared with the fast NO analyzer. Additionally, it can be observed that the result of the exhaust gas analyzer is smoother. Increasing and decreasing rate is also lower than that of the fast NO analyzer. It is due to not only the difference in the response time of the analyzer

itself but also the longer sampling line of the exhaust gas analyzer. However, the total amount of measured NO by the two sets of equipment agrees well with the calculation of the integral on time.

For a quantitative analysis of the results, a 5-second average value was obtained using the raw data. The left side of Figure 6.6 shows the 5-second average profiles of the predicted and measured NO and NO_x. The measurement delay of the exhaust gas analyzer is corrected. The right side describes the degree of matching of the model and measurement using the 5-second window. It can be observed that the model predicts the NO and NO_x emission during the emission cycles well with a high R2 values.

From the results, the total amount of NO and NO_x can be calculated using the air flow rate and injected fuel mass. Additionally, because the distance of each cycle is known, the mass per km can be obtained. The results are shown in Table 6.2. The total mass per km of NO and NO_x the emissions during emission cycle showed errors within 7.6 %.

The main sources of error of the NO_x estimation model are inaccurate input parameters, such as injection quantity and air flow rate from the ECU. Another source of error is error from the EGR model. It was observed that the 1% of error in EGR estimation could cause over 12 % of error in NO estimation in the low EGR region in previous study [90]. Additionally, the limit of the EZM can be the source of error. It was reported that the EZM over-estimates the NO as a function of BMEP [105]. The model assumptions can also cause error when the combustion temperature is very high that the characteristic time for equilibrium of NO formation is short enough to affect the calculation of NO formation rate. The sensitivity analysis is needed in future works.

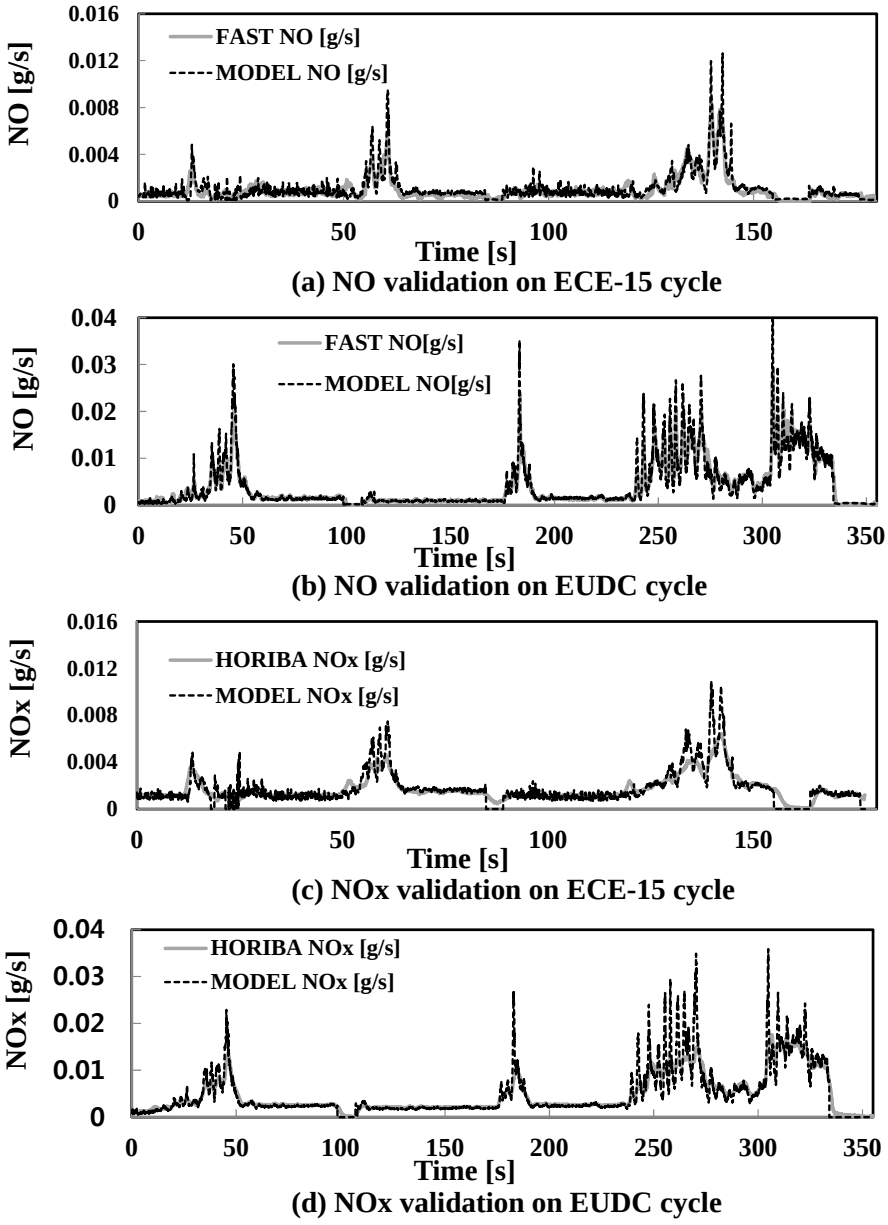

Figure 6.4 The validation results of NO and NOx estimation of the model during ECE-15 and EUDC cycle.

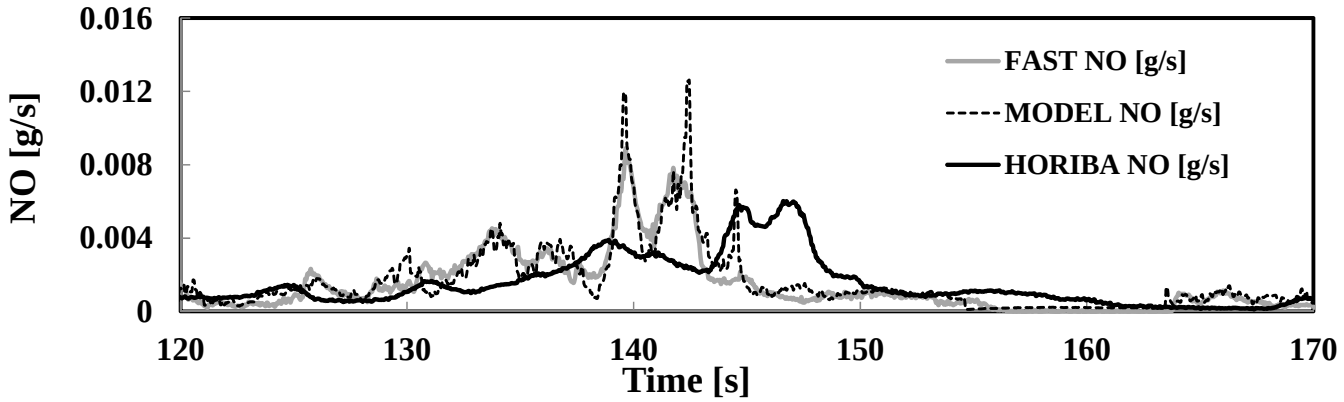

Figure 6.5 The comparison of measurement characteristics between fast NO analyzer and exhaust gas analyzer during part of the ECE-15 cycle.

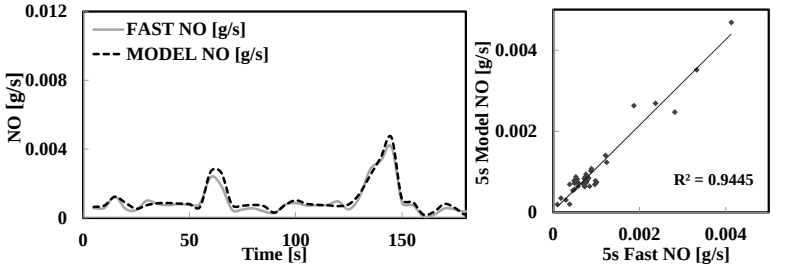

(a) 5s average NO validation on ECE-15 cycle

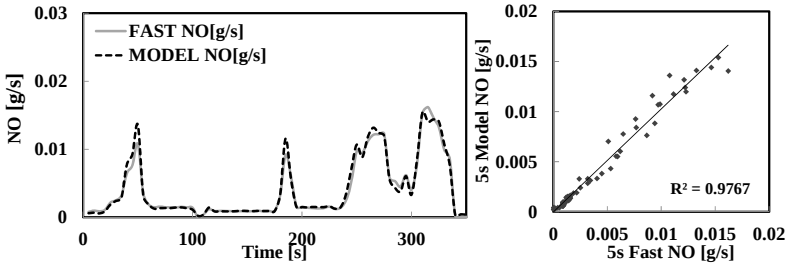

(b) 5s average NO validation on EUDC cycle

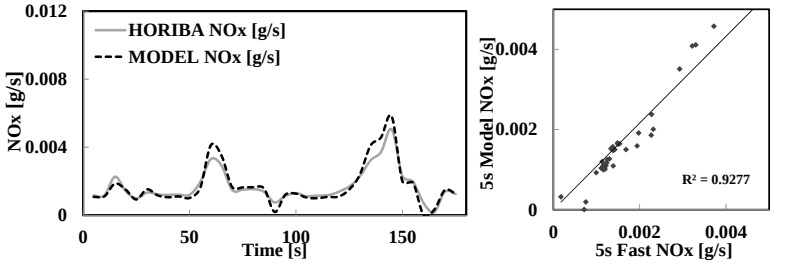

(c) 5s average NOx validation on ECE-15 cycle

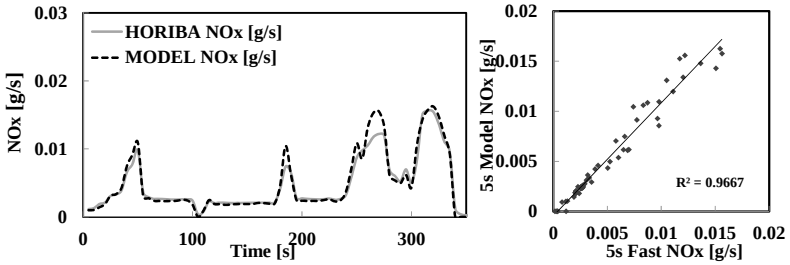

(d) 5s average NOx validation on EUDC cycle

Figure 6.6 The validation results of 5s average NO and NOx estimation of the model on ECE-15 and EUDC cycle.

Table 6.2 ECE-15 and EUDC cycle results.

[g/km]	Horiba	Fast NO	Model
ECE-15 (NO)	0.052	0.048	0.051
ECE-15 ((NOx)	0.075	X	0.073
EUDC (NO)	0.211	0.206	0.195
EUDC (NOx)	0.247	X	0.239

Chapter 7. Conclusion

In this study, the physics-based NO_x estimation model based on in-cylinder pressure and data available from ECU was developed. The model used extended Zeldovich mechanism for NO_x estimation and the calculation process was simplified by investigation using CFD. The merits of the developed model are:

1. Because the model uses only one empirical constant, mapping and training procedure are convenient. Therefore, the model could be easily applied to the engine using a few engine measurement data from the engine development or test process.

2. The process of calculating and predicting the NO formation is simple; therefore, the model can predict the cycle-to-cycle NO formation in real time.

3. The model can reflect changes in engine operating conditions because it makes use of the in-cylinder pressure. Thus, the model demonstrates good agreement with the CFD results for the overall NO range.

From the sensitivity analysis, it was found that EGR had a huge impact on the NO estimation model. Thus, EGR measurement was carefully done during the experiment. The model was verified using a light duty Diesel engine for not only steady state operating conditions but also for simple transient operations. From the steady state validation, the model showed ± 10 ppm error under 100 ppm NO region and ± 10 % error under 150 ppm NO region compared to the experimental results. The real-time model was also compared to the measurement using a fast NO_x analyzer in the transient state varying engine speed, EGR rate, load and so on. The results showed that the model predicts the real-time NO well.

Additionally, an empirical NO_2 estimation model was developed using experimental data to predict the total NO_x emissions. From the analysis, the

NO_2/NO_x ratio can be expressed as a function of the amount of NO. Additionally, the EGR estimation model that can estimate the cylinder-by cylinder EGR was used as an input to the NO_x estimation model. From the validation during the ECE-15 and EUDC cycles, the model predicted the transient NO and NO_x well and showed a potential as a virtual NO_x sensor. The results showed that the error of the total mass per kilometer of NO and NO_x for the ECE-15 and EUDC cycle was less than 7.6 %.

It can be concluded that the presented model can reliably estimate engine-out NO_x. Therefore, this model can be applied to an engine as a good tool for controlling engine-out NO and after-treatment systems without the need for the NO_x sensor. Moreover, the estimation model can be applied to 1-D simulations, such as GT-SUITE and AMESIM, and it shows improved NO_x estimation results than that of their own NO_x model as the model is able to predict the NO level as same standard as the 3-D CFD simulation.

Bibliography

1. SANJAY, M.C., *A review of NOx formation under gas-turbine combustion conditions.* Combustion Science and Technology, 1993. **87**(1-6): p. 329-362.

2. MAURO, A.G., et al., *Mild combustion for fuel-NOx reduction.* Combustion Science and Technology, 2004. **176**(7): p. 1035-1054.

3. Hasegawa, T., *Prediction Methodology of Fuel-NOx Emissions in Gasified Fuels' Combustion.* International Journal of Gas Turbine, Propulsion and Power Systems, 2010. **3**(1).

4. Williams, A., et al., *A review of NOx formation and reduction mechanisms in combustion systems, with particular reference to coal.* Journal of the Institute of Energy, 1997. **70**(484): p. 102-113.

5. Danzon, M.A., R. Van Leeuwen, and M. Krzyzanowski, *Air quality guidelines for Europe*2000: World Health Organization, Regional Office for Europe.

6. Brunekreef, B. and S.T. Holgate, *Air pollution and health.* Lancet, 2002. **360**: p. 1233-1242.

7. EPA. Available from: http://www.epa.gov/air/nitrogenoxides/.

8. Berglund, M., et al., *Health risk evaluation of nitrogen oxides.* Scandinavian Journal of Work, Environment & Health, 1993: p. 1-72.

9. Crutzen, P.J., *The influence of nitrogen oxides on the atmospheric ozone content.* Quarterly Journal of the Royal Meteorological Society, 1970. **96**(408): p. 320-325.

10. Ricciardolo, F.L., et al., *Nitric oxide in health and disease of the respiratory system.* Physiological reviews, 2004. **84**(3): p. 731-765.

11. Kone, B.C., *Nitric oxide in renal health and disease.* American journal of kidney diseases, 1997. **30**(3): p. 311-333.

12. Pacher, P., J.S. Beckman, and L. Liaudet, *Nitric oxide and peroxynitrite in health and disease.* Physiological reviews, 2007. **87**(1): p. 315-424.

13. Lee, S.D., *Nitrogen oxides and their effects on health*1980: Ann Arbor Science Publishers.

14. Heywood, J.B., *Internal combustion engine fundamentals*1988, New York: McGraw-Hill.

15. Kummer, J., *Catalysts for automobile emission control.* Progress in Energy and Combustion Science, 1980. **6**(2): p. 177-199.

16. Heck, R.M., R.J. Farrauto, and S.T. Gulati, *Catalytic air pollution control*1995: Wiley Online Library.

17. Heck, R.M. and R.J. Farrauto, *Automobile exhaust catalysts.* Applied Catalysis A: General, 2001. **221**(1): p. 443-457.

18. Hosoya, M. and M. Shimoda, *The application of diesel oxidation catalysts to heavy duty diesel engines in Japan.* Applied Catalysis B: Environmental, 1996. **10**(1–3): p. 83-97.

19. Sharp, C., *Diesel emission regulation and emission control technologies [R].* Southwest Research Institute Internal Report, 2011.

20. Zelenka, P., W. Cartellieri, and P. Herzog, *Worldwide diesel emission standards, current experiences and future needs.* Applied Catalysis B: Environmental, 1996. **10**(1–3): p. 3-28.

21. Rexeis, M. and S. Hausberger, *Trend of vehicle emission levels until 2020 – Prognosis based on current vehicle measurements and future emission legislation.* Atmospheric Environment, 2009. **43**(31): p. 4689-4698.

22. Dieselnet. *Emission Standards >> European Union 'Cars and Light Trucks'*. Available from: http://www.dieselnet.com/standards/eu/ld.php.

23. Dieselnet. *Emission Standards >> United States 'Cars and Light-Duty Trucks-Tier 2'*. Available from: http://www.dieselnet.com/standards/us/ld_t2.php.

24. Röpke, S., G. Schweimer, and T. Strauss, *NOx formation in diesel engines for various fuels and intake gases.* SAE Paper, 1995. **950213**.

25. Ladommatos, N., et al., *The dilution, chemical, and thermal effects of exhaust gas recirculation on diesel engine emissions-Part 1: effect of reducing inlet charge oxygen.* SAE Paper, 1996. **961165**.

26. Ladommatos, N., et al., *The effects of carbon dioxide in exhaust gas recirculation on diesel engine emissions.* Proceedings of the Institution of Mechanical Engineers, Part D: Journal of Automobile Engineering, 1998. **212**(1): p. 25-42.

27. Ladommatos, N., et al. *The dilution, chemical, and thermal effects of exhaust gas recirculation on Diesel engine emissions–part 3: Effects of water vapour,"*. in *SAE International, International Spring Fuels and Lubricants Meeting*. 1997.

28. Kreso, A.M., et al., *A study of the effects of exhaust gas recirculation on heavy-duty diesel engine emissions*1998: Society of Automotive Engineers.

29. Ladommatos, N., et al., *The effect of exhaust gas recirculation on combustion and NOx emissions in a high-speed direct-injection diesel engine.* SAE Paper, 1996. **960840**.

30. Pierpont, D., D. Montgomery, and R. Reitz, *Reducing particulate and NOx using multiple injections and EGR in a DI diesel.* SAE Paper, 1995. **950217**.

31. Chan, M., S. Das, and R.D. Reitz, *Modeling multiple injection and EGR effects on diesel engine emissions.* SAE Paper, 1997. **972864**.

32. Park, C., S. Kook, and C. Bae, *Effects of multiple injections in a HSDI diesel engine equipped with common rail injection system.* SAE Paper, 2004. **2004-01-0127**.

33. Kimura, S., et al., *New combustion concept for ultra-clean and high-efficiency small DI diesel engines.* SAE Paper, 1999. **1999-01-3681**.

34. Kimura, S., et al., *Ultra-clean combustion technology combining a low-temperature and premixed combustion concept for meeting future emission standards.* SAE Paper, 2001. **2001-01-0200**: p. 01-0200.

35. Hasegawa, R. and H. Yanagihara, *HCCI combustion in Dl diesel engine.* SAE TRANSACTIONS, 2003. **112**(3): p. 1070-1077.

36. Walter, B. and B. Gatellier, *Development of the high power NADI concept using dual mode diesel combustion to achieve zero NOx and particulate emissions.* SAE Paper, 2002. **2002-01-1744**.

37. Kanda, T., et al., *PCCI Operation with Fuel Injection Timing Set Close to TDC.* SAE Technical paper, 2006. **2006-01-0920**.

38. Jacobs, T.J., et al., *Lean and rich premixed compression ignition combustion in a light-duty diesel engine.* SAE TRANSACTIONS, 2005. **114**(3): p. 382-393.

39. Lee, S. and R.D. Reitz, *Spray targeting to minimize soot and CO formation in premixed charge compression ignition (PCCI) combustion with a HSDI diesel engine.* SAE Paper, 2006. **2006-01-0918**.

40. Alriksson, M. and I. Denbratt, *Low temperature combustion in a heavy duty diesel engine using high levels of EGR.* SAE Paper, 2006. **2006-01-0075**.

41. Colban, W., P. Miles, and S. Oh, *Effect of intake pressure on performance and emissions in an automotive diesel engine operating in low temperature combustion regimes.* SAE Technical paper, 2007(2007-01): p. 4063.

42. Yun, H., et al., *Development of premixed low-temperature diesel combustion in a HSDI diesel engine.* SAE SP, 2008. **2168**: p. 29.

43. Sarangi, A., G. McTaggart-Cowan, and C. Garner, *The effects of intake pressure on high EGR low temperature diesel engine combustion.* SAE Technical paper, 2010. **2010-01-2145**.

44. Singh, S., et al., *Simultaneous optical diagnostic imaging of low-temperature, double-injection combustion in a heavy-duty DI diesel engine.* Combustion Science and Technology, 2007. **179**(11): p. 2381-2414.

45. Fang, T., et al., *Spray and combustion visualization in an optical HSDI diesel engine operated in low-temperature combustion mode with bio-diesel and diesel fuels.* SAE Paper, 2008: p. 01-1390.

46. Genzale, C.L., R.D. Reitz, and M.P. Musculus, *Effects of spray targeting on mixture development and emissions formation in late-injection low-temperature heavy-duty diesel combustion.* Proceedings of the Combustion Institute, 2009. **32**(2): p. 2767-2774.

47. Kashdan, J.T., P. Anselmi, and B. Walter, *Advanced injection strategies for controlling low-temperature diesel combustion and emissions.* SAE International Journal of Engines, 2009. **2**(1): p. 1835-1856.

48. Martin, G.C., et al., *Early direct-injection, low-temperature combustion of diesel fuel in an optical engine utilizing a 15-hole, dual-row, narrow-included-angle nozzle.* SAE International Journal of Engines, 2009. **1**(1): p. 1057-1082.

49. Cheng, A., et al., *Effects of fuel volatility on early direct-injection, low-temperature combustion in an optical diesel engine.* Energy & fuels, 2010. **24**(3): p. 1538-1551.

50. Genzale, C.L., R.D. Reitz, and M.P. Musculus, *Optical diagnostics and multi-dimensional modeling of spray targeting effects in late-injection low-temperature diesel combustion.* SAE International Journal of Engines, 2010. **2**(2): p. 150-172.

51. Hountalas, D., T. Zannis, and G. Mavropoulos, *Potential Benefits in Heavy Duty Diesel Engine Performance and Emissions from the Use of Variable Compression Ratio.* SAE Technical paper, 2006. **2006-01-0081**

52. Yoshimoto, Y., M. Onodera, and H. Tamaki, *Reduction of NOx, smoke, and BSFC in a diesel engine fueled by biodiesel emulsion with used frying oil.* SAE Paper, 1999. **1999-01-3598**.

53. Yoshimoto, Y. and H. Tamaki, *Reduction of NOx and smoke emissions in a diesel engine fueled by biodiesel emulsion combined with EGR.* SAE Paper, 2001. **2001-01-0649**.

54. Nazar, J. and A. Ramesh, *Studies on Dual Fuel Operation of Karanja OIl and Its Bio-Diesel with LPG as the Inducted Fuel.* SAE Paper, 2006. **2006-01-0237**.

55. Curran, S., et al., *In-cylinder fuel blending of gasoline/diesel for improved efficiency and lowest possible emissions on a multi-cylinder light-duty diesel engine.* SAE Paper, 2010: p. 01-2206.

56. Kokjohn, S. and R. Reitz. *Characterization of Dual-Fuel PCCI Combustion in a Light-Duty Engine*. in *International Multidimensional Engine Modeling User's Group Meeting, https://imem. cray. com/2010/Meeting-2010/7*. 2010.

57. Chen, S. and O. Yanakiev, *Transient NOx emission reduction using exhaust oxygen concentration based control for a diesel engine.* SAE Paper, 2005. **2005-01-0372**.

58. Catania, A.E., R. Finesso, and E. Spessa, *Predictive zero-dimensional combustion model for DI diesel engine feed-forward control.* Energy Conversion and Management, 2011. **52**(10): p. 3159-3175.

59. Touns, M., P. Menegazzi, and P. Rouchon, *NOx trap model for lean-burn engine control.* SAE Paper, 2003. **2003-01-2292**.

60. Nieuwstadt, M.v. and O. Yanakiev, *A diesel lean NOx trap model for control strategy verification.* SAE Paper, 2004. **2004-01-0526**.

61. Parks, J., et al., *Nitrogen selectivity in lean NOx trap catalysis with diesel engine in-cylinder regeneration.* SAE Paper, 2005. **2005-01-3876**.

62. He, Y., *Development and application of a lean NOx trap model.* SAE Paper, 2006. **2006-01-0686**.

63. Willand, J., et al., *Selective Non-Catalytic NoDx Reduction in Diesel Engines Using Aqueous Urea.* SAE Paper, 1998. **982651**.

64. Koebel, M., M. Elsener, and M. Kleemann, *Urea-SCR: a promising technique to reduce NOx emissions from automotive diesel engines.* Catalysis Today, 2000. **59**(3): p. 335-345.

65. Song, Q. and G. Zhu, *Model-based closed-loop control of urea SCR exhaust aftertreatment system for diesel engine.* SAE, Warrendale, PA, Tech. Rep, 2002. **2002-01-0287**.

66. Hammer, T., et al., *Plasma-enhanced selective catalytic reduction: Kinetics of nox-removal and byproduct formation.* SAE TRANSACTIONS, 1999. **108**(4): p. 2035-2041.

67. Hammer, T., *Plasma-Enhanced Selective Catalytic Reduction of NoDx in Diesel Exhaust: Test Bench Measurements.* SAE Paper, 1999. **1999-01-3633**.

68. Müller, W., et al., *Selective Catalytic Reduction – Europe's NOx Reduction Technology.* SAE Paper, 2003. **2003-01-2304**.

69. Schmieg, S.J. and J.-H. Lee, *Evaluation of supplier catalyst formulations for the selective catalytic reduction of NOx with ammonia.* SAE TRANSACTIONS, 2005. **114**(4): p. 1786-1794.

70. Hosoya, M., et al., *The Study of NOx and PM Reduction Using Urea Selective Catalytic Reduction System for Heavy Duty Diesel Engine.* SAE Paper, 2007. **2007-01-1576**.

71. Cho, I., S. Lee, and H. Kang, *A Study on the NOx Reduction of Urea-Selective Catalytic Reduction (SCR) System in a Heavy-Duty Diesel.* SAE Paper, 2007. **2007-01-3447**.

72. Narayanaswamy, K. and Y. He, *Modelling of Copper-Zeolite and Iron-Zeolite Selective Catalytic Reduction (SCR) Catalysts at Steady State and Transient Conditions.* SAE Paper, 2008-01-0615. **2008-01-0615**.

73. Schmieg, S.J., R.J. Blint, and L. Deng, *Control strategy for the removal of NOx from diesel engine exhaust using hydrocarbon selective catalytic reduction.* SAE International Journal of Fuels and Lubricants, 2009. **1**(1): p. 1540-1552.

74. Lu, X., et al., *Experimental studies on the dual-fuel sequential combustion and emission simulation.* Energy, 2013. **51**(0): p. 358-373.

75. Timoney, D., et al., *The development of a semi-empirical model for rapid NOx concentration evaluation using measured in-cylinder pressure in diesel engines.* Proceedings of the Institution of Mechanical Engineers, Part D: Journal of Automobile Engineering, 2005. **219**(5): p. 621-631.

76. Andersson, M., et al., *A Real Time NOx Model for Conventional and Partially Premixed Diesel Combustion.* SAE Technical paper, 2006. **2006-01-0195**.

77. Arrègle, J., et al., *Sensitivity study of a NOx estimation model for on-board applications.* SAE Paper, 2008. **2008-01-0640**.

78. Arrègle, J., et al., *On board NOx prediction in diesel engines: a physical approach.* Automotive Model Predictive Control, 2010: p. 25-36.

79. Hountalas, D., N. Savva, and R. Papagiannakis. *Development of a New Physically Based Semi-empirical NO x Model Using the Measured Cylinder Pressure*. in *THIESEL 2010 Conference on Thermo-and Fluid Dynamic Processes in Diesel Engines*. 2010.

80. Guardiola, C., et al., *Semiempirical in-cylinder pressure based model for NOx prediction oriented to control applications.* Applied Thermal Engineering, 2011. **31**(16): p. 3275-3286.

81. Lianglin, W., G. Ying, and S. Wei. *Prediction of the NOx Dynamic Emissions for a Heavy Duty Diesel Engine SCR Application*. in *Power and Energy Engineering Conference (APPEEC), 2011 Asia-Pacific*. 2011. IEEE.

82. Andersson, M., et al., *A predictive real time NOx model for conventional and partially premixed diesel combustion.* SAE Paper, 2006. **2006-01-3329**.

83. Seykens, X., et al., *Experimental validation of extended NO and soot model for advanced HD diesel engine combustion.* SAE Int. J. Engines, 2009. **2**(1): p. 606-619.

84. Willems, F., et al., *Cylinder Pressure-Based Control in Heavy-Duty EGR Diesel Engines Using a Virtual Heat Release and Emission Sensor.* SAE Technical paper, 2010. **2010-01-0564**.

85. Hegarty, K., et al., *Semi-Empiric Model Based Approach for Dynamic Prediction of NOx Engine Out Emissions on Diesel Engines.* SAE Technical paper, 2010. **2010-01-0155**.

86. Traver, M.L., R.J. Atkinson, and C.M. Atkinson, *Neural network-based diesel engine emissions prediction using in-cylinder combustion pressure.* SAE TRANSACTIONS, 1999. **108**(4): p. 1166-1180.

87. Traver, M.L., C.M. Atkinson, and R.J. Atkinson, *A Neural Network-Based Virtual NOx Sensor for Diesel Engines.* combustion, 2000. **5**(6): p. 7-9.

88. Wang, Y.Y., Y. He, and S. Rajagopalan, *Design of Engine-Out Virtual NOx Sensor Using Neural Networks and Dynamic System Identification.* SAE International Journal of Engines, 2011. **4**(1): p. 828-836.

89. Johri, R., A. Salvi, and Z. Filipi. *Real-Time Transient Soot and NOx Virtual Sensors for Diesel Engine using Neuro-Fuzzy Model Tree and Orthogonal Least Squares*. 2011. ASME 2011 Internal Combustion Engine Division Fall Technical Conference.

90. Park, W., et al., *Prediction of real-time NO based on the in-cylinder pressure in Diesel engines.* Proceedings of the Combustion Institute, 2013. **34**(2): p. 3075-3082.

91. CD-adapco, *STAR-CD v4.10 Methodology*2009.

92. Colin, O. and A. Benkenida, *The 3-zones extended coherent flame model (ECFM3Z) for computing premixed/diffusion combustion.* Oil & gas science and technology, 2004. **59**(6): p. 593-609.

93. Colin, O., A. Pires da Cruz, and S. Jay, *Detailed chemistry-based auto-ignition model including low temperature phenomena applied to 3-D*

engine calculations. Proceedings of the Combustion Institute, 2005. **30**(2): p. 2649-2656.

94. Campbell, J., A. Gosman, and G. Hardy, *Analysis of premix flame and lift-off in diesel spray combustion using multi-dimensional CFD.* SAE International Journal of Engines, 2009. **1**(1): p. 571-590.

95. Reitz, R. and R. Diwaker, *Effect of drop breakup on fuel sprays*, 1986, Society of Automotive Engineers, Inc., Warrendale, PA.

96. Aamir, M. and A. Watkins. *Dense propane spray analysis with a modified collision model*. in *Procceedings of the 15th European Conference on Liquid atomization and spray systems (ILASS-Europe 1999), Toulouse, France*. 1999.

97. Bai, C. and A. Gosman, *Development of methodology for spray impingement simulation.* SAE Paper, 1995. **950283**.

98. Zeldovich, Y.B., *The oxidation of nitrogen in combustion and explosions.* Acta Physicochimica URSS, 1946. **21**(4): p. 577-628.

99. Technologies, G., *GT-SUITE Engine Performance Application Manual*, 2009.

100. Kee, R.J., et al., *CHEMKIN-III: A FORTRAN chemical kinetics package for the analysis of gas-phase chemical and plasma kinetics*1996: Sandia National Laboratories Livermore, CA.

101. Patel, A. and S.-C. Kong, *Development and validation of a reduced reaction mechanism for HCCI engine simulations.* SAE Paper, 2004. **2004-01-0558**.

102. Yu, S., *Study on the engine control using the in-cylinder pressure in diesel engine*, 2012, SNU.

103. Woo, K.W. and S.I. Yeo, *Dalton's Law vs, Amagat's Law for the Mixture of Real Gases.* 1995.

104. Lee, J., et al., *The Development of Real-time NOx Estimation Model and its Application* SAE Paper, 2013. **2013-01-0243**.

105. Miller, R., et al., *A Super-Extended Zel'dovich Mechanism for NOx Modeling and Engine Calibration.* SAE Paper, 1998. **980781**.

초 록

디젤 엔진에 대한 배기 규제가 강화됨에 따라 새로운 연소 기법을 이용하여 엔진 자체의 배출물을 줄이거나 후처리 장치 등을 이용하여 최종 배출물을 줄이는 등의 노력이 이루어지고 있다. 특히, 질소 산화물(NOx) 감소를 위한 실린더 내 연소제어, 동시에 후처리 장치의 효율을 최적화하기 위해서는 실시간으로 배출되는 NOx 배출량에 대한 정보가 필요하다.

따라서 물리적, 현상학적 모델을 사용한 가상 NOx 센서에 대한 많은 연구가 보고되고 있다. 기존 연구들은 비교적 정확하게 NOx 배출량을 예측하고 있지만 실시간 애플리케이션으로써 활용하기에는 현재 차량에 장착 중인 엔진 제어 장치의 계산 능력에 비해 모델이 너무 복잡하거나, 경험식을 피팅하기 위해 많은 보정 상수가 사용되고, 통계적 수학적 모델 등의 경우에는 많은 트레이닝이 필요한 등의 여러 가지 제한 요인이 있었다.

본 연구에서는 선행 연구의 한계를 극복하기 위해 실시간 실린더 압력과 ECU 에서 얻을 수 있는 데이터에 기반한 실시간 NOx 예측 모델을 개발하였다. CFD 는 실험 과정에서 직접 얻을 수 없는 NO 의 형성 과정을 자세히 설명 할 수 있기 때문에, 물리적 분석과 함께 CFD 결과의 분석을 통해 모델을 개발하였다. 또한 실린더 내 압력이 엔진 연소특성의 변화를 잘 반영하기 때문에, 다양한 엔진의 작동 조건에서 NO 의 배출량을 예측할 수 있도록 연소압력이 사용되었다. 개발된 NO 예측 모델은 간단한 계산 과정으로 이루어졌기 때문에 실시간으로 사이클 별 NO 를 예측할 수 있었다. 검증 결과는 제안된 모델이 엔진에서 배출되는 NO 를 잘 예측하는 것을 보여주었고, 따라서 개발된 모델이 NO 센서 대용으로써 엔진과 후처리 장치의 제어를 위한 유용한 도구로써 시스템에 적용될 수 있음을 확인하였다. 가상 NO 센서로 사용될 수 있는 것 이외에도, 개발된 NO 예측 모델은 GT-SUITE 와

AMESim 과 같은 1 차원 시뮬레이션에 적용되어 CFD 모델과 동일한 수준으로 NO 수준을 예측할 수 있는 가능성을 가지고 있다.

이후, 개발 된 NO 예측 모델은 정상 상태와 과도 엔진 작동 상태에서 NO 의 실시간 추정을 위한 기존의 엔진 제어 장치를 우회한 임베디드 시스템에 구현되었다. 모델의 결과는 NEDC 전 영역을 커버하는 대표적인 정상 상태의 동작 점에서 엔진에서 배출되는 실시간 NO 측정값과 비교되었다. 또한 다양한 조건에서 모델의 예측성을 검증하기 위해 배기가스 재순환율과 주분사시기를 베이스 조건 대비 변화시켰다. 정상상태 검증 결과 HP-EGR 76 케이스에서 실험 결과와 R^2=0.96 의 높은 예측 정도를 확인할 수 있었다. 또한 과도상태에서의 NO 예측 정도를 검증하기 위해 고속 NOx 분석기를 사용하여 엔진 속도, 부하 변경 등의 간단한 램프 조건에서 모델 결과와 비교하였다. 또한 유럽의 배출가스 측정 모드인 ECE-15 와 EUDC 사이클에서 고속 NOx 분석기 결과를 사용하여 모델을 검증하였다. 추가적으로, NO 만이 아닌 전체 NOx 를 예측할 수 있도록 정상상태 실험 결과 기반의 경험식을 사용한 NO_2 예측 모델을 제안하였다. 실시간 NOx 예측 모델에 정확한 과도상태 EGR 값을 제공하기 위해 실험실에서 개발된 EGR 예측 모델 또한 적용 되었다.

주요어 : 질소 산화물(NO_x), 실린더 압력(In-cylinder pressure), 디젤엔진(Diesel engine), CFD(Computational Fluid Dynamics), 가상 질소 산화물 센서(Virtual NO_x sensor)
학번 : 2007-22992